DIPARTIMENTO DI SCIENZE DELLA VITA

DOTTORATO DI RICERCA IN SCIENZE DELLA VITA

XXXIII CICLO

Functional proteomic investigation of extracellular vesicles: Rai $^{+/+}$ vs Rai $^{-/-}$ astrocytes and released vesicles in EAE and bronchoalveolar lavage fluid-extracted extracellular vesicles in Idiopathic Pulmonary Fibrosis

Settore Scientifico Disciplinare: BIO/10

Relatore: Prof. *Luca Bini*

Correlatore: Dr. *Claudia Landi*

Coordinatore: Prof. *Massimo Valoti*

Tesi di: *Enxhi Shaba*

Anno Accademico 2019/2020

SUMMARY

ABSTRACT

In the recent years, extracellular vesicles (EVs) drew a growing interest in scientific community, especially for their intrinsic role of cell-cell communication entities between local and distant targets. Given these appealing features, functional proteomics of EVs is a considerably valuable approach for the investigation of not only their functions, but also of their potentialities, as it provides a wider and enriched scenario of various physio-pathological molecular mechanisms. Considering this background, we performed two different functional proteomic studies on EVs in two different pathologic conditions.

The first study emerged from recent investigations on protein ShcC/Rai role in experimental autoimmune encephalomyelitis (EAE), as its deficiency resulted in disease protection and astrocytes were identified as accountable for the establishment of a local protective environment. Therefore, our analysis focused on the differences in protein content of astrocytes, as well as of their released extracellular vesicles, between $Rai^{+/+}$ and $Rai^{-/-}$ in a not stimulated and IL-17-stimulated conditions, applying 2DE, image analysis, mass spectrometry identification of differential proteins and enrichment analysis. Curiously, our proteomic data showed that both the vesicular and cellular differential proteins indicate the overall involvement of macro molecular areas, such as oxidative stress response, ECM and cellular remodelling, glutamate metabolism, EMT mechanisms and metabolic reprogramming, shifting astrocytes towards a neuroprotective response.

Concurrently, a second study was conducted to characterize and explore the individual impact on Idiopathic Pulmonary Fibrosis (IPF) pathogenesis of not only the vesicular component of bronchoalveolar lavage fluid (BALF), but also its fluid counterpart. Indeed, to the best of our knowledge, our study is the first shotgun proteomic investigation of EV isolated from BALF of IPF patients. To this purpose, ultracentrifugation was chosen as EVs isolation technique and its purification was assessed by TEM, 2DE and LC-MS/MS. Interestingly, our 2DE data and scatter plot analysis showed a considerable difference of EVs proteome with respect to whole BALF and to its fluid counterpart proteome, highlighting the importance of pre-fractioning of complex samples to the advantage of low-abundant protein species in biomarkers discovery. Remarkably, enrichment analysis results draw attention on a systemic metabolic dysregulation in disease development and highlight relevant molecular pathways that result distinctive but complementary in IPF pathogenesis.

ABBREVIATIONS

%V : percentage of relative volume

2DE : Two-dimensional gel electrophoresis

A2BAR : A2B adenosine receptor's

ABC : Ammonium Bicarbonate

ACN : Acetonitrile

ACTA : actin aortic smooth muscle

ACTB : actin cytoplasmic 1

ADAM10 : Disintegrin and metalloproteinase domain-containing protein 10

ALIX : ALG-2-interacting protein X

ALS : Amyotrophic Lateral Sclerosis

AND : Adiponectin

ANXAII : Annexin 2

AP-1 : Activator protein 1

ARDS : Acute Respiratory Distress Syndrome

ARF6 : ADP-ribosylation factor 6

BAFF : B-Cell Activating Factor

BAL : Bronchoalveolar Lavage

BALF : Bronchoalveolar Lavage Fluid

BBB : Blood Brain Barrier

BCR : B-Cell Receptor

BP : Biological Process

CFTR : Cystic fibrosis transmembrane conductance regulator

CHAPS : 3-[(3-cholamidopropyl) dimethylammonia]-1-propanesulfonate hydrate

CHCA : α-cyano-4-hydroxycinnamic acid

CISK : Cytokine-independent survival kinase

CNS : Central Nervous System

COPD : Chronic Obstructive Pulmonary Disease

CREB1 : Cyclic AMP-responsive element-binding protein 1

CTD-ILD : ILD associated with connective tissue disease

DAP : Differentially Abundant Protein

DAS : Differentially Abundant Spot

DLCO : Diffusing Capacity of the Lung for Carbon Monoxide

DTE : Dithioerythritol

EAE : Experimental Autoimmune Encephalomyelitis

ECM : ExtraCellular Matrix

EGFR : Epidermal growth factor receptor

ELF : epithelial lining fluid

EMT : Epithelial-Mesenchymal Transition

ENOA/ENO1 : alpha-enolase

ErbB2 : Receptor tyrosine-protein kinase erbB-2

ERP44 : endoplasmic reticulum resident protein 44

ESCRT : Endosomal Sorting Complex Required for Transport

ETS1 : Protein C-ets-1

EVs : Extracellular Vesicles

FGF : Fibroblast growth factor

FVC : Forced vital capacity

GAPDH : Glyceraldehyde-3-phosphate dehydrogenase

GATA-2 : Endothelial transcription factor GATA-2

GFAP : Glial Fibrillary Astrocytic Protein

GLI-3 : Transcriptional activator GLI3

GLNA : Glutamine synthetase

GO : Gene Ontology

HDAC1: Histone deacetylase 1

HIF-1 : Hypoxia-inducible factor 1

HP : Hypersensitivity Pneumonitis

HSBP1 : Heat shock factor-binding protein 1

HSF-1 : Heat-shock factor 1

HSR : heat shock response

IFNγ : Interferon-gamma

IIP : Idiopathic Interstitial Pneumonia

ILD : Interstitial Lung Disease

IPF : Idiopathic Pulmonary Fibrosis

KLHL9 : Kelch-like protein 9

LAMP1 : Lysosome-associated membrane glycoprotein 1

LEG2 : Galectin-2

MAP4 : Microtubule-associated protein 4

MAPK : Mitogen-activated protein kinase

MBP : Myelin Basic Protein

MCP-1 : Monocyte chemoattractant protein-1

MDD : Multidisciplinary discussion

MHC : Major Histocompatibility Complex

MIP-1α : Macrophage inflammatory protein 1-alpha

MKL1 : Megakaryoblastic leukemia 1

MMP : Matrix metalloproteinase

MOG : Myelin oligodendrocyte protein

MS : Mass Spectrometry

MS : Multiple sclerosis

MV : Microvesicle

NDUS2/NDUFS2 : NADH dehydrogenase (ubiquinone) iron-sulfur protein 2, mitochondrial

NK : Natural Killer

NO : Nitric Oxide

NS : Not stimulated

PARP1 : Poly(ADP-ribose) polymerase-1

PBS : Phosphate Buffer Saline

PCA : Principal Component Analysis

PDIA3 : protein disulfide-isomerase A3

PEA15 : astrocytic phosphoprotein PEA-15

PKA : Protein kinase A

PKCα : Protein kinase C alpha

PLA2 : phospholipase A2 activity

PMF : Peptide Mass Fingerprinting

PPARγ : Peroxisome proliferator-activated receptor-γ

PRDX6 : Peroxiredoxin-6

PSB2/PSMB2 : Proteasome subunit beta type-2

PTMs : Post-Translational Modifications

RAAS : Renin-Angiotensin-Aldesterone system

RAB11B : Ras-related protein Rab-11A

RAB27A : Ras-related protein Rab-27A

RAGE : receptor for advanced glycation end products

RBGPR : rab3 GTPase-activating protein non-catalytic subunit

ROCK : Rho-associated protein kinase

ROS : Reactive Oxygen Species

S100A6/S10A6 : Calcyclin

SDS : Sodium Dodecyl Sulphate

SHC3 : ShcC/Rai

SODC/SOD1 : superoxide dismutase (Cu-Zn)

TCR : T-cell receptor

TEM : Transmission Electron Microscopy

TFA : Trifluoroacetic acid

TGF : Tumor Growth Factor

TNF : Tumor-necrosis factor

tPA : Tissue plasminogen activator

TPC6B : Trafficking protein particle complex subunit 6B

TSG101 : Tumor susceptibility gene 101 protein

TSTD2 : Thiosulfate sulfurtransferase/rhodanese-like domain-containing protein 2

UBE2N : Ubiquitin-conjugating enzyme E2 N

UIP : Usual Interstitial Pneumonia

VEGF-A : Vascular endothelial growth factor A

YY1 : Transcriptional repressor protein YY1

INTRODUCTION

PROTEOMICS and SYSTEMS BIOLOGY

Proteomics is the characterization of the entire observable protein complement of a biological system, also referred to as "proteome". This term was coined for the first time in 1994 by Mark Wilkins identifying the overall protein content of any cell that is characterized with regard to their expression, function, localization, interactions, post-translational modifications and turnover, at a particular time (1). The human proteome is way more complex than the human genome, considering that starting from about 19000-20000 coding-genes, about 1 million proteins could be obtained. This complexity was explained by the potentiality of a single gene in encoding multiple proteins through a variety of pre- and co-transcriptional events. In addition to these processes, transcripts could undergo several post-translational modifications (PTMs), further increasing proteome complexity (2,3). Consequently, as a protein may undergo these events exerting different functions according to their state, a further definition was required to better distinguish each form of a single protein. To this purpose, the term "proteoform" or "protein species" was coined to indicate the smallest unit of the proteome defined by its structural formula comprising full amino acid sequence and every post translational modification (4,5). Additionally, while human genome is relatively static, human proteome is highly dynamic since protein profiles may change in relation to time and a variety of extracellular and intracellular stimuli, providing a snapshot-in-time of a particular biochemical system. For these reasons, proteomics might be considered as the most valuable and highly potential data set to characterize a biological system (6). In fact, proteomics combined with other so-called "OMIC sciences" such as genomics, epigenomics transcriptomics and metabolomics, might offer alternative and intriguing insights, improving our understanding in many research areas. Consequently, the integration and interaction of the different components of the OMIC cascade had given rise to a new study field known as "systems biology" (7). This interdisciplinary research area consists of several study fields such as biology, computer science, engineering, bioinformatics and others providing a holistic view of the biological processes as the interaction of biomolecules in an intricate biological network of genes, transcripts, proteins and metabolites. Moreover, it allows to look at the whole picture instead of the sum of parts, changing perspective for a global evaluation (8). Therefore, as a result of the new high-throughput technologies developed in the recent decades, a

huge amount of data from all these different fields of study is rapidly generated (9–11). As a result, this global information at different scales of organization might be used for a wider perspective that starts from genes and proteins, on through subcellular interactions and pathways, ending in more complex systems like cells, tissues, organs and whole organisms (12). For this reason, biology and omics technologies play a crucial role in the better understanding of molecular systems, starting from the simplest structures and progressively towards the more complex ones. In particular, this increasing knowledge may contribute to future advances in medicine, leading to the development of more sensitive and efficient biomarkers and to precision and individualization of treatments (9).

PROTEOMICS TECHNOLOGIES AND APPLICATIONS

Protein separation is a central feature of all analytical strategies in proteomics, due to the extreme complexity of proteomes themselves. Consequently, several separation techniques have been developed during the last decades in order to improve sensitivity and efficacy of the subsequent proteomic analysis, such as chromatographic approaches as well as gel-based separation methods (1). Although the development of alternative gel-free approaches has led, nowadays, to a switch towards mass-spectrometric proteomic analysis, electrophoretic separation techniques continue to be some of the most versatile and widely used approaches to study the proteome of a biological system. Indeed, one of the main advantages of these methods is the separation and identification of thousands of individual proteins species, including proteoforms and post-translational modifications (13,14) Gel-based methods consists of the well-known and widely used SDS-PAGE, which is a good resolving technique for the separation of proteins according to their size, thus facilitating the estimation of molecular weight (6). In addition, an upgrade is represented by 2D-electrophoresis, which consists in the separation of complex protein mixtures according to two largely orthogonal parameters, moreover two dimensions: their “isoelectric point” (pI) and their apparent molecular weight (Mr). Consequently, depending on the gel size, polyacrylamide polymerization degree and pH gradient used, 2-DE can resolve up to 5000 different protein species simultaneously and can detect and quantify less than 1 ng of protein per spot (15). First, proteins separate according to their isoelectric point along an immobilized pH gradient (IPG) strips and this step is commonly called “isoelectric focusing” (IEF). Then, IPG strips are aligned along the top of an SDS-polyacrylamide gel and once electric field is applied, proteins migrate from the strip into the gel, separating according to their molecular weight, as a classic one-dimensional electrophoresis. The resulting 2D gels are then

digitalized, therefore 2D maps are analyzed using specific image analysis softwares, allowing also a relative protein quantification between different samples. After image analysis, differential spots of interest might be excised and then processed for identification by mass spectrometry, such as MALDI-TOF (14). This proteomic approach has both several advantages and disadvantages: on one side, 2-DE is characterized by a very high resolution at the protein level and is efficiently successful for the separation of proteoforms and post-translationally modified proteins. On the other side, it is also characterized by low reproducibility and low sensitivity in the detection of proteins with too low or too high pH values (pH <3 and pH>10), and too high or too low molecular masses (smaller than 10 kDa and larger than 150-200 kDa) (7).

Among the numerous techniques through which proteins can be investigated on a large scale, mass spectrometry (MS) has gained great popularity. Indeed, great improvements of technology and methodology in this field applied to proteomic studies provide always novel strategies to speed biological discovery (16). In particular, as a response to the progressively increasing high demand of high resolution, sensitivity and accuracy in proteomics, novel MS approaches have been developed. On example is the so-called "shotgun proteomics", named for its similarity to "genome shotgun sequencing", a method used from 1995 to 2005, which was aimed to reconstruct whole genomes from random DNA fragments; similarly, the proteomic counterpart operates at the level of protein fragments in order to randomly map complex protein mixtures (17). Although the shotgun approach might be considered as quite simple, it actually results in a highly increased complexity of the generated peptide mixture, requiring very sensitive and efficient separation. Furthermore, as the starting point is represented by already fragmented proteins, this method could lead to a loss of information, such as post-translational modifications or no identification of low abundance proteins, because almost only most abundant peptides are detected (16). For these reasons, the combination with efficient and rapid separation instruments and approaches to mass spectrometry became increasingly important, especially for the analysis of complex human body fluids. Especially, liquid chromatography (LC), often at nano- and micro-scale, is particularly applied for identification of proteins, as often proteomics faces some challenges due to complexity and dynamic range of proteins of various samples. To this purpose, sometimes a depletion of high-abundance proteins and fractioning has to be performed for sample pre-treatment (18).

Given this, two main distinct proteomic approaches might be distinguished: top-down and bottom-up. The former is greatly represented by 2DE as it consists, first, in high-resolution separation of intact proteins, then proteins digestion into peptides, followed by the MS identification by Peptide Mass Fingerprinting (PMF) of selected protein species resulted from differential image analysis.

Conversely, the latter is well represented by Tandem Mass Spectrometry (LC-MS/MS) as it consists, first, in proteins digestion into peptides, then chromatographic separation leading to MS/MS identification of peptides-originating proteins (19).

FUNCTIONAL PROTEOMICS

Nowadays, proteomic results consist of long lists of proteins identified by high-throughput mass spectrometry technologies, thereby the most challenging question is how to extract functional and biological information from this enormous proteomic data. To this purpose, several commercial and open source tools have been developed to facilitate the understanding and interpretation of data (20). On one hand, a strong necessity of a functional classification of genes and gene products led to the development of the so-called "Gene Ontology" (http://geneontology.org/), which consists of a structured and controlled vocabulary for the description of the biology of a gene and its products in an organism at the molecular and cellular level. Conceptually, an ontology is a formal representation of knowledge that provides definitions of entities, their attributes and relationships to other objects. Precisely, in order to properly describe the knowledge of a gene and its products, three main sub-ontologies were set up: biological processes (P), molecular function (F) and cellular component (C) (21,22). Consequently, this association of biological entities to one or multiple GO term allows to carry out a so-called "enrichment analysis", which provides a further and deeper understanding of biological functions and processes enriched in a large-scale proteomic dataset. In other words, a GO-term enrichment analysis compares the abundance of specific GO-terms in the dataset with the natural abundance in the organism or a reference dataset and to this purpose a p-value is calculated for the all the overrepresented GO-terms, representing the significantly enriched functions in the dataset.

However, in most cases proteins work in collaboration with others in order to regulate cellular processes and, indeed, they are often assembled into specific pathways in which they perform their activities. Moreover, pathways and cellular processes regulated by particular proteins have been regularly annotated. Given this concept, specific pathways could be identified as active as correlated to the expression of certain proteins; thereby, differential protein expression data can be used to carry out a so-called "pathway enrichment analysis". Indeed, changes in the expression level of particular proteins in a biological sample compared to its control pattern of expression allow the prediction of potential pathways that are differentially regulated (23). Accordingly, "pathway analysis" might be defined as a data analysis aimed to identify activated pathways or pathway modules from functional proteomic data (20,24). In addition to linear pathways, several tools enable also to build, overlay, visualize and infer protein interaction networks from functional proteomic and other systems biology

data, performing a so-called “network analysis”. In contrast to pathway analysis, network analysis aims to construct comprehensive network diagrams derived from both prior experimental sources and new in silico predictions, extracting system-level biological meanings (25). Given these points, pathway and network analysis approaches applied in proteomics provide several advantages: first, pathway analysis of proteomic data might be directly interpreted in signaling pathways; second, network analysis of proteomic results might be associated to direct evidences supported by protein-protein interaction data validated by in-vitro experiments; third, both analysis can be visualized in a functional protein network with transcriptional factors (24).

EXTRACELLULAR VESICLES

In the recent years, extracellular vesicles (EVs) became a strong field of interest, especially for their potential applications in biomedical research. Interestingly, their existence and main activities have been discovered not so long ago. From their first appearance in scientific papers in 1983 (26–28), extracellular vesicles’ conception has progressively evolved, leading their accepted role in cell-cell communication. Indeed, new paradigm of cell communication was set up and it consists of three main parts: a proximal element that packages and secretes a single or multiple signaling molecules sequestered in EVs; the EVs that travel to a target cell(s) in order to trigger a biological response; a distal element which receives and processes the EVs-mediated information (29).

Accordingly, extracellular vesicles are defined as lipid bound vesicles secreted by cells into the extracellular space and they can be classified upon their biogenesis, release pathway, size, content and function. Nonetheless, three main subtypes can be differentiated by their biogenesis: exosomes (20-150 nm in size), microvesicles (MVs) (100-1000 nm in size) and apoptotic bodies (200-5000 nm in size) (30). Extracellular vesicles’ content varies considerably according to biogenesis, cell type of origin and physiological conditions. Mainly, EVs are loaded with various proteins, lipids and nucleic acids and the pattern of cargos is specific per vesicle and cell type (31). Despite the wide research on profiling EVs proteome, it is rather difficult to outline the specific and fixed protein composition of different types of vesicles, due to variables such as isolation techniques, cell types and culture conditions. Nevertheless, many common proteins might be identified, especially those related to the formation, release and uptake of vesicles. Thus, ESCRT (Endosomal Sorting Complex Required for Transport family proteins are frequently enriched in vesicle fraction, such as ALIX and TSG101 then, proteins involved with the EV formation and release, such as RAB27A, RAB11B and ARF6, are commonly detected. Additionally, many tetraspanins, such as CD63, CD81 and CD9, are often

identified, together with proteins involved in signal transduction (EGFR), antigen presentation (MHC I and II classes) and other transmembrane proteins (LAMP1, TfR) (32,33).

As primary role of EVs is cell-cell communication between local and distant cells, particularly explicit their function of molecular messengers through an autocrine and paracrine manner with a proximal or distal radius of action from their site of origin (34). Upon uptake by target cells in physiological conditions, EVs can exert multiple functions on several biological processes as they may contribute to processes like blood coagulation, wound healing and regulation of immune responses. Nevertheless, vesicles are also involved in pathological events, as they may contribute to neoplastic, autoimmune, inflammatory and infectious diseases' development and progression (35).

Given these unique physical and biological properties, EVs became extremely attractive, especially for their potential therapeutic uses. On one side, they might be used as powerful delivery tools for therapeutic agents into various types of tissues. For example, several studies suggested the ability of some EVs to cross the Blood Brain Barrier (BBB), making them very interesting for the treatment of brain pathologies. Furthermore, as vesicles might be considered like proper messengers, they are prone to be taken-up by target cells, delivering their cargo into the cytosol. This feature sheds light on the opportunity to target intracellular molecules, for instance oncogenes (36). On the other side, as EVs are reported to reflect the phenotype of cells of origin, they have been proposed as diagnostic biomarkers of several pathologies, such as cancer, infectious diseases, autoimmune and inflammatory disorder. In particular, they could be used as bodily fluid-extracted biomarkers, being extremely beneficial as it would limit the need for collection of tissue samples and other invasive procedures (37).

CHAPTER I

Rai $^{+/+}$ vs Rai $^{-/-}$ astrocytes and released vesicles in EAE

ABSTRACT

Multiple sclerosis (MS) is an autoimmune disease characterized by a strong neuroinflammatory status mainly due to the Central Nervous System (CNS) infiltration of myelin-specific proinflammatory CD4+ T cells, especially the Th1 and Th17 subtypes. These autoreactive cells further increase the neuroaxonal damage and demyelination by promoting the activation of other inflammatory cells, such as microglia, astrocytes and macrophages, and this highlights a relevant involvement of the local CNS microenvironment in the disease onset and development. Recent studies on the protein ShcC/Rai, a member of the Shc family of signaling adapters, demonstrated that its deficiency in mouse model protected from EAE (experimental autoimmune encephalomyelitis) and astrocytes were confirmed as the resident cells responsible for the establishment of this local protective environment. Furthermore, growing evidence suggests the emerging role of extracellular vesicles (EVs) as new players, considering their ability to modulate the local microenvironment and to shape the immune response through their content. Thereby, the aim of our study is to evaluate, through a functional proteomic approach, the differences in protein content of astrocytes, as well as of their released extracellular vesicles, between $Rai^{+/+}$ and $Rai^{-/-}$ in a not stimulated and IL-17-stimulated conditions.
By proteomic and enrichment analysis of $Rai^{+/+}$ versus $Rai^{-/-}$ astrocytes' EVs, also after their IL-17 stimulation, the differential identified proteins modulate common molecular pathways, such as oxidative stress response, glutamate homeostasis, ECM/cellular adhesion remodeling and cellular migration, with a strong involvement of WNT- β catenin molecular pathway. In addition, analogous analysis of EVs releasing-astrocytes suggested that the mainly involved pathways are oxidative stress response, ubiquitin-proteasome pathway, energetic metabolism and EMT events via β catenin.
In conclusion, proteomic data provided an overview of the after-effects of Rai deficiency at cellular and vesicular level suggesting the involvement of various proteins, each related to distinct molecular pathways. However, an interesting remark must be reported on how all differential proteins seem to be involved in macro molecular areas, such as oxidative stress response, ECM and cellular adhesions remodelling, glutamate metabolism, EMT mechanisms and metabolic reprogramming.

INTRODUCTION

MULTIPLE SCLEROSIS: OVERVIEW

Multiple sclerosis (MS) is a chronic inflammatory and autoimmune disease of the central nervous system (CNS), predominantly associated with recurrent and intermittent inflammatory episodes resulting in the demyelination and subsequent damage of axons and neurons in the brain, optic nerve and spinal cord (38). Despite the etiology and specific pathophysiological processes of the disease are not yet fully understood, current knowledge suggests the involvement of the immune system, which abnormally directs itself against CNS axons via the activation of mainly autoreactive T cells that target the myelin sheath. Specifically, the myelin sheath is a lipid-based structure that covers axons with the purpose of improving axonal conduction of electrical impulses back and forth from the brain to the rest of the body through the spinal cord. Consequently, the result of the immune cell infiltration across the BBB from the periphery into the CNS is a strong inflammation, demyelination, gliosis and subsequent neuroaxonal degeneration. Particularly, when myelin is destroyed or compromised, electrical impulses are not transmitted correctly. Events of myelin regeneration occur; however, they lead to the formation of hardened scar tissue. As a result, the disease is characterized by confluent demyelinated areas in the white and grey matter of the brain and spinal cord that are called “plaques” or lesions, which indicate a loss of myelin sheaths and oligodendrocytes, affecting every physical, sensory, mental and emotional activity (39).

Unfortunately, the main cause of MS is still unknown, however the most accepted hypothesis is that of a multifactorial cause, where both genetic and environmental factors contribute to an individual’s disease risk. In particular, a complex interaction of genetic and environmental factors and random events affects not only the probability of occurrence of those pathogenic events, but also the ability of the CNS repair, functional plasticity and physical and cognitive activities.

IMMUNOPATHOLOGY

Although in the past multiple sclerosis was often referred to as a primarily neurodegenerative disorder with secondary immune involvement, interesting and enlightening evidences had implemented new players in the complex pathological events leading to the disease and this shifted the definition of MS towards an immune-mediated pathology of the CNS. Accordingly, all evidences confirmed also the involvement of both the innate and adaptive immune system in the pathogenic events, as well as a

strong inflammatory component starting from the earliest stage of the disease throughout the entire course (40). Adaptive immune players are mainly autoreactive B and T cells and, as demyelination is a key feature of MS, myelin protein-derived antigens have been suggested to be the main autoreactive targets, such as a proteolipid protein called "myelin basic protein (MBP)" and the "myelin oligodendrocyte glycoprotein (MOG)" (41). As a result, even though no certain causes have been identified, the adaptive immune system is activated, especially CD8+ cytotoxic T cells, differentiated CD4+ T helper 1 (T_H1) and T_H17 cells, and B cells, thus they infiltrate into the CNS from the periphery mainly by direct crossing of the BBB. Indeed, T_H1 and T_H17 cells are the main CD4+ T cell subsets involved, whose relevance in the pathogenesis of the disease is still deeply investigated. Moreover, evidences in MS patients showed the presence of myelin-reactive peripheral CD4+ T cells with an enhanced expression of both respective T_H1 and T_H17 cell signature cytokines IFNγ and IL-17A, which contribute considerably to the inflammatory status of the disease (40,42).

Even if neurodegeneration in MS is thought to be the final result of a cascade of events primarily affecting axons and neurons, chronic CNS inflammation, mainly exerted by infiltrating adaptive immune cells, contributes to neurodegeneration through the action of cells of the innate immune system, which have become or are already resident within the CNS. In detail, the principal players of the innate immune system involved in MS pathogenesis are CNS macrophages, monocytes-derived macrophages and microglia (43).

ASTROCYTES IN MULTIPLE SCLEROSIS

Even though in the past astrocytes were considered to be passive reactors to the altered immune response in multiple sclerosis pathogenic process, recently these particular cells have gained increasing interest from the scientific community, which completely revolved the common knowledge on this particular cell type. In contrast to previous knowledge that astrocytes are relatively stable cells, providing mainly structural and metabolic support to neuronal cells and to the BBB, recent evidences suggest that astrocytes are, instead, extremely dynamic and that they carry out several functions directed at the maintenance of the homeostasis of the brain (44). In detail, astrocytes are the most abundant and heterogeneous type of glial cells that account for approximately 30% of the entire glial population. Additionally, astrocytes form the so-called "glia limitans" through the distal end feet of their processes and they use them to wrap blood vessels or meninges. For this reason, one of the main function of these glial cells is to contribute to the maintenance of the BBB integrity and to form an additional barrier that can further restrict the infiltration of peripheral cells into the CNS (45). Astrocytes exert multiple physiological functions in the CNS: first, they do not only

contribute to the BBB integrity maintenance, but also to the blood-flow regulation process and to the extracellular matrix (ECM) formation. Second, they maintain homeostasis of neurons and axons by regulating the transport and passage of fluids, ions, toxins and neurotransmitters, such as glutamate, extracellular potassium, ATP and water. Indeed, astrocytes connect to several neuronal synapses with their processes by forming the so-called "tripartite synapses", regulating neuronal synaptic transmission. Third, astrocytes are metabolically coupled to neurons, promoting the synthesis of metabolic substrates, such as glycogen and lipoproteins, and providing antioxidants, such as glutathione and thioredoxin. Fourth, astrocytes, especially those aligning myelinated axons, have a vital role in communicating with oligodendrocytes during developmental myelination. In detail, astrocytes directly provide oligodendrocytes with nutrients and substrates to support the metabolically-demanding process of myelin sheath formation and maintenance.

Thus, this deep astrocytic involvement in the normal CNS functions suggests that astrocytes might actually be active players in the physio-pathological mechanisms of the disease, especially because they are able to influence the surrounding microenvironment and cells by the release of different factors (44–46). In fact, several evidences suggest that reactive astrocytes may assume different phenotypes according to the stimuli they receive, specifically "A1" or "A2" phenotypes. In particular, A1-type astrocytes, i.e. the "neurotoxic" phenotype, are induced by inflammation and they secrete neurotoxic factors; in contrast, A2-type astrocytes, i.e. the "neuroprotective" phenotype, express and release neurotrophic factors (47). Accordingly, astrocyte dual reactivity is regulated by two main canonical pathway, i.e., NF-kB and STAT3 cascades, each characterizing a detrimental or beneficial phenotype, respectively. In detail, NF-kB is a regulator of innate and adaptive immunity that is involved in cell survival, differentiation and proliferation processes. Notably, astrocytic NF-kB signaling is mainly activated via pro-inflammatory cytokines' mediation, such as IL-17, TNF-α and IL-1β and its up-regulation contribute to initiating and maintaining inflammation in the CNS. Particularly, its activation promotes the expression of pro-inflammatory chemokines and cytokines, cell adhesion molecules as well as an impairment of glutamate uptake and a decrease in lactate release. Conversely, STAT3 pathway is activated in response to CNS inflammation and it determines a decrease in inflammation, leukocyte infiltration and demyelination. Interestingly, evidences reported that activated astrocytes provide neuronal protection via ERK and/or STAT3 signaling during inflammation, suggesting a key role of this pathway in the neuroprotective A2 phenotype (45). Nevertheless, the concept of A1/A2 polarization is nowadays considered an oversimplification as reactive astrocytes may also exceed the A1/A2 dichotomy and assume a range of profiles with simultaneously shared and unique features. Moreover, distinct astrocytic phenotypes may coexist or

develop sequentially during different phases of a pathology: reactive astrocytes may first produce pro-inflammatory cytokines and ROS and then in a second phase, they may promote anti-inflammatory and neuroregenerative processes through the release of neurotrophic factors (47).

THE PROTEIN ADAPTOR ShcC/Rai AND MULTIPLE SCLEROSIS

Following the numerous evidences on the Th1 and Th17 cells' role in the MS pathogenesis, it is interesting to focus our attention on specific intracellular factors involved in the activation and differentiation of these autoreactive T cells in order to better characterize their function and their subsequent potential manipulation for therapeutic purposes. Interestingly, several studies have been focusing on the role and activity of a specific protein, known as Rai or ShcC. In detail, ShcC/Rai belongs to the Shc family of protein adaptors, whose members participate in the signalling pathways triggered by tyrosine kinase-coupled surface receptors that regulate several cellular processes, such as proliferation, differentiation, survival and motility. Rai is expressed mainly in the nervous system, indeed its function in different cell types has been evaluated. In neuronal cells, Rai acts as an adaptor recruited to the activated tyrosine kinase receptor Ret and, thereby, mediates the activation of the PI3K/Akt signalling pathway triggering a pro survival effect. Accordingly, Rai in neurons mediates survival signals following the exposure to stress stimuli, such as oxidative stress and hypoxia (48). Nonetheless, several studies reported the expression of this adaptor also in other tissues such as enteric glial cells, endothelial cells and smooth muscle cells of the gastrointestinal tract, indicating potential functions of this adaptor outside of the CNS (49). In fact, the Rai expression was also detected in both T and B lymphocytes, even though in lower levels than in neuronal cells. Interestingly, *Savino et al.* reported that Rai results to exploit opposite functions in lymphocytes and neurons: *in vitro* and *in vivo* evidences demonstrated that Rai attenuates TCR and BCR signalling leading to an impairment of lymphocytes activation and survival (48). Specifically, *Ferro et al.* demonstrated that Rai is recruited to phosphorylated CD3 in response to TCR engagement and, simultaneously, impairs the interaction of ZAP-70 to CD3/TCR complex, thereby it does not allow the PI-3K/Akt pathway activation and inhibits the TCR signal transduction. Indeed, Rai $^{-/-}$ mice displayed splenomegaly, spontaneous T- and B-cell activation and autoantibody production, leading to the development of a lupus-like autoimmune disease, supporting the inhibitory activity of Rai in T and B lymphocytes (50). Additionally, *Savino et al.* proved that Rai negatively regulates $CD4^+$ T cells differentiation to the Th17 lineage and that limits indirectly Th1 development *in vivo* (51). Following these encouraging evidences, *Ulivieri et al.* focused on the potential pathogenic effect of the Th17 cells associated with Rai deficiency on MS development, using the "experimental autoimmune

encephalomyelitis (EAE)", the MS experimental model. Unexpectedly, the results showed that Rai deficiency protects mice from EAE displaying a delay in disease onset and a decrease severity, despite an expected enhanced myelin-specific Th17 cells production and their unaltered ability to infiltrate into the CNS. Indeed, after the injection of MOG-specific T cells from Rai $^{-/-}$ mice into Rai $^{+/+}$ ones, the disease resulted even more severe, whereas the injection of WT MOG-specific T cells into Rai $^{-/-}$ mice showed a protection from the disease. These data suggested that Rai is essential for the EAE development and that the CNS, in its absence, is protected from an immune-mediated damage. Looking for another CNS-resident player which might be responsible for this protective action, *Ulivieri et al.* demonstrates the Rai expression also in spinal cord astrocytes and in primary astrocyte cultures generated from the brain of newborn mice. In fact, astrocytes are able to directly or indirectly interact with infiltrating autoreactive T cells in CNS, and in particular they might modulate the inflammatory environment. As a result, the evidence-supported explanation of this protective phenotype relies on the impaired ability of Rai $^{-/-}$ astrocytes to produce proinflammatory mediators, such as IL-6 which is markedly involved in MS neurodegeneration, in response to specific factors released from infiltrating myelin-reactive T cells, such as IL-17. In fact, while both microglia and astrocytes are targets of Th1-released inflammatory factors, Th17-released ones act selectively on astrocytes, suggesting their role as central mediators of T-cell mediated neuroinflammation. Specifically, this reduced expression of proinflammatory factors is due to a decreased in IL-17-dependent activation of the NF-kB pathway. Moreover, Rai $^{-/-}$ astrocytes showed also reduced production of NO and an increased expression of the immune-suppressive cytokines IL-10 and IL-27. In summary, data revealed that Rai-deficient mice are protected from the pathology due to CNS-resident astrocytes, which establish a local protective environment by attenuating their response to inflammatory signals, although there's an improved development of encephalitogenic Th17 cells which cross the BBB and infiltrate into the CNS (52). Recent studies have further investigated the Rai $^{-/-}$ astrocytes phenotype to better understand how they explicit this protective action in the microenvironment. Specifically, *Ulivieri et al.* demonstrated that Rai-deficient astrocytes present an increased ectonucleotidase activity by upregulating CD39 expression following the exposure to conditioned media from encephalitogenic T cells. Specifically, this enzyme converts extracellular ATP into adenosine, exerting an immunosuppressive activity by inhibiting TCR signaling and thus, T cells activation and proliferation. Thus, elevated extracellular ATP (eATP) represents a danger signal as it boosts T-cell activation and Th17 differentiation, promoting neuroinflammation; on the other hand, adenosine exploits strong anti-inflammatory and immunosuppressive action. Consequently, these evidences suggested Rai as a negative regulator of astrocyte mediated adenosine-

dependent T-cell suppression and further highlight neuroprotective mechanisms of Rai $^{-/-}$ astrocytes against T-cell dependent neurodegeneration. Moreover, additional data provide evidence that Rai $^{-/-}$ astrocytes shift towards the neuroprotective A2 phenotype as they up-regulate the expression of A2-specific transcripts, such as Emp1 and S100a10, by enhancing STAT3 signaling pathway. In particular, this phenotype reports an increased phosphorylated STAT3 (pSTAT3) and a decreased phosphorylated NF-kB (pNF-kB). In conclusion, these data support the neuroprotective feature of Rai deficiency astrocytes (53). Given these interesting findings, the aim of our study was to evaluate, through a functional proteomic approach, the differences in protein content of extracellular vesicles, as well as of the astrocytes they originate from, between Rai$^{+/+}$ and Rai $^{-/-}$ in a not stimulated and IL-17-stimulated conditions.

MATERIALS & METHODS

Astrocytes and released EVs sample preparation for 2DE

Rai $^{+/+}$ (WT) and Rai $^{-/-}$ (KO) astrocytes, as well as their released EVs, were prepared and provided by the research group directed by Prof. Cristina Ulivieri of the Molecular Immunology Laboratory directed by Prof. Cosima Baldari of the Life Sciences Department at the University of Siena. 20 x 10^6 Rai WT or Rai KO astrocytes, each respectively not stimulated (NS) and stimulated with IL-17, and their respective released EVs were prepared for 2DE. First EVs concentration was detected by NanoDrop (NanoDrop ND-1000 spectrophotometer) and both cellular and vesicular samples were solubilized in a denaturation solution composed of 8 M Urea, 2 M Thiourea, 4% w/v 3-[(3-cholamidopropyl) dimethylammonia]-1-propanesulfonate hydrate (CHAPS) and 1% w/v dithioerythritol (DTE). Astrocytes' protein concentration was then detected by Bradford assay (54) and eventually, traces of bromophenol blue were added to samples carrying 60 µg of protein in 350 µl solution for the analytical run and 700 µg in average in 450 µl solution for the preparative run.

2D-Electrophoresis

2D-Electrophoresis (2DE) was performed using the Immobiline polyacrylamide system (55). Immobilized nonlinear pH 3-10 gradient on strips 18 cm in length (GE Healthcare, Uppsala, Sweden) were employed in the first dimensional run. Runs were carried out utilizing the Ettan™ IPGphor™ system (GE Healthcare, Uppsala, Sweden), specifically analytical strips were pre-rehydrated with 350 µl of sample at 16 °C with the following electrical conditions: 30V for 8h, 200 V for 2 h, from 200 V to 3500 V in 2 h, 3500 V for 2 h, from 3500 V to 5000 V in 2 h, 5000 V for 3 h, from 5000 V to 8000 V in 1 h, 8000 V for 3 h, from 8000 V to 10000 V in 1 h, 10000 V for the rest of the run until to reach a total of 90,000 VhT. Carrier ampholytes were added to samples, at 0.2% for the analytical runs and at 2% for the preparative ones. Mass Spectrometry (MS)-preparative strips were pre-rehydrated with 350 µl of samples at 16°C for 12 h at 30 V and successively, the remaining 100 µl were loaded by cup at the cathodic ends, at 16°C applying the following voltage conditions: 200 V for 8 h, from 200 V to 3500 V in 2 h, 3500 V for 2 h, from 3500 V to 5000 V in 2 h, 5000 V for 3 h, from 5000 V to 8000 V in 1 h, 8000 V for 3 h, from 8000 V to 10000 V in 1 h, 10000 V for 10 h for a total of 90,000 VhT. At the end of the first dimensional run, strips were washed with deionized water and equilibrated with two buffers: the first composed of 6 M Urea, 2% w/v Sodium Dodecyl Sulphate (SDS), 2% w/v DTE, 30% v/v glycerol and 0.05 M Tris-HCl pH 6.8 for 12 min; the second one composed of 6 M Urea, 2% w/v SDS, 2.5% w/v Iodoacetamide, 30% v/v glycerol, 0.05 M Tris-

HCl pH 6.8 and a trace of bromophenol blue for 5 min. The second dimension was then performed at 40 mA/gel constant current on 9-16% SDS polyacrylamide linear gradient gels (size: 18 x 20 cm x 1.5 mm) at 9°C (55). Analytical gels were stained with ammoniacal silver nitrate, while preparative gels underwent a mass spectrometry-compatible silver staining (56); then, both were digitized with Image Scanner III laser densitometer supplied with the LabScan 6.0 software (GE Healthcare). 2D image analysis was performed using Image Master 2D Platinum 6.0 software (GE Healthcare, Uppsala, Sweden). First, an Intra Class analysis was performed by matching all gels of the same condition to its "Master gel" chosen by the user taking into consideration the resolution and the number of spots as criteria. In detail, 4 gels for WT NS, 3 for KO NS, 4 for WT IL-17, and 3 for KO IL-17 were used for EVs image analysis, while 3 gels for the same conditions were used for astrocytes image analysis. Secondly, an Inter Class analysis was performed by matching all "Master gels" to each other. Gel comparison resulted in quantitative and qualitative protein differences, validated by a statistical analysis.

Statistical analysis of proteomic data

Non-parametrical tests (Kruskal-Wallis and Dunn´s multiple test) were adopted to compare the percentage of relative volume (%V) of the 2DE protein spots among the groups. Through Benjamini-Hochberg test, the type I errors in null hypothesis were evaluated for each multiple comparison. Only differentially abundant spots with a p-value ≤ 0.05 and at least two-fold change in the ratio of the %V means were considered statistically significant.

Heatmap and PCA analysis

In order to visualize the behavior of the differentially abundant spots in the considered conditions was performed a heatmap analysis using the normalized %V values of the statistically significative abundant spots. In particular, the clustering of protein spots was performed using Ward´s clustering method and Euclidean distance. The above-mentioned analysis and the related figures were obtained by RStudio Desktop 1.1.463 (Integrated Development for RStudio, Inc., Boston, USA, https://www.rstudio.com). Differential spots were also used to perform multivariate analysis by Principal Component Analysis (PCA) simplifying the amount of data (%V variables) by linear transformation. By PCA it is possible visualize experimental groups in a two-dimensional plane on the basis of the differential spot patterns. PCA was performed by RStudio Desktop 1.1.463 (Integrated Development for RStudio, Inc., Boston, USA, https://www.rstudio.com)

MALDI-TOF MS protein identification

MS-preparative gels were manually cut to excise differential electrophoretic spots, which were destained first in a solution 30 mM potassium ferricyanure and 100 mM sodium tiosulphate anhydrous, later in 200 mM ammonium bicarbonate and dehydrated in 100% acetonitrile (ACN). The protein spots were then rehydrated and digested overnight at 37 °C in trypsin solution. Digested protein solution was placed on MALDI target, dried, covered with matrix solution of 5mg/ml α-cyano-4-hydroxycinnamic acid (CHCA) in 50% v/v ACN and 5% v/v trifluoroacetic acid (TFA) and dried again. MS analysis was then performed with UltrafleXtreme™ MALDI-ToF/ToF instrument equipped with a 200 Hz smartbeam™ I laser in the positive reflector mode according to defined parameters: 80 ns of delay; ion source 1: 25 kV; ion source 2: 21.75 kV; lens voltage: 9.50 kV; reflector voltage: 26.30 kV; and reflector 2 voltage: 14.00 kV. The applied laser wavelength and frequency were 353 nm and 100 Hz, respectively, and the percentage was set to 46%. Final mass spectra were produced by averaging 1500 laser shots targeting five different positions within the spot. Spectra were acquired automatically and the Flex Analysis software version 3.0 (Bruker) was used for their analysis and for assigning the peaks. The applied software generated a list of peaks up to 200, using a signal-to-noise ratio of 3 as threshold for peak acceptance. Recorded spectra were calibrated using peptides arising from trypsin auto-proteolysis as internal standard. The resulting mass lists were filtered for contaminant removal: mass matrix-related ions, trypsin auto-lysis and keratin peaks. Peptide Mass Fingerprinting (PMF) search was performed using MASCOT (Matrix Science Ltd., London, UK, http://www.matrixscience.com) setting up the following search parameters: *Mus musculus* as taxonomy, Swiss-Prot/TrEMBL as databases, 100 ppm as mass tolerance, one admissible missed cleavage site, carbamidomethylation (iodoacetamide alkylation) of cysteine as fixed modification and oxidation of methionine as a variable modification.

Network and pathway analysis

Network and pathway analysis were performed submitting the accession number of the identified proteins to the MetaCore 6.8 network building tool (Clarivate Analytics, Philadelphia, Pennsylvania, USA, http://portal.genego.com). This software shows a network of protein interactions, graphically represented by “nodes” (proteins) and “arches” (interactions), by the “shortest-path” algorithm. This algorithm builds a hypothetical network connecting two experimental proteins directly or indirectly using one MetaCore database protein, based on information from scientific literature data and annotated databases of protein interactions and metabolic reactions. Moreover, the software can

establish a hierarchical list of pathway maps, prioritized according to their statistical significance ($p \leq 0.001$), and each of these is equivalent to a canonical map that has multiple sequential steps of interactions, defining a well-established signalling mechanism. In particular, each step is also well-defined, experimentally validated and accepted in the research field.

Real-Time PCR and immunoblotting

Validations were carried out by the research group directed by Prof. Cristina Ulivieri of the Molecular Immunology Lab directed by Prof. Cosima Baldari of the Life Science Department at the University of Siena. In detail, total RNA was extracted using RNeasy Plus Mini Kit (Quiagen) according to manufacturer's instructions. RNA purity and concentration were confirmed using Nanodrop ND 1000 Spectrophotometer (Thermo Scientific). First-strand cDNAs were generated using the reverse transcription polymerase chain reaction (RT-PCR) carried out using iScript ™ cDNA Synthesis Kit (Bio-Rad). Real-time quantitative PCR (RT-qPCR) was performed using SsoFast™ EvaGreen supermix kit (Bio-Rad). The cDNA fragments corresponding to GLNA, S100A6 and PRDX6 were amplified using specific pairs of primers. All samples were run in duplicate on 96-well optical PCR plates (Sarstedt AG). Gene expression data were presented relative to the expression of housekeeping gene GADPH.

Protein extraction was obtained by astrocytes lysis in 1% (v/v) Triton X-100 in 20 mM Tris-HCl (pH 8), 150 mM NaCl in the presence of Protease Inhibitor Cocktail set III (Cal BioChem) and 0.2 mg Na orthovanadate/ml. Extractions were resuspended in 10 µl of loading sample buffer and loaded on a 10% SDS-PAGE, then transferred to nitrocellulose membrane (GE Healthcare Life Sciences) for immunoblotting analysis. Immunoblots of Rai WT and KO NS were carried out using anti-GLNA and anti-S100A6 mouse IgG antibodies (Santa Cruz Biotechnologies, USA). Nitrocellulose membranes were washed three times, 10 minutes each, with a blocking solution of 3% powder milk (p/v) and Triton X100 0.1% (p/v) in Phosphate Buffer Solution (PBS) pH 7.4. Then, they were incubated with primary antibodies, following manufacturer's instructions. At this step, membranes were washed again three times, 10 minutes each, with the same previous blocking solution, followed by the incubation with secondary goat anti-mouse (Bio-Rad Laboratories) at 1:3000 in blocking solution for 2 hours. After incubation, membranes were washed three times per 10 minutes each with blocking solution, then washed in Triton X100 0.5% (p/v) in PBS pH 7.4 for 30 minutes. Eventually, they were washed twice (30 minutes each) with Tris H-Cl 0.05 M pH 6.8 and then detection was

carried out using Amersham ECL Western Blotting Detection Reagent (Cytiva, formerly GE Healthcare Life Sciences).

RESULTS

EVs proteomic analysis

Proteomic content of EVs released from WT and KO astrocytes not stimulated (NS) and stimulated with IL-17, was investigated by 2DE. Image analysis of WT NS vs KO NS showed a mean of 694 spots per gel, extrapolating 14 differentially abundant spots validated by statistics, 8 identified by MS (Table 1; Figure 1A). On the other hand, proteomic analysis of EVs from WT IL-17 vs KO IL-17 showed a mean of 660 spots in each gel and by image and statistical analyses we extrapolated 7 differentially abundant spots (DASs), of which 6 identified (Table 1; Figure 1B). Table 1 reports the spot number, corresponding to the number present in Figure 1A, B, the protein name, the UniProt abbreviation, the accession number and the theoretical pI and MW of the identified proteins. Moreover, MS results (such as score, number of matched peptides, sequence coverage) and statistical values (Kruskal Wallis and Dunn's Test) were reported. As can be observed in Figure 1A and Table 1, all the identified proteins in WT NS vs KO NS were rab3 GTPase-activating protein non-catalytic subunit (RBGPR), protein disulfide-isomerase A3 (PDIA3), thiosulfate sulfurtransferase/rhodanese-like domain-containing protein 2 (TSTD2), alpha-enolase (ENOA), glutamine synthetase (GLNA), kelch-like protein 9 (KLHL9), all lowly abundant in KO NS condition. Interestingly, protein S10A6 was present only in WT NS. Microtubule-associated protein 4 (MAP4) is a common differential abundant protein (DAP) between the two analyses and showed an opposite behavior as it was low abundant in KO NS and highly abundant in KO IL-17. Furthermore, identified proteins in WT IL-17 vs KO IL-17, all highly abundant in KO IL-17, were actin cytoplasmic 1 (ACTB), peroxiredoxin-6 (PRDX6), heat shock factor-binding protein 1 (HSBP1) and actin aortic smooth muscle (ACTA). In addition, endoplasmic reticulum resident protein 44 (ERP44) was detected as qualitative difference in KO IL-17. Figure 2A and B reports the heatmap analysis of significant differential spots in WT NS vs KO NS and WT IL-17 vs KO IL-17, respectively. While in NS condition we observed a predominance in low abundant proteins in KO with respect to WT, in IL-17 stimulated condition we observed an opposite behavior.

PCA analysis showed a characteristic sample distribution relies on the differential protein pattern for the analyzed conditions. In particular, in Figure 3A we observed that WT NS samples were well distinct from KO NS relies on PC1. On the other hand, in Figure 3B also samples from WT IL-17 were separated from KO IL-17 with respect to the PC1.

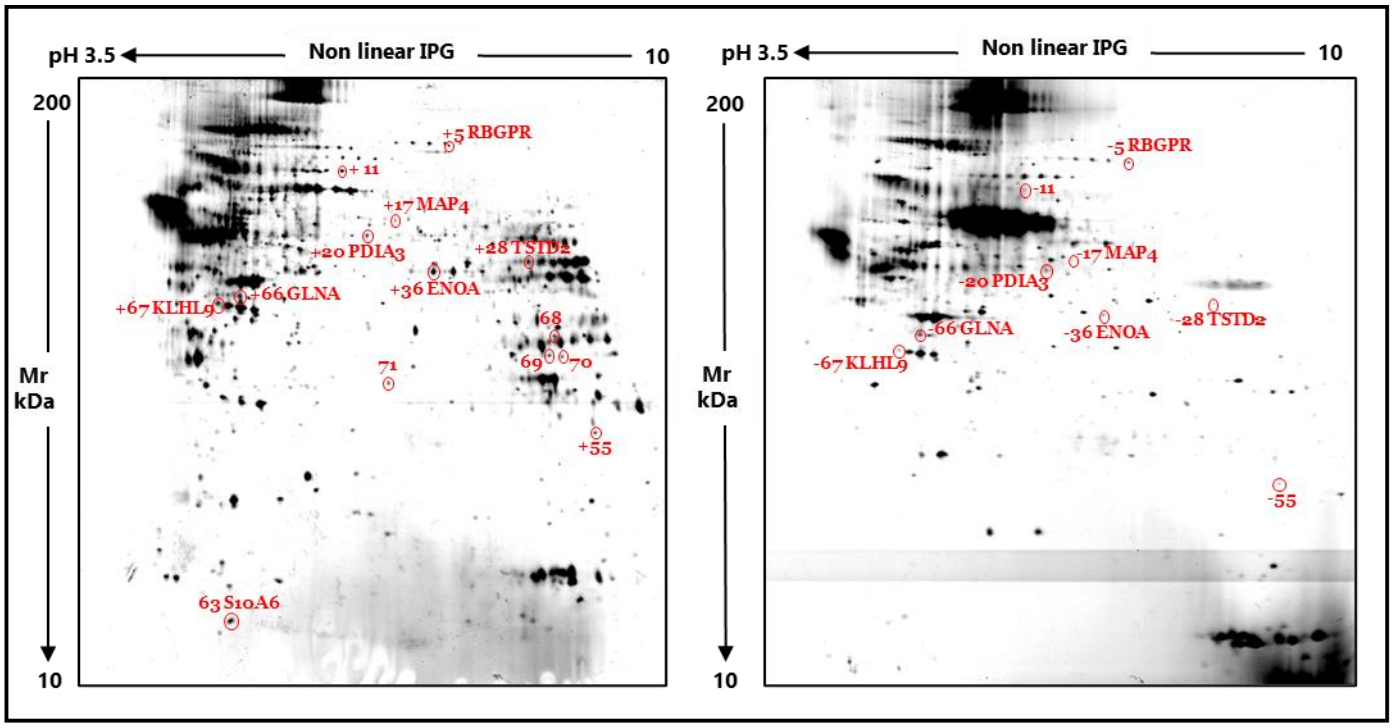

A. Rai WT vs Rai KO NS EVs

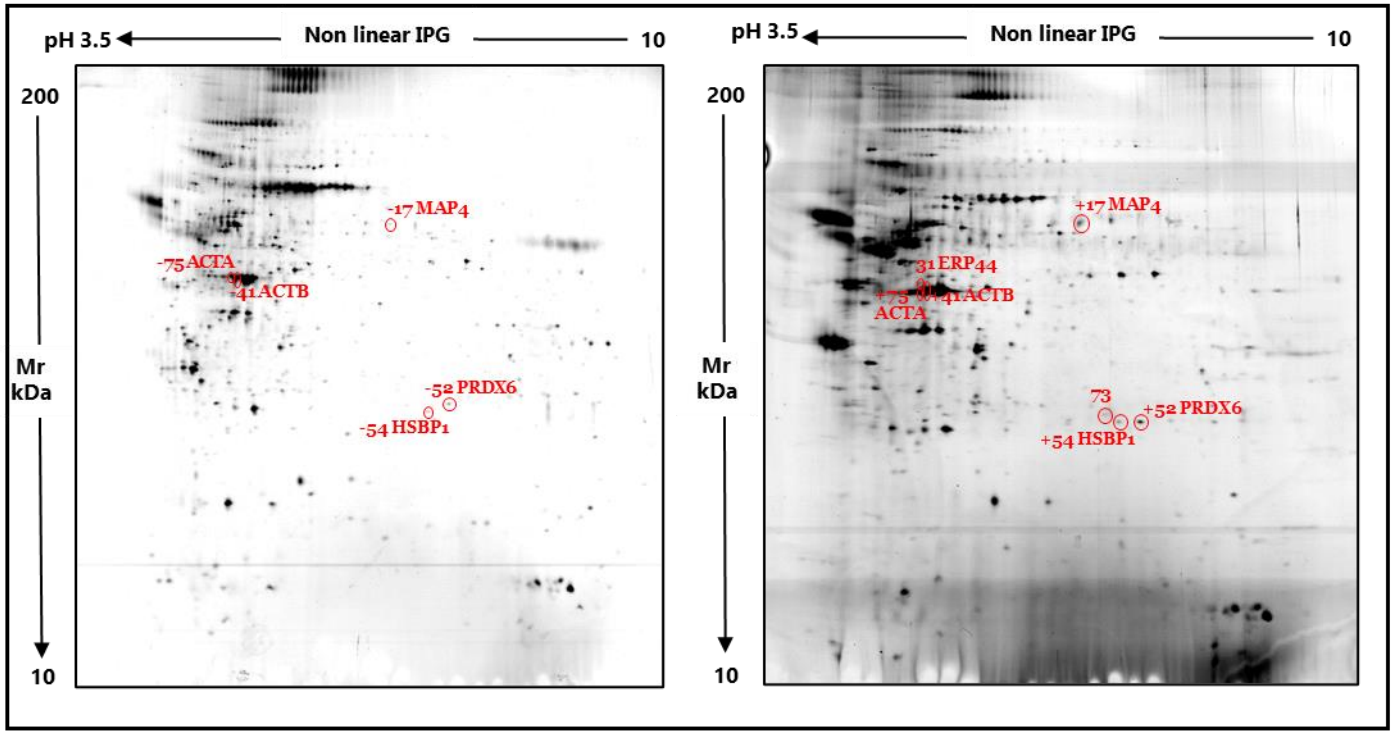

B. Rai WT vs Rai KO IL-17 EVs

Figure 1. Two-dimensional electropherograms of astrocytes' EVs

Two-dimensional gels show patterns of proteins ranging from 200 to 10 kDa in molecular weight and from 3.5 to 10 pH in isoelectric point. Red circles highlight DAS in the considered conditions

Spot Number	Protein name	Uniprot Abbreviation	Acession Number	Theoretical pI - MW (kDa)	MASCOT search results			NS			IL17		
					Score	No. matched peptides	Seq. Coverage	Kruskal Wallis	Rai WT - Rai KO	Rai KO - Rai WT	Kruskal Wallis	Rai WT - Rai KO	Rai KO - Rai WT
5	**Rab3 GTPase-activating protein non-catalytic subunit**	**RBGPR**	Q8BMG7	5.84 - 154035	86	11/18	8%	**0,02**	**2,73**	0,37	0,29	3,57	0,28
17	**Microtubule-associated protein 4**	**MAP4**	P27546	4.90 - 117927	78	6/6	7%	**0,04**	**6,99**	0,14	**0,02**	0,18	**5,54**
20	**Protein disulfide-isomerase A3**	**PDIA3**	P27773	5.88 - 57099	268	23/31	38%	**0,04**	**3,4**	0,29	0,61	1,64	0,61
28	**Thiosulfate sulfurtransferase/rhodanese - like domain-containing protein 2**	**TSTD2**	Q3U269	7.10 - 56833	78	7/9	11%	**0,01**	**34,79**	0,03	0	0	0
31	**Endoplasmic reticulum resident protein 44**	**ERP44**	Q9D1Q6	5.09 - 47222	143	11/18	30%	0,12	2,01	0,5	**5E-05**	0	**0.06 (%V mean)**
36	**Alpha-enolase**	**ENOA**	P17182	6.37 - 47453	215	14/16	36%	**0,03**	**13,62**	0,07	0,2	0	0.1 (%V mean)
41	**Actin, cytoplasmic 1**	**ACTB**	P60710	5.29 - 42052	122	9/14	26%	0,56	0,66	1,52	**0,002**	0,44	**2,3**
52	**Peroxiredoxin-6**	**PRDX6**	O08709	5.71 - 24969	195	10/10	44%	0,36	0,37	2,68	**0,03**	0,5	**2**
54	**Heat shock factor-binding protein 1**	**HSBP1**	Q9CQZ1	6.12 - 23057	100	6/9	33%	0,76	1,21	0,83	**0,01**	0,37	**2,73**
63	**Protein S100-A6**	**S10A6**	P14069	5.30 - 10101	89	4/4	30%	**0,02**	**0.09 (%V mean)**	0	0,14	0.08 (%V mean)	0
66	**Glutamine synthetase**	**GLNA**	P15105	6.64 - 42834	85	7/14	13%	**0,01**	**2**	0,5	0,21	2,46	0,41
67	**Kelch-like protein 9**	**KLHL9**	Q6ZPT1	6.00 - 70210	79	7/11	8%	**0,002**	**4,36**	0,23	0,79	1,22	0,83
75	**Actin, aortic smooth muscle**	**ACTA**	P62737	5.23 - 42381	214	14/17	37%	0,147845	0	0.44 (%V mean)	**0,03**	0,42	**2,38**

Table 1. MALDI TOF identification of differentially abundant spots of EVs Rai WT vs Rai KO NS and IL-17

Table reports spot number, protein name, UniProt abbreviation, UniProt Accession number, Thoretical isoelectric point and molecular weight (kDa), Mascot search results including score, number of matched peptides and sequence coverage, p-value , Kruskal Wallis) and fold-change in both NS and IL-17 comparisons.

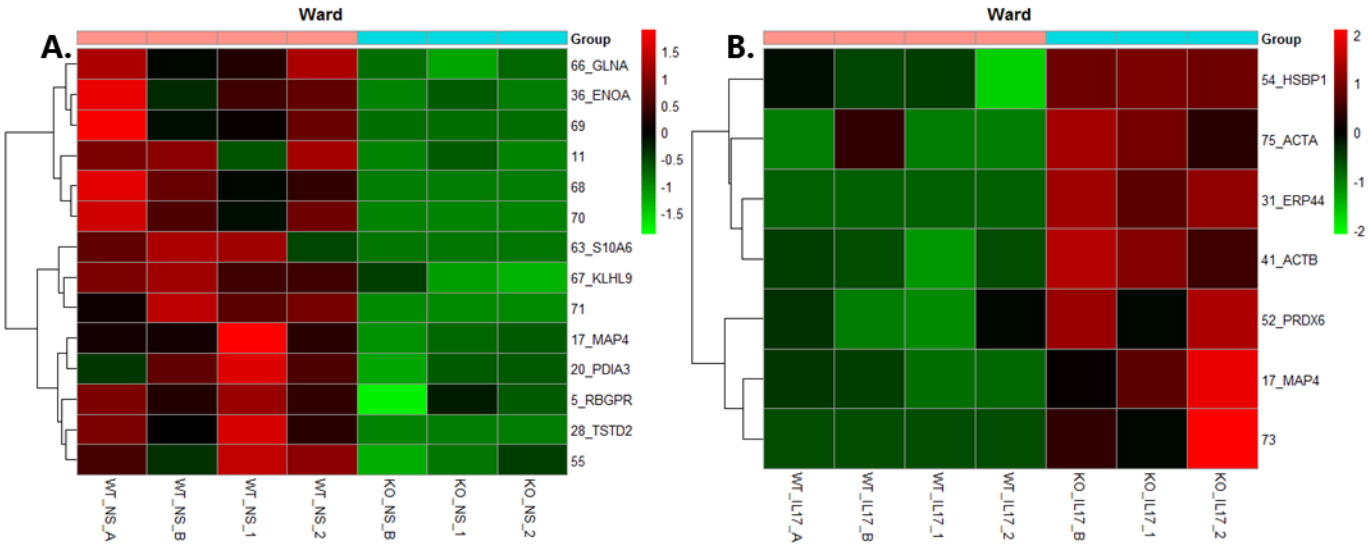

Figure 2. EVs cluster analysis

Heatmap of **A)** Rai WT NS vs Rai KO NS and **B.** Rai WT IL-17 vs Rai KO IL-17

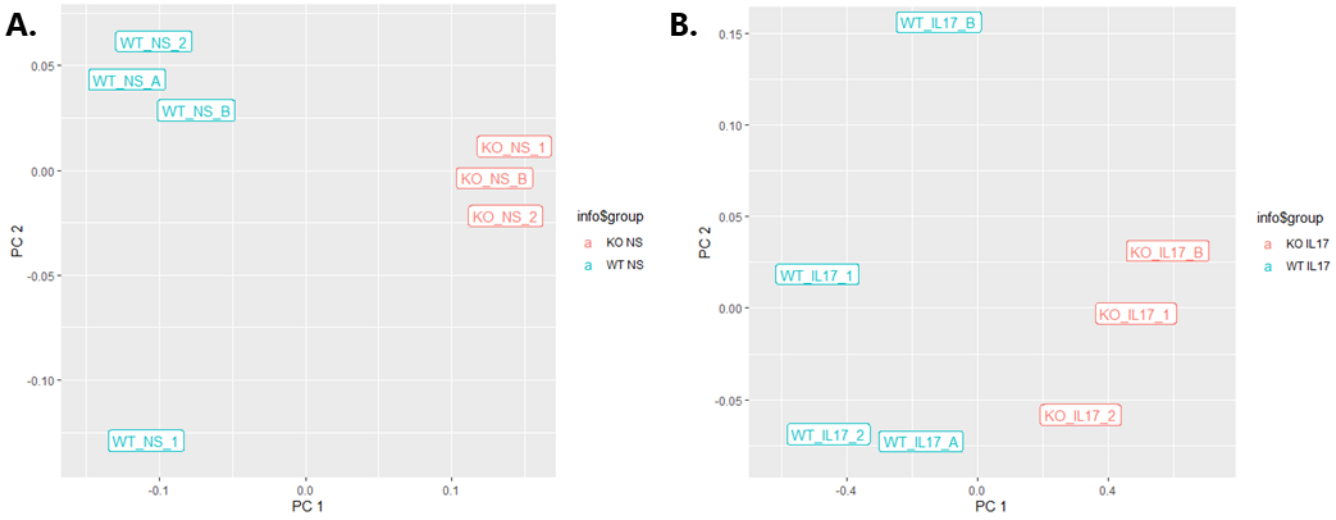

Figure 3. EVs Principal Component Analysis

PCA of **A)** Rai WT NS vs Rai KO NS and **B)** Rai WT IL-17 vs Rai KO IL-17

EVs-releasing astrocytes proteomic analysis

Simultaneously, a 2DE analysis of WT and KO EVs-releasing astrocytes, not stimulated and stimulated with IL-17 was performed. Image analysis of WT and KO not stimulated astrocytes resulted a mean of 2914 spots per gel, evidencing 22 DASs of statistic relevance, of which 8 were identified by MS (Table 2; Figure 4A). Although the investigation of IL-17 stimulated WT and KO astrocytes is still in progress, its image analysis resulted a mean of 2252 spots per gel, indicating 5 statistically significant differential spots, of which 1 was identified by MS so far (Table 2; Figure 4B). Table 2 follows the same structure of the previous table listing all differential spots values and MS identification data, referring directly to the corresponding number in Figure 2A, B. In detail, the identified proteins in the WT NS vs KO NS astrocytes were alpha-enolase (ENOA), astrocytic phosphoprotein PEA-15 (PEA15), NADH dehydrogenase (ubiquinone) iron-sulfur protein 2, mitochondrial (NDUS2), which resulted all lowly abundant in KO NS, then ubiquitin-conjugating enzyme E2 N (UBE2N), Trafficking protein particle complex subunit 6B (TPC6B) and Galectin-2 (LEG2), proteasome subunit beta type-2 (PSB2), and superoxide dismutase (Cu-Zn) (SODC), which instead resulted highly abundant in KO NS. Accordingly, the heatmap in Figure 5 displays this remarkable homogeneous distribution of up- and down-regulated proteins between the wild-type and the knock-out conditions. Furthermore, PCA of WT NS vs KO NS astrocytes in Figure 6 shows that each condition presents a distinctive profile as WT and KO samples clearly separate with respect to the PC1.

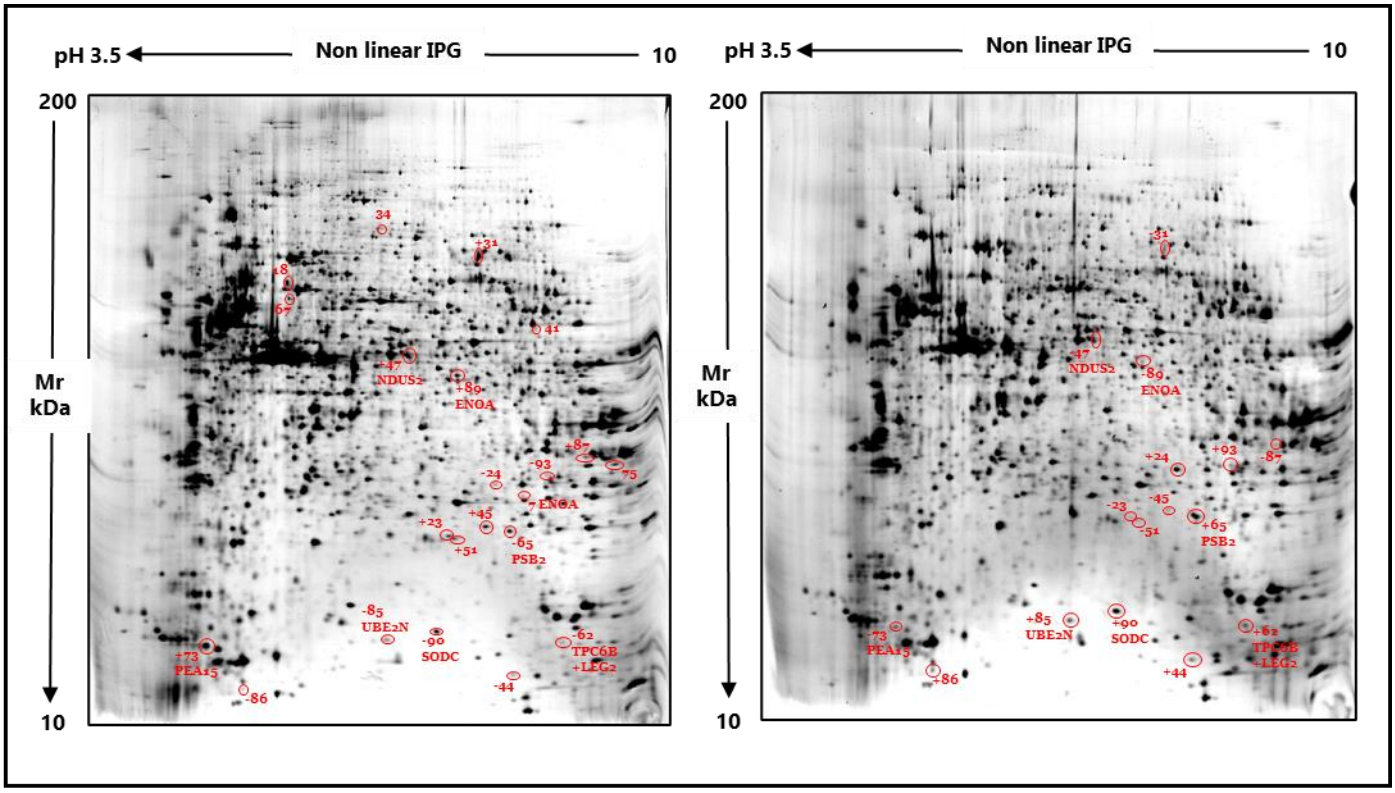

A. Rai WT vs Rai KO NS astrocytes

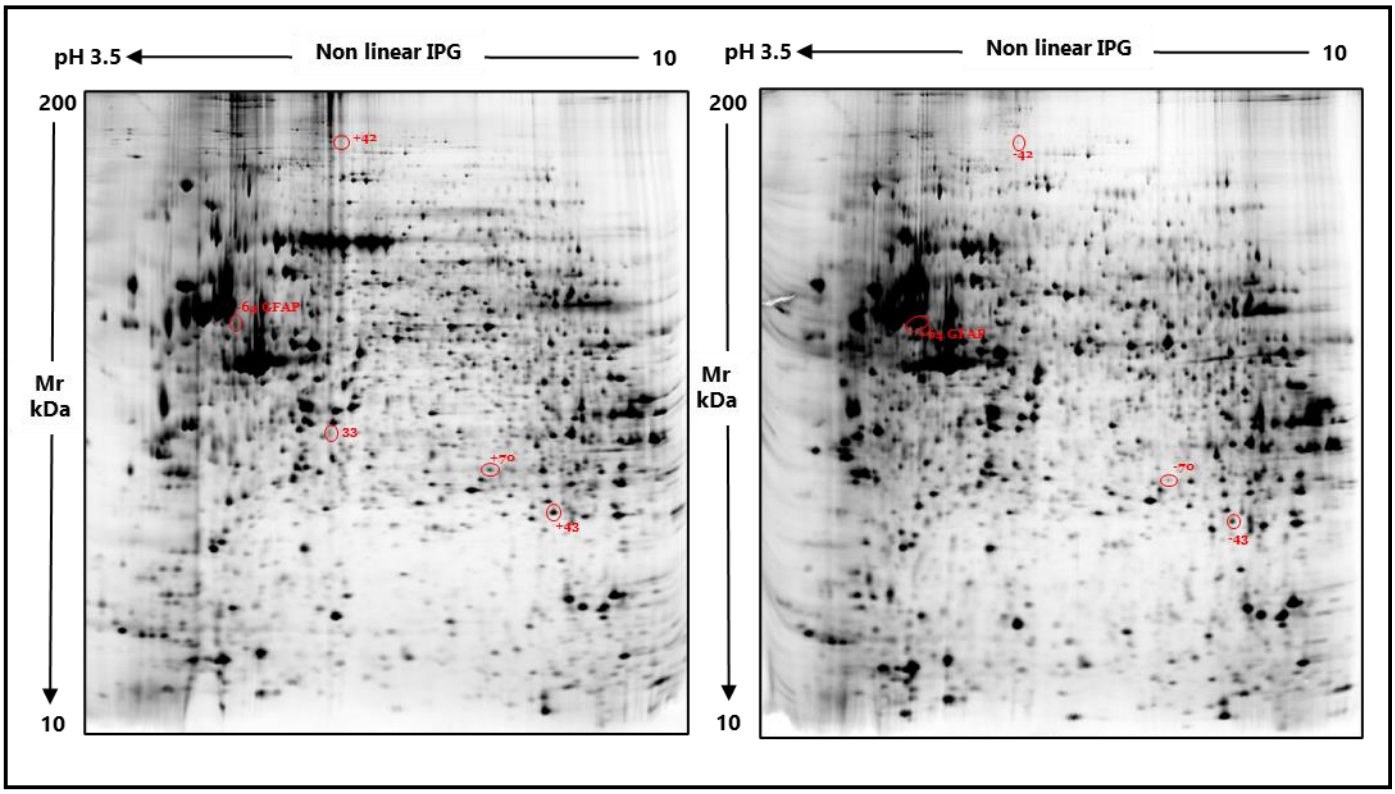

B. Rai WT vs Rai KO IL-17 astrocytes

Figure 4. Two-dimensional electropherograms of astrocytes

Two-dimensional gels show patterns of proteins ranging from 200 to 10 kDa in molecular weight and from 3.5 to 10 pH in isoelectric point

Spot Number	Protein name	Uniprot Abbreviation	Acession Number	Theoretical pI - MW (kDa)	MASCOT search results			NS			IL17		
					Score	No. matched peptides	Seq. Coverage	Kruskal Wallis	Rai WT - Rai KO	Rai KO - Rai WT	Kruskal Wallis	Rai WT - Rai KO	Rai KO - Rai WT
7	Alpha-enolase	ENOA	P17182	6,37 - 47453	31	13	27	**3,71E-03**	**0.01 (% V mean)**	0	6,25E-01	0	0
47	NADH dehydrogenase [ubiquinone] iron-sulfur protein 2, mitochondrial	NDUS2	Q91WD5	6,52 - 52991	93	35	59	**4,29E-02**	**2,60**	0,38	3,76E-01	0,90	1,11
62	Trafficking protein particle complex subunit 6B + Galectin-2	TPC6B + LEG2	Q9D289 Q9CQW5	8,88 - 18152 7,01 - 14984	28 30	6 4	44 41	**4,36E-02**	0,46	**2,19**	9,97E-02	0,56	1,77
64	Glial fibrillary acidic protein	GFAP	P03995	5,27 - 49927	68	27	53	7,02E-02	0,71	1,40	**2,14E-02**	0,43	**2,32**
65	Proteasome subunit beta type-2	PSB2	Q9R1P3	6,52 23063	92	22	55	**5,75E-03**	0,38	**2,64**	2,07E-01	0,66	1,53
73	Astrocytic phosphoprotein PEA-15	PEA15	Q62048	4,94 - 15102	50	8	59	**4,44E-02**	**3,25**	0,31	1,16E-01	2,50	0,40
85	Ubiquitin-conjugating enzyme E2 N	UBE2N	P61089	6,13 - 17184	75	13	65	**3,50E-02**	0,41	**2,41**	1,35E-01	0,73	1,37
89	Alpha-enolase	ENOA	P17182	6,37 - 47453	74	27	55	**3,50E-02**	**3,72**	0,27	4,09E-01	1,19	0,84
90	Superoxide dismutase [Cu-Zn]	SODC	P08228	6,02 - 16104	85	11	49	**4,36E-02**	0,44	**2,26**	2,45E-01	0,87	1,15

Table 2. MALDI TOF identification of differentially abundant spots of astrocytes Rai WT vs Rai KO NS and IL-17

Table reports spot number, protein name, UniProt abbreviation, UniProt Accession number, Theoretical of isoelectric point and molecular weight (kDa), Mascot search results including score, number of matched peptides and sequence coverage, p-value (Dunn's test) and fold-change in both NS and IL-17 comparisons.

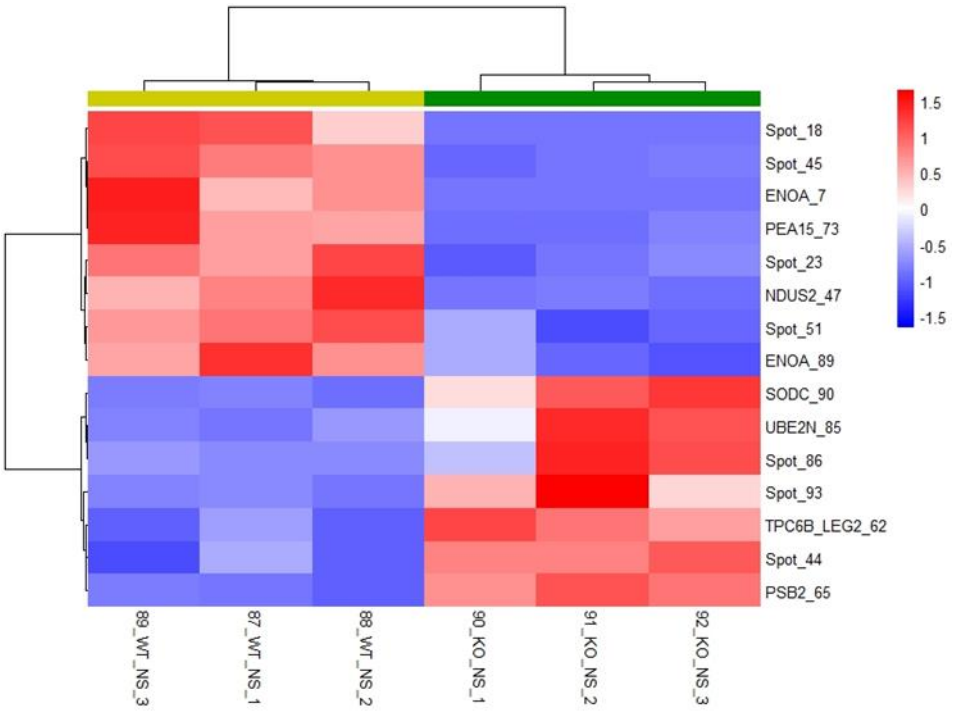

Figure 5. Astrocytes cluster analysis

Heatmap of Rai WT NS vs Rai KO NS astrocytes

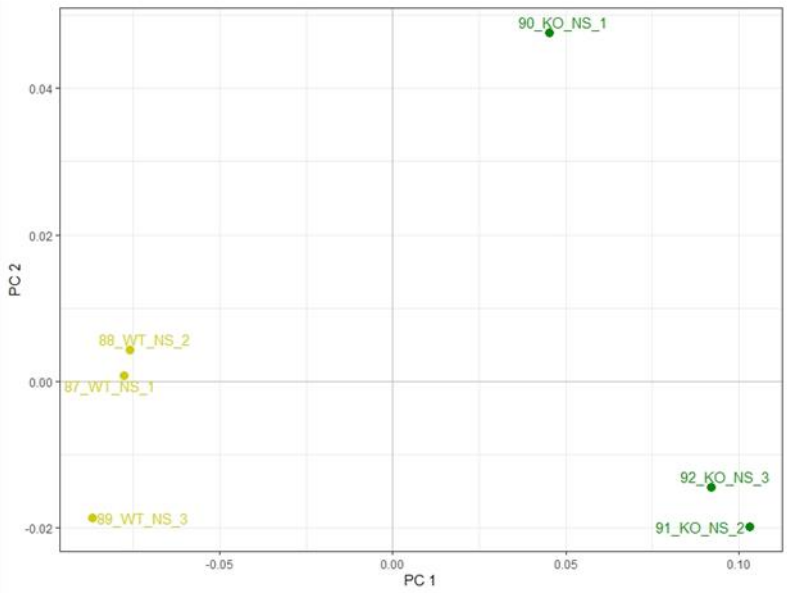

Figure 6. Astrocytes Principal Component Analysis

PCA of Rai WT NS vs Rai KO NS astrocytes

EVs enrichment analysis

Enrichment analysis performed by MetaCore software shed light on protein functions and on the potential involvement of the identified proteins in specific molecular pathways. As it is possible to observe in Figure 7, 8, 9, Table 3 and 4, we reported the protein networks and the most significant pathway maps obtained from the DAPs found in the WT vs KO NS and IL-17 EVs comparisons, as well as the WT vs KO NS astrocytes analysis, respectively. As protein Rai plays a central role in our study, we decided to perform a second network analysis for each of three comparisons, including protein Rai in order to visualize its potential influence on the DAPs. First, Figure 7A shows WT NS vs KO NS EVs DAPs network, conversely Figure 7B, WT NS vs KO NS EVs + Rai network. Both interaction maps share MAP4, GLNA, ENOA and PDIA3 as central hubs; in addition, RBGPR was central hub in the net in Figure 7A, while protein Rai (SHC3) was central hub in the network in Figure 7B. Light blue lines represents canonical paths starting from SHC3 and involving Ras cascade until the induction of ERK1/2. In turn, ERK1/2 was related with MAP4 (Figure 7B). All DAPs have a cytoplasmic localization and the MetaCore software suggests the involvement of particular transcriptional factors with nuclear localization, such as c-myc, ETS1, p53, AP-1 and RARalpha in both cases. In addition, the software indicates also the involvement of also HDAC1, which results correlated with ENOA and GLNA.

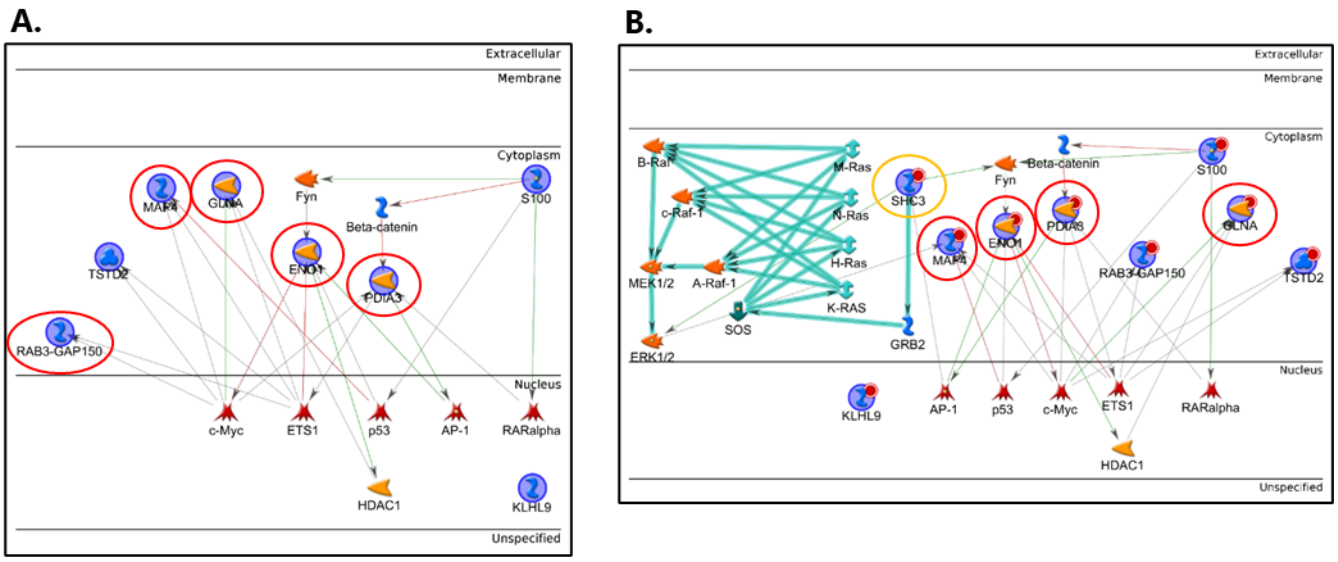

Figure 7. EVs DAPs networks

(A.) Network of EVs WT vs KO NS differentially abundant spots, **(B.)** also implemented with Rai (marked in yellow). Central hubs are marked in red.

Then, pathway analysis, reported in Table 3, was performed with and without Rai; however, no differences in molecular pathways were observed. DAPs result particularly involved in these pathways: p53 signaling in Prostate Cancer, beta-catenin-dependent transcription regulation in colorectal cancer, Nitrogen metabolism, WNT signaling in HCC, neurophysiological process GABAergic neurotransmission, HIF-1 in gastric cancer, immune response of antigen presentation by MHC class I classical pathway, role of thyroid hormone in the regulation of oligodendrocyte differentiation in multiple sclerosis, development regulation of cytoskeleton proteins in oligodendrocytes differentiation and myelination, signal transduction mTORC1 upstream signaling, glycolysis and gluconeogenesis and Histidine-glutamate-glutamine metabolism.

Enrichment by Pathway Maps					EVs - WT NS vs KO NS			
#	Maps	Total	min(pValue)	Min FDR	p-value	FDR	In Data	Network Objects from Active Data
1	p53 signaling in Prostate Cancer	33	1,378E-02	3,288E-02	1,651E-02	3,848E-02	1	MAP4
2	Beta-catenin-dependent transcription regulation in colorectal cancer	36	1,502E-02	3,288E-02	1,800E-02	3,848E-02	1	Calcyclin
3	Nitrogen metabolism	36	1,502E-02	3,288E-02	1,800E-02	3,848E-02	1	GLNA
4	Transcription_P53 signaling pathway	39	1,626E-02	3,288E-02	1,948E-02	3,848E-02	1	MAP4
5	WNT signaling in HCC	40	1,668E-02	3,288E-02	1,998E-02	3,848E-02	1	GLNA
6	Development_Role of Thyroid hormone in regulation of oligodendrocyte differentiation	48	1,999E-02	3,288E-02	2,394E-02	3,848E-02	1	GLNA
7	Neurophysiological process_GABAergic neurotransmission	51	2,122E-02	3,288E-02	2,542E-02	3,848E-02	1	GLNA
8	HIF-1 in gastric cancer	51	2,122E-02	3,288E-02	2,542E-02	3,848E-02	1	ENO1
9	Immune response_Antigen presentation by MHC class I, classical pathway	54	2,246E-02	3,288E-02	2,689E-02	3,848E-02	1	PDIA3
10	Role of Thyroid hormone in regulation of oligodendrocyte differentiation in multiple sclerosis	55	2,287E-02	3,288E-02	2,739E-02	3,848E-02	1	GLNA
11	Development_Regulation of cytoskeleton proteins in oligodendrocyte differentiation and myelination	58	2,411E-02	3,288E-02	2,886E-02	3,848E-02	1	MAP4
12	Signal transduction_mTORC1 upstream signaling	74	3,068E-02	3,835E-02	3,670E-02	4,517E-02	1	PDIA3
13	Glycolysis and gluconeogenesis	94	3,884E-02	3,924E-02	4,642E-02	4,691E-02	1	ENO1
14	Transcription_HIF-1 targets	95	3,924E-02	3,924E-02	4,691E-02	4,691E-02	1	ENO1
15	Histidine-glutamate-glutamine metabolism	95	3,924E-02	3,924E-02	4,691E-02	4,691E-02	1	GLNA

Table 3. EVs pathway analysis

Excel report of 10 most significant enriched pathway maps of EVs WT vs KO NS proteins: maps, p-value, FDR, number of proteins associated, network objects.

Since the IL-17 stimulation, in the second part of the EVs analysis, we wondered its potential influence on the DAPs, with and without Rai, as previously performed. To this purpose, we added IL-17 protein to both networks obtained from WT IL-17 vs KO IL-17 (Figure 8A) and WT IL-17 vs KO IL-17 + Rai (Figure 8B). Both networks highlight three common central hubs: IL-17, MAP4 and actin. In addition, MKL1 is central hub in WT IL-17 vs KO IL-17 while protein Rai (SHC3) is central hub in WT IL-17 vs KO IL-17 + Rai. MetaCore software also suggests the involvement of GATA-2 transcriptional factor. Similar to the previous comparison, most of the considered proteins have cytoplasmic localization.

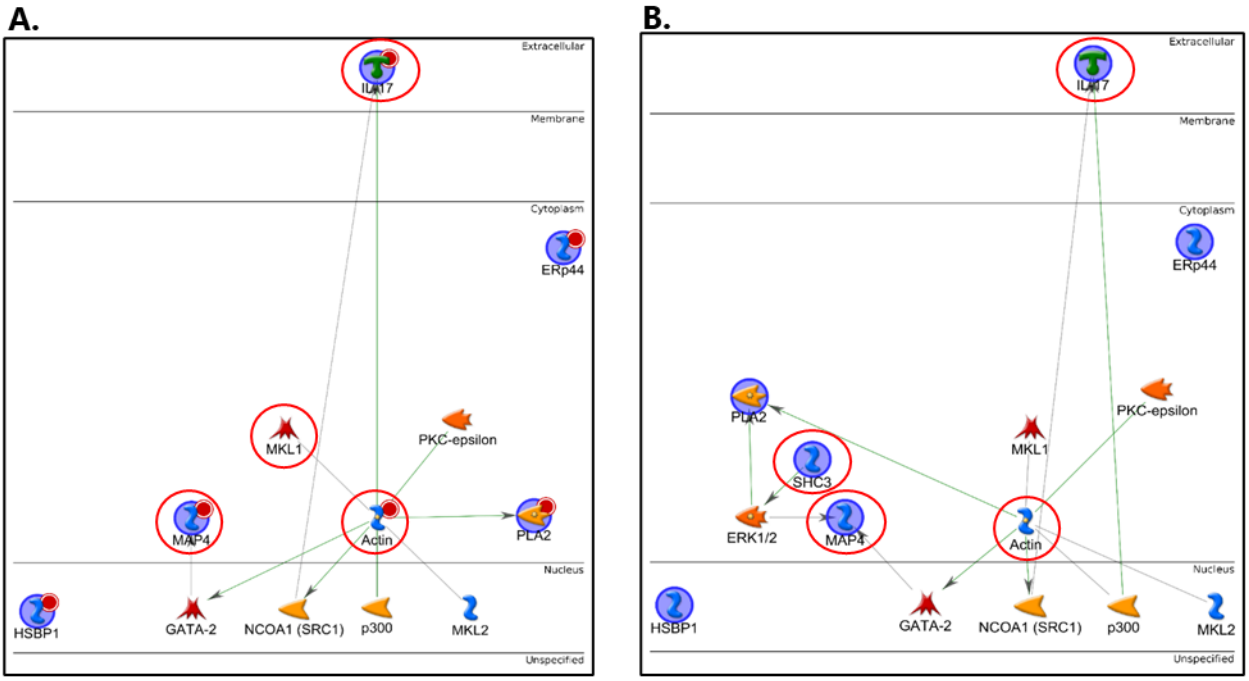

Figure 8. EVs IL-17 network analysis

(A.) Network of EVs WT vs KO IL-17 differentially abundant spots, **(B.)** also implemented with Rai (marked in yellow). Central hubs are marked in red.

Pathway Maps analysis, reported in Table 4, shows the involvement of the following pathways: possible regulation of HSF-1/ chaperone pathway in Huntington's disease, p53 signaling in prostate cancer, dysregulation of adiponectin secretion from adipocytes in obesity, type 2 diabetes and metabolic syndrome X, retinal ganglion cell damage in glaucoma, glucocorticoids-mediated inhibition of pro-constrictory and pro-inflammatory signaling in airway smooth muscle cells, regulation of cytoskeleton proteins in oligodendrocyte differentiation and myelination, plasmalogen biosynthesis, oxidative stress in adipocyte dysfunction in type 2 diabetes and metabolic syndrome X,

TNF-alpha and IL-1 beta-mediated regulation of contraction and secretion of inflammatory factors in normal and asthmatic airway smooth muscle and immune response by CD16 signaling in NK cells.

Enrichment by Pathway Maps					EVs - WT IL-17 vs KO IL-17			
#	Maps	Total	pValue	Min FDR	p-value	FDR	In Data	Network Objects from Active Data
1	Possible regulation of HSF-1/ chaperone pathway in Huntington's disease	21	7,033E-03	2,297E-02	7,033E-03	2,297E-02	1	PLA2
2	p53 signaling in Prostate Cancer	33	1,103E-02	2,297E-02	1,103E-02	2,297E-02	1	MAP4
3	Dysregulation of Adiponectin secretion from adipocytes in obesity, type 2 diabetes and metabolic syndrome X	38	1,270E-02	2,297E-02	1,270E-02	2,297E-02	1	ERp44
4	Transcription_P53 signaling pathway	39	1,303E-02	2,297E-02	1,303E-02	2,297E-02	1	MAP4
5	Retinal ganglion cell damage in glaucoma	45	1,502E-02	2,297E-02	1,502E-02	2,297E-02	1	NSGPeroxidase
6	Glucocorticoids-mediated inhibition of pro-constrictory and pro-inflammatory signaling in airway smooth muscle cells	49	1,635E-02	2,297E-02	1,635E-02	2,297E-02	1	PLA2
7	Development_Regulation of cytoskeleton proteins in oligodendrocyte differentiation and myelination	58	1,933E-02	2,297E-02	1,933E-02	2,297E-02	1	MAP4
8	Plasmalogen biosynthesis	64	2,132E-02	2,297E-02	2,132E-02	2,297E-02	1	PLA2
9	Oxidative stress in adipocyte dysfunction in type 2 diabetes and metabolic syndrome X	64	2,132E-02	2,297E-02	2,132E-02	2,297E-02	1	PLA2
10	TNF-alpha and IL-1 beta-mediated regulation of contraction and secretion of inflammatory factors in normal and asthmatic airway smooth muscle	65	2,165E-02	2,297E-02	2,165E-02	2,297E-02	1	PLA2
11	Immune response_CD16 signaling in NK cells	69	2,297E-02	2,297E-02	2,297E-02	2,297E-02	1	PLA2

Table 4. EVs IL-17 pathway analysis

Excel report of 10 most significant enriched pathway maps of EVs WT vs KO IL-17 proteins: maps, p-value, FDR, number of proteins associated, network objects.

EVs-releasing astrocytes enrichment analysis

Concurrently, we applied the same enrichment conditions previously set in the EVs analysis to the WT vs KO NS astrocytes investigation, thus Figure 9A and B reports protein networks without and with Rai, respectively. As previous networks, canonical pathways are highlighted in blue. Both networks in Figure 9A and B share the same central hubs which are ENO (ENOA), SOD1 (SODC), E2N(UBC13) (UBE2N), Proteasome 20s core (PSB2) and PEA15. In particular, in both cases all DAPs have a cytoplasmic localization except for NDUS2 (NDUFS2) which locates on the membrane; furthermore, network analysis suggests a wider interaction network including both nuclear-localized factors such as, NOTCH1, ESR, PR, p53, c-Myc, GLI-3, YY1, GLI-3R and HIF-1, and membrane-located ones, such as ErbB2 and EGFR. In addition, Figure 9B shows the interaction of SHC3 (Rai) with Fyn and then suggests an indirect interaction with ENO.

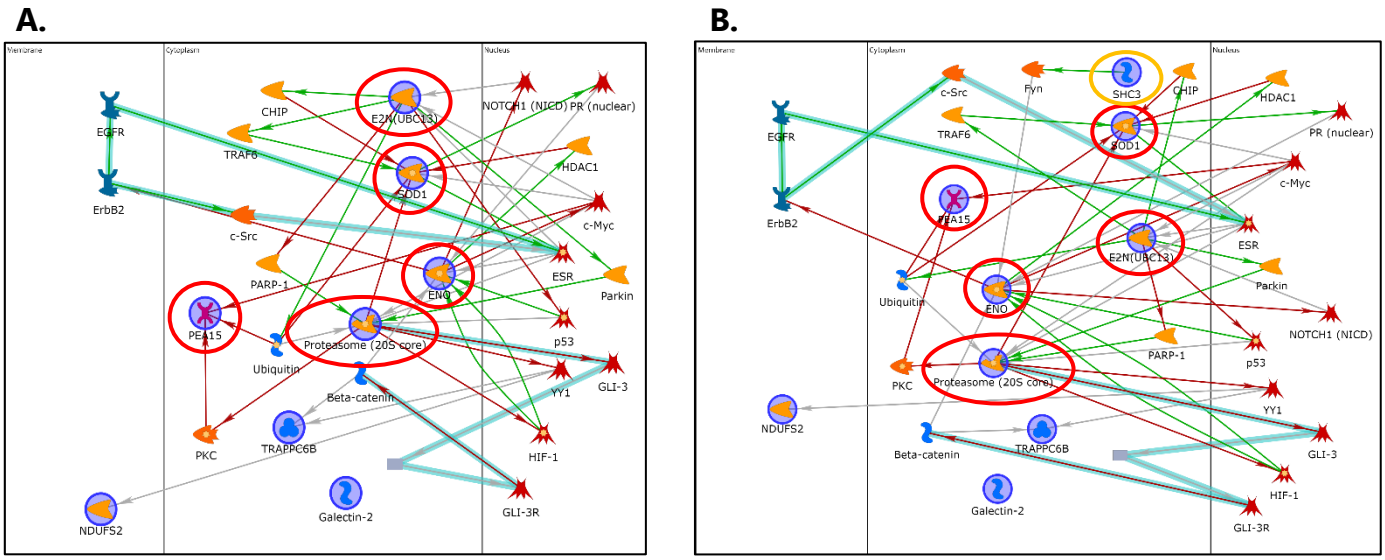

Figure 9. Astrocytes NS network analysis

(A.) Network of astrocytes WT vs KO NS differentially abundant spots, **(B.)** also implemented with Rai (marked in yellow). Central hubs are marked in red.

Thus, pathway analysis was carried out still with and without Rai, even though no differences in pathways came out. In detail, Figure 9C lists the 10 most significant pathways such as TGF-beta induction of EMT via ROS, putative ubiquitin pathway, CREB1-dependent transcription deregulation in Huntington's disease, IL-17-induced CIKS-dependent NF-KB and MAPK signaling, IL-1 beta-dependent CFTR expression, BAFF-induced non-canonical NF-KB signaling, ROS-mediated activation of MAPK via inhibition of phosphatases, Erk interactions, lipoxins and resolvin E1 inhibitory action on neutrophil functions.

Enrichment by Pathway Maps					ASTRO - WT NS vs KO NS			
#	Maps	Total	pValue	Min FDR	p-value	FDR	In Data	Network Objects from Active Data
1	Development_TGF-beta-induction of EMT via ROS	20	9.933E-03	3.854E-02	9.933E-03	3.854E-02	1	SOD1
2	Proteolysis_Putative ubiquitin pathway	23	1.142E-02	3.854E-02	1.142E-02	3.854E-02	1	E2N(UBC13)
3	CREB1-dependent transcription deregulation in Huntington's Disease	26	1.290E-02	3.854E-02	1.290E-02	3.854E-02	1	SOD1
4	Apoptosis and survival_IL-17-induced CIKS-dependent NF-kB signaling and mRNA stabilization	28	1.388E-02	3.854E-02	1.388E-02	3.854E-02	1	E2N(UBC13)
5	IL-1 beta-dependent CFTR expression	31	1.536E-02	3.854E-02	1.536E-02	3.854E-02	1	E2N(UBC13)
6	Immune response_BAFF-induced non-canonical NF-kB signaling	32	1.585E-02	3.854E-02	1.585E-02	3.854E-02	1	E2N(UBC13)
7	Apoptosis and survival_IL-17-induced CIKS-dependent MAPK signaling pathways	32	1.585E-02	3.854E-02	1.585E-02	3.854E-02	1	E2N(UBC13)
8	Oxidative stress_ROS-mediated activation of MAPK via inhibition of phosphatases	34	1.684E-02	3.854E-02	1.684E-02	3.854E-02	1	SOD1
9	Signal transduction_Erk Interactions: Inhibition of Erk	34	1.684E-02	3.854E-02	1.684E-02	3.854E-02	1	PEA15
10	Immune response_Lipoxins and Resolvin E1 inhibitory action on neutrophil functions	35	1.733E-02	3.854E-02	1.733E-02	3.854E-02	1	SOD1

Table 5. Astrocytes NS pathway analysis

Excel report of 10 most significant enriched pathway maps of astrocytes WT vs KO NS proteins: maps, p-value, FDR, number of proteins associated, network objects.

Not stimulated vesicular and cellular pathways' comparison

In order to obtain a broader perspective of the knock-out untreated condition, we performed also an additional pathway analysis, illustrated in Table 6, this time including all DAPs resulted from the WT vs KO NS EVs and cells. Specifically, the report highlights HIF-1 signaling and glycolytic and gluconeogenesis processes, both mediated by ENO1, and immune response-associated processes, mediated by PSMB2 and PDIA3.

Enrichment by Pathway Maps					ASTROCITI - WT NS vs KO NS				EVs - WT NS vs KO NS			
#	Maps	Total	min(pValue)	Min FDR	p-value	FDR	In Data	Network Objects from Active Data	p-value	FDR	In Data	Network Objects from Active Data
1	HIF-1 in gastric cancer	51	2.102E-02	3.311E-02	2.930E-02	4.462E-02	1	ENO1	2.102E-02	3.311E-02	1	ENO1
2	Immune response_Antigen presentation by MHC class I, classical pathway	54	2.224E-02	3.311E-02	3.100E-02	4.462E-02	1	PSMB2	2.224E-02	3.311E-02	1	PDIA3
3	Glycolysis and gluconeogenesis	94	3.846E-02	3.886E-02	5.343E-02	5.620E-02	1	ENO1	3.846E-02	3.886E-02	1	ENO1
4	Transcription_HIF-1 targets	95	3.886E-02	3.886E-02	5.399E-02	5.620E-02	1	ENO1	3.886E-02	3.886E-02	1	ENO1

Table 6. Pathway analysis Rai WT NS vs Rai KO NS astrocytes and EVs proteomic data

Excel report of most significant enriched pathway maps of WT vs KO NS astrocytes and EVs differential proteins: maps, p-value, FDR, number of proteins associated, network objects.

Protein validation by qRT-PCR and western blot

Furthermore, three vesicular DAPs were further validated at a cellular level by qRT-PCR and immunoblotting. Specifically, glutamine synthase (GLNA) and S100A6 were confirmed down-regulated in the KO NS condition both at a transcriptional level, shown in Figure 10A and C respectively, and at a protein level, shown in Figure 11A and B respectively. Moreover, PRDX6 was confirmed up-regulated transcriptionally in the IL-17-stimulated KO astrocytes, as shown in Figure 10B. Nonetheless, validation experiments are still in progress by the Molecular Immunology Lab, in order to progressively implement our data.

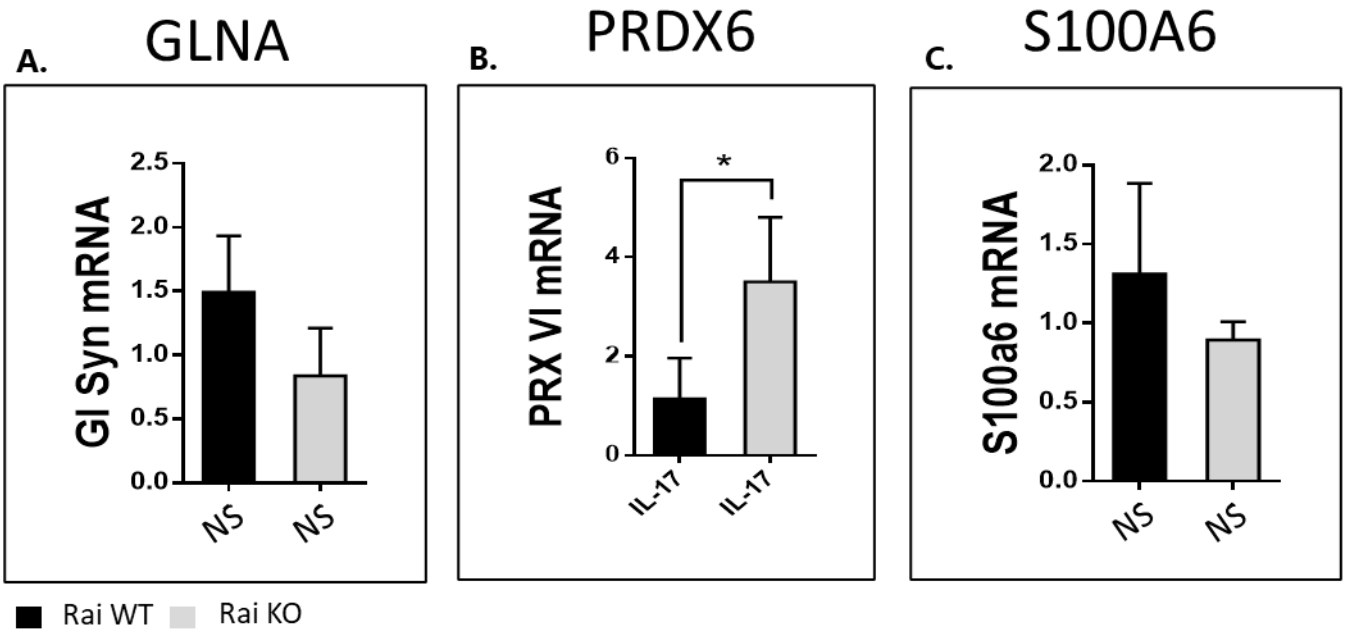

Figure 10. Quantitative Real-Time PCR (RT-qPCR) of three vesicular proteins at cellular level

qRT-PCR of (**A.**) GLNA transcripts in not stimulated astrocytes, (**B.**) PRDX6 transcripts in IL-17-stimulated astrocytes and (**C.**) S100A6 transcripts in not stimulated astrocytes. The levels of different transcripts were normalized to GAPDH, used as housekeeping gene. Data are presented as mean value ± SD.

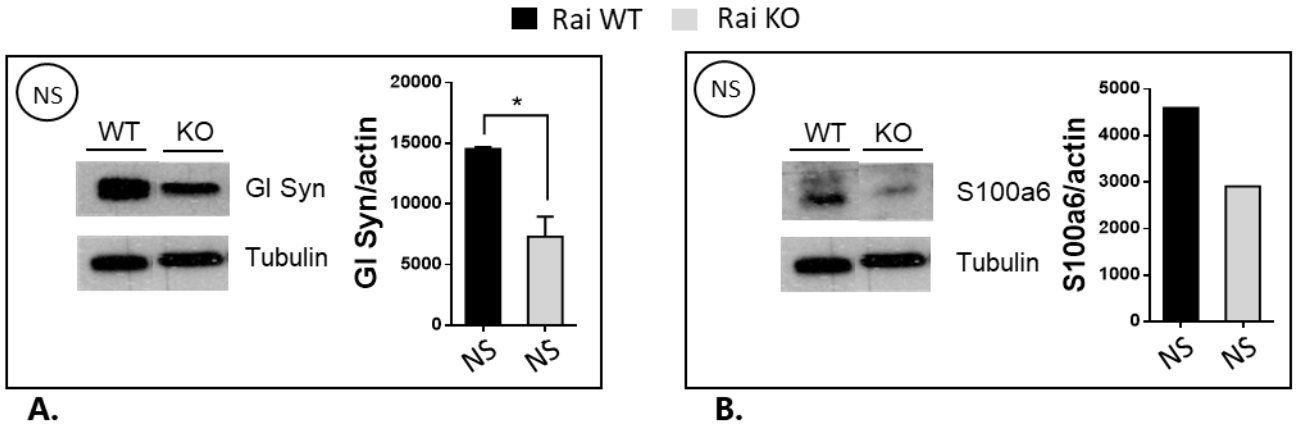

Figure 11. Immunoblotting analysis of GLNA and S100A6 in not stimulated astrocytes

Immunoblot analysis of glutamine synthase (Gl Syn) (**A.**) and of S100a6 (**B.**) in protein extractions of wild-type (WT) and knock-out (KO) not stimulated astrocytes. A control blot of the same filter is shown. Right, the quantification by densitometric analysis of the levels of GLNA (**A.**) and S100A6 (**B.**) relative to tubulin are shown with Rai WT astrocytes taken as 1. Data are presented as mean value ± SD. ANOVA * $p < 0.05$.

DISCUSSION

In the light of the compelling evidences about astrocytes ability to exhibit a potential neuroprotective phenotype via modulation of the local microenvironment, as well as the protective effect resulting from Rai deficiency (52,53), we aimed at evaluating differences in protein content of astrocytes and their released EVs $Rai^{+/+}$ and $Rai^{-/-}$ (WT NS vs KO NS), also after IL-17 stimulation (WT IL-17 vs KO IL-17), used to mimic autoreactive Th17 lymphocytes inflammatory input. To this purpose, our study included 2DE analysis and MS identification of statistically differential proteins, followed by network and pathway analysis. Thus, interesting data were further confirmed by qRT-PCR and immunoblotting.

Glutamate homeostasis, cellular adhesion remodeling, cellular migration, ECM remodeling as target pathways of DAPs in NS EVs

Our functional proteomic data revealed interesting results. First of all, the major part of the DASs found in WT NS vs KO NS EVs resulted less abundant in KO NS vesicles, suggesting that Rai absence may led to a lower release of these protein species into the vesicles. The protein network obtained from the specific DAPs showed that RBGPR, GLNA, ENOA, PDIA3, were central hubs. As protein Rai plays a central role in our study, we introduced this protein in a second network to visualize its potential influence on the DAPs. In the second net, also Rai (SHC3) was considered central hub, although no differences in pathway maps were reported.

One interesting protein is RBGPR, which is a regulatory subunit of a GTPase activating protein and it has specificity for Rab3 subfamily involved in exocytosis of neurotransmitters and hormones (57), suggesting that protein Rai could have effects on vesicles release and recycling.

Another protein is GLNA, whose main activity is to catalyze the ATP-dependent conversion of glutamate and ammonia to glutamine (58,59), as also suggested by Pathway Maps Analysis report "Histidine-glutamate-glutamine metabolism". Indeed, as widely demonstrated, glutamate metabolism is considerably involved in neurodegenerative diseases (60,61), for instance multiple sclerosis (62), as several studies report excessive exposure to glutamate to induce serious neuronal damage (58). However, GLNA has numerous functions, indeed, pathway maps analysis shows that it is also involved in other molecular paths such as nitrogen metabolism, WNT signaling, oligodendrocytes differentiation regulated by thyroid hormones proper of multiple sclerosis (63), and GABAergic neurotransmission. Interestingly, our analysis detected a low abundance of GLNA in KO

untreated EVs, which was also correlated to diminished transcripts inside astrocytes, confirmed by qRT-PCR.

In addition, it was reported that GLNA acetylation leads to the modulation of genes related to nitrogen metabolism(64), in accordance with our pathway analysis data. Indeed, our net suggests the interaction between GLNA and HDAC1 and in turn, HDAC1 interacts with ENOA regulating in part its acetylation. Highly acetylated ENOA is important in the maintenance of activated lymphocytes by increasing glycolysis-derived energy supply (65).

ENOA is another crucial protein found differentially abundant in KO NS EVs. Despite its main function as glycolytic enzyme, this protein mediates different activities according to its multiple cellular localizations. In particular, under inflammatory conditions it migrates from cytoplasm to cell surface where acts as a plasminogen receptor, promoting the extracellular matrix (ECM) degradation and consequent infiltration of inflammatory cells. In addition, surface enolase might activate proteolytic enzymes (MMPs) and may induce the production of proinflammatory cytokines (IL-6, IL-1β, TNF-β and TNF-α) and chemokines (MCP-1 and MIP-1α), as well as the production of reactive oxygen species (ROS) and nitric oxide (NO) (66). Interestingly, pathway analysis results indicate that ENOA is correlated to HIF-1α activity. This transcriptional factor was reported to suppress oligodendrocyte apoptosis mediated by hypoxic conditions and preventing demyelination. Additionally, it acts on genes encoding proteins that mediate hypoxic adaptive responses such as oxygen transport and cellular metabolism (67). Furthermore, *Mutze et al* reported that the expression of ENOA and PDIA3, another protein that we found diminished in KO EVs, decreases upon inhibition of Wnt/β-catenin signaling (68). In detail, PDIA3 is a multi-functional protein of the protein disulfide isomerases (PDIs) family, playing critical roles in modulating inflammation, apoptosis and oxidative stress in various pathologic conditions. Indeed, a recent study reported that PDIA3 KO mice mitigated neuroinflammation after traumatic brain injury in mice, as evidenced by the reduced expression of pro-inflammatory IL-6, TNF-α and IL-1β, while an enhanced expression of anti-inflammatory regulator IL-10. In addition, these PDIA3 KO-associated anti-inflammatory activities were correlated with a decrease in phosphorylated NF-κB/p65 and attenuated oxidative stress. This finding, associated with our PDIA3 down-regulation in KO EV, potentially supports the Rai KO astrocytes polarization towards a neuroprotective A2 phenotype (69). Remarkably, ENOA was also correlated to different suggested transcriptional factors such as AP-1, p53, c-myc, ETS and also to Fyn, a Src family kinases, reported to be fundamental for cell motility and cell migration through the extracellular matrix with simultaneous remodeling of intercellular adhesions (70). This process is primarily assisted by up-regulation of the extracellular matrix–degrading enzymes MMPs, in

particular MMP-2 and MMP-9, and disruption of cell-cell adhesion such as methylation of E-cadherin and degradation of β-catenin (70). Curiously, adding Rai to the WT vs KO NS EVs network, an interaction between Rai, Fyn and ENOA is reported, suggesting its potential involvement in altered adhesions and ECM remodeling processes.

Our network also reports that Fyn and β-catenin are connected with S100 family proteins. In particular, we found S10A6 only present in WT NS EVs, and qRT-PCR analysis also reported a down-regulation of S10A6 transcripts in KO NS astrocytes, suggesting that Rai could influence its production and release. In agreement with our MetaCore results, *Chen et al* reported that S10A6 alters the expression of epithelial-mesenchymal-transition (EMT)-related markers via β-catenin activation inducing EMT and promoting cell migration and invasion in a β-catenin-dependent manner (71). Since the multiple sclerosis microenvironment is known to present an excessive activation of the glutamatergic pathway playing an important part in the pathophysiology of multiple sclerosis (62), *Yamada et al* reported S10A6 as interesting protein because up-regulated in activated astrocytes in response to extracellular glutamate. In addition, an *in vitro* analysis by *Leclerc et al* reported that neuronal apoptosis might be mediated by extracellularly secreted S10A6 through its binding to the transmembrane receptor for advanced glycation end products (RAGE) via ROS dependent processes (72). As our enrichment analysis surprisingly showed, the differential identified proteins, acting through different molecular ways, lead to the same interesting molecular events. In particular, they contribute to glutamate homeostasis, cellular adhesion remodeling, cellular migration, ECM remodeling with strong involvement of WNT-β-catenin molecular pathway.

Plasmalogen biosynthesis, oxidative stress, regulation of cytoskeleton in oligodendrocyte differentiation and myelination, adiponectin secretion and EMT as target pathways of DAPs in IL-17 stimulated EVs

Secondly, astrocytes were treated with IL-17, in order to simulate the inflammatory stimulus released by autoreactive T-cells in EAE. Proteomic investigation of the harvested vesicles revealed appealing results. Enrichment analysis performed on DAPs showed a network with MAP4, Actin and a database in house protein MKL1, as central functional hubs. In addition, we applied the same experimental design performing an additional network analysis with Rai protein added, and interestingly Rai resulted central hub.

Although PRDX6 is not a central hub, pathway maps analysis showed some interesting molecular ways related to this protein, such as plasmalogen biosynthesis, oxidative stress in adipocyte

dysfunction in type 2 diabetes and metabolic syndrome X. In detail, PRDX6 is a Ca^{2+}-independent intracellular protein that could locate in the cytosol, lysosomes and lysosomal-related organelles and expresses glutathione peroxidase and lysophosphatidylcholine acyl transferase activities (73). Recently, it was demonstrated that PRDX6 explicates a novel phospholipase A2 activity (PLA2), through which it plays an important role for phospholipid metabolism (73) and, as suggested by MetaCore analysis, for plasmalogen biosynthesis, a particular class of ether-linked phospholipids. Curiously, myelin, which is a lipid-rich multi lamellar sheath featured by high energetic demands and low antioxidant capacity, is unusually rich in plasmalogens, as it's fundamental in protection against oxidative damage (74). In addition, the Rai introduction into the WT vs KO IL-17 net shows an indirect interaction of Rai (SHC3) with PLA2 through ERK1/2 molecular way. Indeed, *Liu et al* reported SHC3 to potentiate ERK activation (75), PLA2s activities positively regulated upstream by PI3-K, PKCα , and ERK1/2 signal, seems to be involved in stimulating endothelial cells migration, proliferation, including BBB modulation, as well as in angiogenesis (76–78).

Another interesting differential protein resulting from our IL-17 stimulated study is MAP4, which resulted the only factor to be dysregulated in both comparisons. In particular, it resulted abundant in KO NS with respect to WT NS and conversely, it resulted highly abundant in KO IL-17. These results marked as MAP4 could be modulated via Rai and IL-17 stimulus. By MetaCore results we can observe that MAP4 is connected with GATA-2 and ERK1/2 as well. Moreover, by pathway maps analysis it resulted involved in p53 signaling and regulation of cytoskeleton proteins in oligodendrocyte differentiation and myelination. Indeed, Jiang et al reported MAP4 as a regulator of invasion and migration in esophageal squamous cancer cell (79). Interestingly, MAP4 together with other MAPS is involved in the regulation of the microtubule network during the differentiation of myelin forming oligodendrocytes (80). Interestingly, it is connected to another central hub MKL1, the key transcriptional co-activator of many actin cytoskeletal genes, regulating genomic accessibility and cell fate reprogramming (81).

Our findings report also a particular chaperone protein ERp44, only present in KO IL-17 vesicles, which our enrichment analysis suggested to be involved in adiponectin folding, as also reported by *Hampe et al* (82). Adiponectin (ADN), because of its anti-inflammatory and immunosuppressive properties, could have protective roles in multiple sclerosis (83). Indeed, adiponectin is reported to inhibits pathogenic Th17 differentiation by suppressing Th17 cytokine IL-17, its associated cytokine IL-6 and the transcription factors of Th17 cells (83). For this reason, the presence of ERp44 only in Rai KO IL-17 vesicles could suggest a potential role in multiple sclerosis protection.

HSBP1 is another protein found increased in the Rai KO IL-17 EVs. This protein is ubiquitously expressed and it localizes in the nucleus where it negatively regulates Heat Shock Factor 1 (HSF-1) activity (84), a heat shock transcriptional factor responsible for activating the heat shock response (HSR), responsible for restoring correct protein folding (85). Indeed, its up-regulation could suggest a beneficial effect, supported also by literature. Specifically, *Eroglu et al* showed that HSBP1 KO mouse modulated genes related to WNT-β catenin signaling leading to EMT (86). Another recent study demonstrated that an astrocytic overexpression of HSPB1 is correlated to an attenuation of motor neurons toxicity in Amyotrophic Lateral Sclerosis (ALS), explicating neuroprotective properties (87).

Astrocytes proteomic analysis reveals antioxidant, proteasome system activity and wound healing response in Rai KO cells

Shedding light also on the cellular proteomic changes due to Rai deficiency, we extrapolated interesting preliminary data, as the IL-17 stimulated WT vs KO cells is still in progress.

Of high relevance, our data report an increased level of SOD1 in Rai KO NS astrocytes and pathway analysis, indeed, suggests the predominant involvement of oxidative stress-related molecular pathways. In detail, SOD1 is the cytoplasmic form of superoxide dismutase, which catalyzes the conversion of superoxide anion to oxygen and hydrogen peroxide, exhibiting antioxidant activities. Interestingly, other studies provided evidence of an increased expression of several antioxidant enzymes, such as superoxide dismutases and peroxiredoxins, in demyelinating multiple sclerotic lesions, especially by astrocytes (88). Accordingly, the observed increased release of antioxidant PRDX6 after IL-17 stimulation and the observed increased intracellular level of antioxidant SOD1 in the untreated state might suggest that Rai KO condition reflects into an enhanced antioxidant response indifferently on the stimulation, therefore it might exhibit a protective phenotype. Moreover, pathway analysis evidences also the SOD1 relation to TGF-beta induced EMT via ROS, highlighting the potential Rai KO astrocytic attempt at repair through the activation of fibrotic response (89,90). Indeed, astrocytes are generally known as responsible of glial scar formation following neuroinflammatory stimuli (45) and this scarring mechanisms are mainly characterized by ECM remodeling (91), Wnt/beta catenin-mediated fibrotic processes (92), TGF-beta-mediated fibrogenesis (93). Another differential protein is galectin-2 (LEG2), whose corresponding human protein might be considered as a functional homologue of galectin-1 (Gal-1) (94). As several studies have demonstrated a more efficient remyelination in presence of Gal-1, this could probably suggest similar

neuroprotective activities for galectin-2 as well (95). An additional differential protein is PEA-15, which is reported to induce ERK cascade inhibition and to establish indirect interactions with PARP1 (Poly (ADP-ribose) polymerase-1) and PKC, as shown in the analysis. Indeed, a recent study reports that PARP1, PEA15 and NF-kB activities might be distinctly regulated by PKC, AKT and ERK1/2, regulating specifically astroglial responses (astrogliosis) (96).

The resulting network suggests also the involvement of the ubiquitin proteasome system (UPS), whose dysfunction is reported to be crucial to all neurodegeneration processes. In detail, our increased proteins in Rai KO cells are two components of this machinery, i.e. proteasome 20S subunit B (PSB2) and ubiquitin conjugating enzyme E2 N (UBE2N) (97). In addition, UBE2N is reported, by pathways analysis, to be involved in the canonical and non-canonical NF-kB signaling pathways (98).

Additionally, as Rai has been also added to the WT vs KO NS astrocytes network in order to explore its potential interactions with the observed DAPs, MetaCore reported an interesting correlation between SHC3 (Rai), Fyn, ENOA and beta catenin, suggesting that Rai could have a potential influence on ENOA activity.

Comprehensive pathway analysis of NS EVs and astrocytes suggests a metabolic reprogramming towards a neuroprotective effect

In order to get a more comprehensive overview of the Rai knock-out status, we performed an additional pathway analysis comparing DAPs of NS EVs and astrocytes. The resulting scenario included the predominant involvement of ENOA, suggesting that Rai deficiency impacts also on cellular energetics. Curiously, numerous studies correlate the ENOA up-regulation with the so-called Warburg effect, a shift in cellular energetic metabolism towards aerobic glycolysis, being at the basis of neoplastic cell survival and maintenance (99,100). Conversely, our analysis highlighted a down-regulation of ENOA both at cellular and vesicular levels, suggesting that Rai knock-out astrocytes may switch their energetic metabolism. An interesting hypothesis may come out from a particular study according to which in EAE activated microglia (particularly mononuclear phagocytes) undergo a polarization from a pro-inflammatory M1 status to an anti-inflammatory M2 mainly characterized by profound metabolic changes. In other words, M1 phenotype is prevalently switched towards aerobic glycolysis, whereas M2 phenotype become more oxidative (101). Furthermore, this metabolic switch is driven by HIF-1α and our pathway analysis of EVs and astrocytes comparison suggests interestingly the involvement of the same factor. As previous findings demonstrated that Rai KO astrocytes expressing specific A2 neuroprotective-associated genes impact the microenvironment in

a protective manner (53), it is therefore possible to postulate that Rai deficiency may have an effect on metabolism reprogramming, affecting astrocytes function and shifting them towards a neuroprotective action. Nonetheless, our analysis is still on its way and further experiments and validation are surely necessary to implement our data and to further extend our understanding of Rai deficiency impact on disease pathogenesis.

CONCLUSION

In conclusion, proteomic data obtained from our analysis provide an overview of the effects of Rai deficiency at cellular and vesicular level suggesting the involvement of various proteins, each related to distinct molecular pathways. However, an interesting remark must be reported on how all differential proteins seem to be involved in macro molecular areas, such as oxidative stress response, ECM and cellular adhesions remodelling, glutamate metabolism, EMT mechanisms and metabolic reprogramming. Consequently, although WT vs KO IL-17 astrocytes analysis' preliminary data must be completed and included in our previous results to get a comprehensive final outline, our findings could represent a promising starting point in the understanding of Rai action in EAE modulation.

CHAPTER II

Bronchoalveolar lavage fluid-extracted extracellular vesicles in Idiopathic Pulmonary Fibrosis

ABSTRACT

In the longtime challenge of identifying specific, easily-detectable and reliable biomarkers of interstitial lung diseases (ILDs), alternative biofluids, such as bronchoalveolar lavage fluid (BALF), have been considerably evaluated. In particular, BALF proteomics is progressively strengthening and providing novel and interesting insights into ILDs' pathogenesis, especially into idiopathic pulmonary fibrosis (IPF). Moreover, interest on the role of extracellular vesicles in IPF pathophysiology is considerably growing as they could represent a valuable source of knowledge, providing an additional point of view in the disease pathogenesis. Although very few, current EVs studies on IPF BALF are focused mainly on miRNAs, thus, to the best of our knowledge, our study is the first shotgun proteomic investigation of EV isolated from BALF of IPF patients. The main purpose of our analysis was to characterize and explore the individual impact on IPF pathogenesis of not only the vesicular component of BALF, but also its fluid counterpart. To this purpose, ultracentrifugation was chosen as EVs isolation technique and its purification was assessed by TEM, 2DE and LC-MS/MS. Interestingly, our 2DE data and scatter plot analysis showed a considerable difference of EVs proteome with respect to whole BALF and to its fluid counterpart proteome. The analysis of protein content and protein functions of the two counterparts evidenced that EVs proteins are predominantly involved in cytoskeleton remodeling, adenosine signaling, adrenergic signaling and C-peptide signaling, while fluid portion's ones result involved in ECM remodeling, pro-inflammatory response, Wnt signaling, angiotensin system and blood coagulation. Interestingly, these results draw attention on a systemic metabolic dysregulation in disease development and highlight relevant molecular pathways that result distinctive but complementary in IPF pathogenesis, as two faces of the same coin.

INTRODUCTION

Bronchoalveolar lavage Fluid

Bronchoalveolar lavage (BAL) is a relatively non-invasive procedure used in pulmonary medicine and it consists in the washing of selected lobes of the lung, usually five times with 20 ml of sterile saline buffer (0.9% w/v NaCl), by fiberoptic bronchoscopy and in the recollection of the fluid. In detail, the fluid derived from BAL procedure consists of cells, both resident alveolar cells and recruited inflammatory cells, their secreted products and proteins from leakage across the endothelial-epithelial barrier; however, it is usually centrifuged to remove its cellular debris resulting in a cell-free supernatant that is commonly referred to as "bronchoalveolar lavage fluid (BALF)". BALF's composition is quite similar to that of other biological fluids, especially plasma, and represents a complex mixture of soluble components such as phospholipids, lipids, nucleic acids, peptides and proteins derived from resident cells or passive and/or active diffusion through the alveolar-capillary barrier (102,103). Especially, BALF proteome consists of a wide variety of proteins, which is estimated to be in the order of 10^6 and is mainly dominated, in both healthy and pathological conditions, by plasma derived proteins, such as albumin, transferrin, alpha 1-antitripsin, haptoglobin and immunoglobulin A and G. In addition, other factors can be detected, such as immune inflammatory mediators, proteolytic factors, heat shock proteins and complement proteins, as well as proteins that are mainly secreted by airway and alveolar epithelial cells, such as surfactant-associated proteins, clara cell proteins and mucin-associated antigens; furthermore, the exclusive origin of these proteins makes them great markers of alveolar-capillary barrier's integrity and permeability, as an abnormal detection of these factors in serum might suggest impairments in epithelial cell function (104).

BALF as diagnostic sample

In order to justify the composition of this fluid and, consequently, to explore its diagnostic potential, the understanding of the physiological composition of the lung is a strong requirement. In particular, the lung is a highly complex organ composed of many types of cells, such as epithelial cells, immune cells, fibroblasts and endothelial cells, and the airways and alveoli are covered with a thin layer of "epithelial lining fluid (ELF)", composed of soluble components responsible for structural integrity of airspaces, maintaining gas-exchange and providing immune protection. Interestingly, the protein composition of ELF is affected by external factors and/or pathologic conditions affecting the lung

and, for this reason, it might reflect the pathogenesis of several pulmonary diseases. Indeed, various external factors, such as inhaled particles, airborne pollutants, infectious agents, and lung diseases induce in ELF biochemical modifications, as well as alterations in the expression of proteins that passively and actively diffuse through the alveolar-capillary barrier. As a result, BAL examination is an optimal tool for ELF assessment and for the diagnosis of potential pulmonary diseases (105). To this purpose, the cytological analysis of BAL is commonly performed for the diagnosis and management of several lung diseases, especially the group of interstitial lung diseases (ILDs). In detail, ILD can be defined as acute and chronic bilateral parenchymal infiltrative lung disease with variable degrees of tissue inflammation and fibrosis, whose aetiology can be either known or unknown. The American Thoracic Society and the European Respiratory Society's classification includes ILDs with known cause, such as pneumoconiosis, ILD associated with connective tissue disease (CTD-ILD) and hypersensitivity pneumonitis (HP), and ILDs with unknown cause, such as sarcoidosis and idiopathic interstitial pneumonias (IIP); particularly, IIPs constitute a heterogeneous group of pathologies, including idiopathic pulmonary fibrosis (IPF) (106). Nonetheless, the diagnostic value of BAL cytological analysis in the differential diagnosis of ILDs is frequently a matter of debate, especially because it must performed in combination with other diagnostic procedures, such as imaging techniques, blood tests, lung function tests, transbronchial biopsy or lung biopsy, physical examination and clinical history (107). Consequently, many forward steps and ameliorations have been made, especially in the BALF proteomics as it's undergoing a considerable evolution by providing nowadays not only qualitative descriptive results, but also clinically applicable and quantitative ones. Indeed, studies on BALF proteome have been gaining considerable attention as directed to the understanding of pathophysiologic biochemical mechanisms and to the further suggestion of potential biomarkers of lung diseases, such as IPF, cystic fibrosis, sarcoidosis, chronic obstructive pulmonary disease (COPD) and acute respiratory distress syndrome (ARDS) (105). In particular, most recent proteomic studies on BALF are focused on the characterization of the pathologically and clinically more interesting low abundance and low molecular weight proteins. Unfortunately, the over-representation, in both healthy and diseased BALF proteomes, of high molecular weight plasma proteins, such as albumin and immunoglobulins, limits the ability of current technologies to analyse the corresponding lower abundance proteins.

Idiopathic Pulmonary Fibrosis (IPF)

Idiopathic pulmonary fibrosis is classified as an interstitial lung disease (ILD), which involves the lung tissue and the interstitium characterized by microscopic pattern of usual interstitial pneumonia (UIP). In particular, IPF can be further defined as a chronic progressive fibroproliferative pathology characterized by fibroblast and myofibroblast deposition in the alveolar walls and uninterrupted production of extracellular matrix, leading to an impairment of parenchymal lung structure and gas exchange. IPF subjects present an extremely poor prognosis, as the median survival is from 3 to 5 years, and respiratory failure is the main cause of death in about 80% of affected individuals. Although IPF etiopathogenesis is not clearly elucidated yet, two main events represent the widest accepted hypothesis: on one hand, an unresolved chronic inflammation and alveolar epithelial alterations and on the other hand, frequent lesions associated with altered wound repair processes, which might lead to the activation, proliferation and migration of mesenchymal cells with further generation of active myofibroblastic foci and excessive accumulation of extracellular matrix. As an early diagnosis of IPF and its discrimination from the other ILDs are particularly difficult, BALF proteomics results to be a valuable source: on one hand, it enriches common knowledge on lung pathophysiology by implementing new information about pulmonary microenvironment events; on the other hand, it might provide sufficiently sensitive and specific prognostic and/or diagnostic biomarkers, which could be easily detected, and new therapeutic targets as well (108,109).

Extracellular vesicles in IPF

A growing number of studies on lung diseases have been investigating the pathophysiologic role of extracellular vesicles (EVs) in several biofluids, such as blood, serum, saliva, sputum and bronchoalveolar lavage fluid. As generally known, EVs are able to transfer regulatory signals, which could be proteins, lipids, DNA, mRNAs and miRNAs, to target cells exploiting a remarkable cell-to-cell communication process. Interestingly, alterations in the composition and content of these vesicles occur during the course of lung diseases, emphasizing their value as a new source of pulmonary diseases biomarkers and potential novel therapeutic vehicles. Currently, most studies have been focusing on EVs, especially exosomes, from BALF, sputum or respiratory cell supernatant in inflammatory pulmonary disorders such as asthma, sarcoidosis and chronic obstructive pulmonary disorder, in order to explore their potential involvement in the dissemination of pulmonary inflammation (110,111). Despite the great interest on EVs' potentiality in lung diseases therapy and diagnosis, few studies focused their attention on EVs' role in IPF. In detail, *Njock et al.* investigated

exosomes from sputum samples of IPF subjects and demonstrated the correlation of three specific exosomal miRNAs (miR-142-3p, miR-33a-5p, let-7d-5p) with disease severity (111). Other reports focused on serum EVs evaluation in IPF patients, as reported for instance by *Yamada et al.*, who reported a correlation of serum EV miR-21-5p with the progression and prognosis of the disease (112). Nonetheless, very few studies investigated extracellular vesicles in BALF samples from IPF subjects. Particularly, most of them drew attention to miRNAs contained within EVs: for instance, *Lee et al.* demonstrated the presence of miRNA-rich-EVs in BALF from healthy mouse model and set up a specific isolation protocol (113), while *Liu et al.* investigated the expression pattern of miRNAs in exosomes from BALF of IPF elderly patients, identifying miR-30a-5p upregulation in IPF subjects compared to control and its target gene, TAB3 (114). Furthermore, *Martin-Medina et al.* demonstrated that EVs from BALF IPF function as carriers of signaling mediator WNT5A, contributing to the pathogenesis of the disease (115). Given these points, current researches are directed to alternative sources of biomarkers, which can be used in combination with conventional ones (such as KL-6, surfactant proteins A and D and matrix metalloproteinases) in order to broaden common knowledge on IPF pathogenesis and to further suggest potential molecular targets.

This study aimed at the proteome characterization of EVs from IPF BALF by first setting up the EVs isolation protocol by ultracentrifugation, followed by a quality control assessment by Transmission Electron Microscopy (TEM) and two-dimensional electrophoresis (2-DE) in order to highlight the different proteomic profiles; as a further step, proteomes identification was carried out by shotgun LC-MS/MS, followed by enrichment analysis of first, exclusive proteins of each complementary fraction, and then of both proteomes.

MATERIALS & METHODS

Population

Two IPF patients, both males, mean age 69 ± 5 years and both ex-smokers, were enrolled in the study. The patients were diagnosed according to ATS/ERS guidelines at Medizinische Hoschschule (MHH) – Pneumology Clinic of Hannover (Germany). Demographic data, smoking habits, onset symptoms and comorbidities were recorded in a database together with other clinical data. Lung function tests were performed according to ATS/ERS guidelines to obtain FVC, DLCO and GAP percentages. Diagnosis of IPF was formulated in a context of multidisciplinary discussion (MDD). After informed consent of the patients, Bronchoalveolar lavage was performed for diagnostic purposes in order to exclude other interstitial lung diseases. Samples were provided by the research group directed by Prof. Antje Prasse at Fraunhofer ITEM, Hannover (Germany).

EVs isolation from IPF BAL Fluid

Human IPF Bronchoalveolar lavage fluid (BALF) samples were first centrifuged at 800 x g for 5 min at 4°C as a routine procedure after their collection from patients in order to separate BALF from the cell component. In particular, BALF samples from two IPF patients were prepared for the analysis, specifically using 15 ml per each as starting volume. First, BALF samples were centrifuged at 12 000 x g for 45 min at 4°C, pellet was discarded and supernatant collected in ultracentrifuge tubes. Second, they were centrifuged at 110 000 x g for 2 h at 4°C (Beckman Coulter Optima XE, Type 70 Ti Fixed-Angle Titanium Rotor, Beckman Coulter Life Sciences, Brea, California, USA). At this step, supernatant was collected in a new tube and stored on ice, as this fraction represented the complementary portion of BALF whole fluid deprived of the extracellular vesicles (BALF EVs-free). Conversely, pellet was resuspended in PBS and filtered into a new ultracentrifuge tube through a 0.22 µm filter; then, it was further centrifuged at 110 000 x g for 70 min at 4°C. Following, supernatant was discarded, pellet was resuspended in PBS and centrifuged again at 110 000 x g for 70 min at 4°C; at this point, pellet was transferred into a new eppendorf (BALF EVs) (116). Eventually, BALF EVs concentration was detected by NanoDrop (NanoDrop ND-1000 spectrophotometer)

Transmission Electron Microscopy (TEM)

As a first checkpoint of BALF EVs isolation, transmission electron microscopy was performed by Eugenio Paccagnini and Dr. Mariangela Gentile, members of the research group directed by Prof. Pietro Lupetti of the Life Sciences Department at the University of Siena. In detail, about 3 µl of BALF EVs sample was loaded onto a 300 mesh formvar coated copper grid for 2 minutes. After blotting the excess, the grid was negatively stained with 2% aqueous ammonium molybdate for 30 s and analyzed using a Thermo Fisher Scientific Tecnai G2 Spirit transmission electron microscope operating at 120 kV equipped with a EMSIS Veleta 2048X2048 CCD camera. Diameter measurements of vesicles was performed using IC Measure software (IC Measure 2.0.0.245, The Imaging Source, Bremen, Germany) on TEM snapshots.

Samples preparation for 2DE analysis

Dialysis of BALF EVs and BALF fluid portion was performed against four changes of distilled water at 4°C for 12 h in order to eliminate salts. Thus, samples were lyophilized and dissolved in lysis buffer (8 M urea, 4% w/v 3-[(3-cholamidopropyl) dimethylammonia]-1-propanesulfonate hydrate (CHAPS), 40 mM Tris base, 1% w/v dithioerythritol (DTE) and trace amounts of bromophenol blue). Before adding bromophenol blue, protein concentration of BALF fluid portion was determined by Bradford assay (54) in order to load 60 µg of protein per gel, while EVs protein content was used.

2D-Electrophoresis

2DE was carried out using the Immobiline polyacrylamide system on a preformed immobilized nonlinear pH gradient from pH 3 to 10, 18 cm in length (Cytiva, formerly GE Healthcare, Uppsala, Sweden). Two-dimensional run was performed using Ettan™ IPGphor™ system (Cytiva, formerly GE Healthcare, Uppsala, Sweden) at 16°C applying the following electrical conditions: 200 V for 8 h, from 200 to 3500 V in 2 h, 3500 V for 2 h, from 3500 to 5000 V in 2 h, 5000 V for 3 h, from 5000 to 8000 V in 1 h, 8000 V for 3 h, from 8000 to 10000 V in 1 h, 10000 V, for a total of 90,000 VhT. Gel strips were rehydrated with lysis buffer and traces of bromophenol blue overnight at room temperature; then, 0.2% carrier ampholyte was added to samples and the run was performed by cup loading, with the cup placed at the cathodic end of the strips. Following the first-dimension run, strips were equilibrated in 6 M urea, 2% w/v SDS, 2% w/v DTE, 30% v/v glycerol and 0.5 M Tris–HCl pH 6.8 for 12 min and for a further 5 min in 6 M urea, 2% w/v SDS, 2.5% w/v iodoacetamide, 30%

v/v glycerol, 0.5 M Tris–HCl pH 6.8 and a trace of bromophenol blue. Then, the second dimension was performed on 9-16% SDS polyacrylamide linear gradient gels (18 x 20 cm x 1.5 mm) and the run was carried out at 40 mA/gel constant current at 9°C until the dye reached the bottom of the gel. Eventually, gels were stained with ammoniacal silver nitrate.

MS-preparative SDS-PAGE

For shotgun proteomic analysis, BALF whole fluid of the same patients were also prepared, thereby, BALF whole fluid and BALF EVs-free were subjected to cold acetone precipitation (1:4) overnight at -20°C. Then, centrifuged at 4542 x g for 10 min at 4 °C, pellet was resuspended in acetone and centrifuged again at 15000 x g for 10 min at 4°C. At this step, the three components per each sample (BALF whole fluid; BALF EVs-free; EVs) were solubilized in a denaturation solution composed of 8 M Urea and 4% w/v CHAPS and their protein concentration was determined by Bradford Assay (54).

MS-preparative SDS-PAGE was carried out utilizing pre-cast 12% polyacrylamide gels (Criterion™ XT Bis-Tris Protein Gel, Bio-Rad, Hercules, California, USA) with Criterion™ Vertical Electrophoresis Cell (Bio-Rad, Hercules, California, USA) with the following voltage conditions: 60 V for stacking gel and 120 V for separation gel. The protein amount loaded was 50 µg for BALF and BALF fluid fraction, and total protein content for EVs. Samples were centrifuged, XT sample buffer and XT reducing agent (Bio-Rad, Hercules, California, USA) were added to each sample and then heated at 95°C for 5 min; then, proteins were alkylated by addition of 40% acrylamyde at a final concentration of 2% and eventually samples were loaded in the gel. After the run, the gel was incubated in a 50% v/v methanol and 10% v/v glacial acetic acid fixing solution for 1 h at gentle agitation; then, stained in Coomassie Blue staining solution composed of 0.1% w/v Coomassie Brilliant Blue R-250, 50% v/v methanol and 10% v/v glacial acetic acid for 20 min at gentle agitation.

Samples preparation for LC-MS/MS

Protein bands were cut out and further minced into $1mm^3$ gel pieces; then, they were destained twice in 50% v/v acetonitrile (ACN)/20 mM Ammonium Bicarbonate (ABC) at 37°C with shaking (Thermomixer, Eppendorf AG, Hamburg, Germany) at 700 rpm for 30 min. Following destaining, gel pieces were dehydrated in 100% ACN at room temperature for 10 min and then solvent was removed in a vacuum centrifuge (Speedvac, Thermo Fischer Scientific™, Waltham, MA, USA) for 30 min. After, a 10 ng/µl Trypsin in 10% v/v ACN/20 mM ABC solution for protein digestion was added to gel pieces, which rehydrated on ice for 60 min; then, they were covered with 10% v/v

ACN/20 mM ABC solution and digestion was performed overnight at 37°C with shaking at 350 rpm. At this point, first digestion was stopped by adding a 50% v/v ACN/5% v/v trifluoroacetic acid (TFA) solution and gel pieces were incubated at 24°C with shaking at 700 rpm for 30 min. Supernatant containing peptide extracts was collected into a new vial dried in a vacuum centrifuge for 30 min. Second, a 50% v/v ACN/0.5% v/v TFA solution was added to gel pieces, incubated with the same previous parameters, supernatant combined to the one already collected and further dried in vacuum centrifuge for 30 min; third, 100% ACN was added to gel pieces and they were incubated at 24°C with shaking at 700 rpm for 20 min. Eventually, supernatant was collected and then dried in a vacuum centrifuge for 3 h.

LC-MS/MS analysis and protein identification

Peptides of mono-dimensional gel digestion were analysed using LC-MS/MS analysis. Particularly, dried samples were dissolved in a 2% v/v ACN/0.1% v/v TFA solution and incubated at 24°C with shaking at 350 rpm for 30 min; after centrifugation at 20000 x g at room temperature for 30 min, supernatants were used for the LC-MS/MS analysis. Particularly, supernatants were transferred to an LC sample vial and an appropriate amount of each sample was injected into a Dionex Ultimate 3000 high-performance LC system (Thermo Fisher Scientific, USA). Peptides were loaded on a trap column (C18 material, 2 cm length, 75 µm ID, Acclaim PepMap, Dionex) with 6 µl/min and washed with 0.1% v/v TFA loading buffer. After 5 minutes, the trap column was switched in line with the nano flow separation column (C18 material, 50 cm length, 75 µm ID, Acclaim PepMap, Dionex) and peptides were eluted with a flow of 250 nl/min and a linear gradient of elution buffer A (0.1% v/v formic acid) and elution buffer B (80% v/v acetonitrile, 0.1% v/v formic acid). The LC system was online connected to the nanoESI source of an LTQ Orbitrap Lumos Mass Spectrometer (Thermo Fisher Scientific, USA). Orbitrap mass analyser recorded the survey scans and the most intense precursor ions of charge state ≥ 2 were selected for collision induced (CID) fragmentation with a normalized collision energy of 38%. Fragments were scanned out in the orbitrap mass analyzer in centroid mode and raw data were processed with MaxQuant software (Version 1.6.50, https://maxquant.net/maxquant/). For peptide identification, MS/MS spectra were searched against the human entries of the UniProtKB/Swiss-Prot database and they were stated identified if false discovery rate (FDR) on protein and peptide level was less than 0.01. Oxidation of methionine residues, N-terminal acetylation, deamidation of asparagine and glutamine residues and propionamidation of cysteine residues were selected as variable modifications; furthermore, a

maximum of two missed cleavages were accepted. A minimum ratio count of one unique or razor peptide was required for quantification. Furthermore, the results for the identified protein groups were further processed for statistical purposes using the Perseus software (Version 1.5.2.6, https://maxquant.net/perseus/). Shotgun experiments were performed at Fraunhofer ITEM, Hannover (Germany) in collaboration with Dr. Alfonso Carleo, member of the Prof. Antje Prasse research group.

Enrichment analysis

Enrichment analysis was performed submitting gene names of identified proteins to the MetaCore 6.8 network building tool (http://portal.genego.com, Clarivate Analytics, Philadelphia, Pennsylvania, USA). Specifically, we first performed an enrichment analysis by GeneGo ontologies biological processes, and then a Pathway Maps analysis. Indeed, the software can establish a hierarchical list of pathway maps, prioritized according to their statistical significance ($p \leq 0.001$), and each of these is equivalent to a canonical map that has multiple sequential steps of interactions, defining a well-established signaling mechanism. In particular, each step is also well-defined, experimentally validated and accepted in the research field.

RESULTS

Quality control assessment of EVs from BALF IPF

Extracellular vesicles were isolated from Bronchoalveolar Lavage Fluid of IPF affected subjects by sequential ultracentrifugation and their purification was assessed by transmission electron microscopy (Figure 1). As illustrated in TEM images in Figure 1A and B, this reproducible and easy-to-perform isolation technique allowed the separation of a wide size range (70-2000 nm) of vesicles with a spherical morphology and sometimes assembled into small aggregates, starting from smaller vesicles of 70-150 nm in size (Figure 1A), to medium and larger vesicles of 150-600 nm and 600-2000 nm in size, respectively (Figure 1B). In order to further evaluate the proper isolation of EVs, 2DE of both EVs and the complementary fluid fraction was performed. The resulted two-dimensional gels show patterns of proteins ranging from 200 to 10 kDa in molecular weight and from 3.5 to 10 pH in isoelectric point. The obtained proteomic profile of EVs (Figure 2A), results to be considerably different from the one of the complementary fluid portion and strongly deviates from the BALF one, as well (Figure 2B and 2C respectively). Conversely, a strong similarity between BALF and fluid fraction 2DE gels is considerably evident.

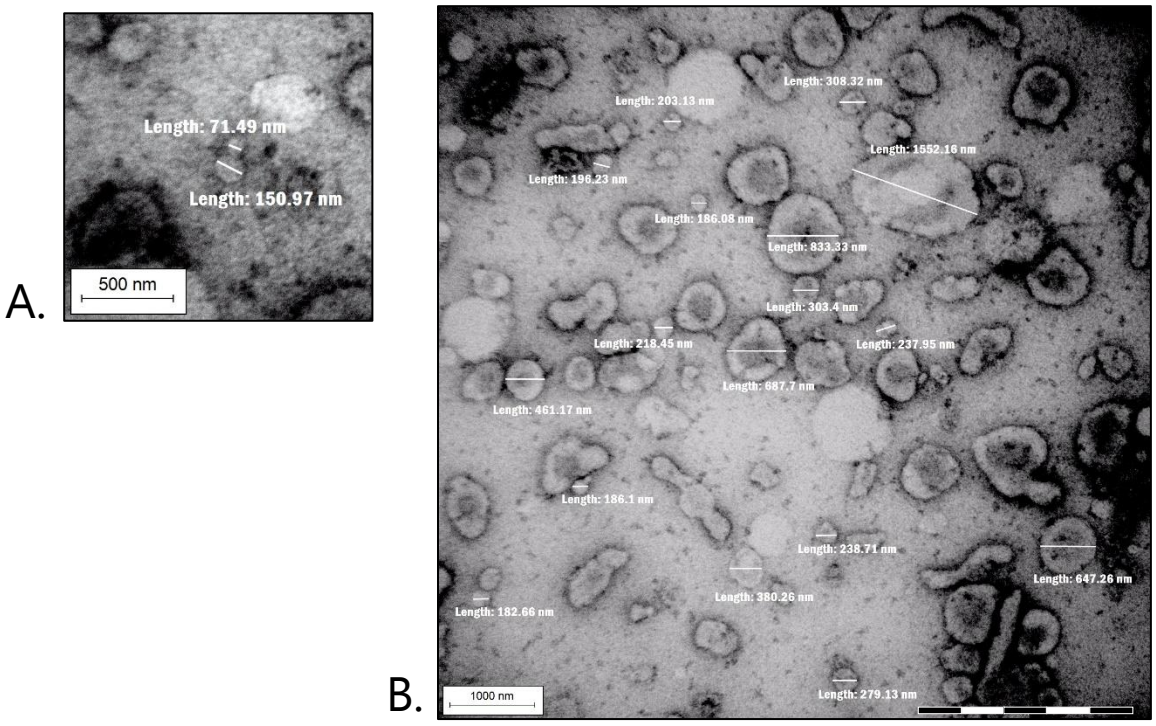

Figure 1. Transmission Electron Microscopy of BALF EVs.
Predominant presence of vesicles ranging from 150 to 600 nm in size **(A. B.),** with limited smaller (70-150 nm) **(A.)** and bigger (600-2000 nm) **(B.)** vesicles.

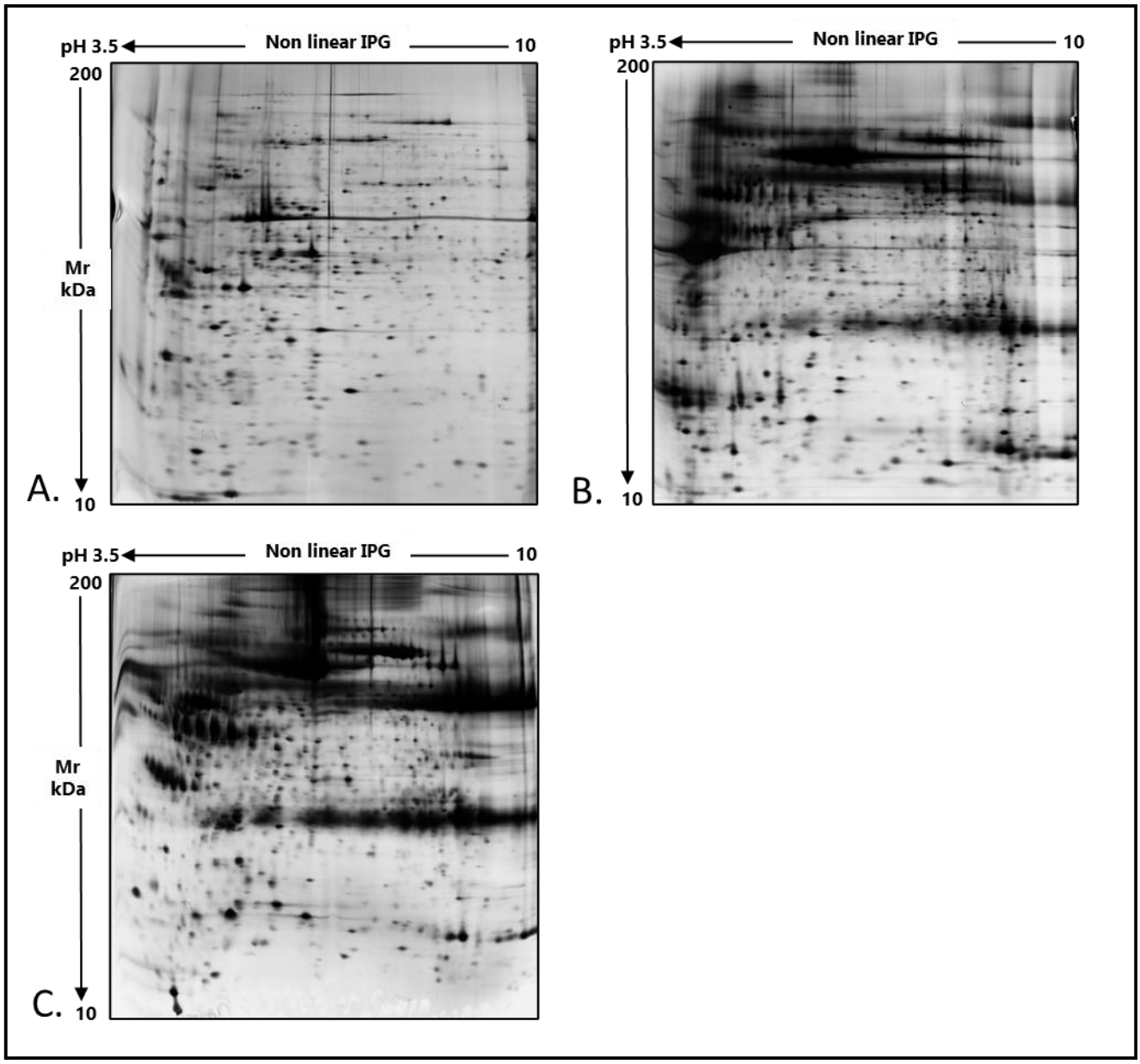

Figure 2. Two-dimensional gel electropherograms of BALF EVs, fluid fraction and whole BALF

(A) 2DE gel of BALF EVs; **(B)** 2DE gel of the fluid fraction; **(C)** 2DE gel of whole BALF

Shotgun Proteomics of BALF EVs and BALF Fluid Portion

Proteomes of the vesicular and of the fluid fractions were identified by shotgun approach. Mass spectrometry results fundamentally consists of label free quantification intensities of each protein in the EVs and in the fluid portion of both samples, number of identified peptides q-value, score, protein IDs, protein names and gene names. In addition, a Venn diagram was also performed submitting the proteome lists of EVs and of the fluid counterpart, which account for 715 and 741 proteins, respectively. As Venn diagram in Figure 3 displays, 271 proteins (26.8%) are EVs exclusive, 297 (29.3%) are fluid portion exclusive and 444 (43.9%) are common to both fractions.

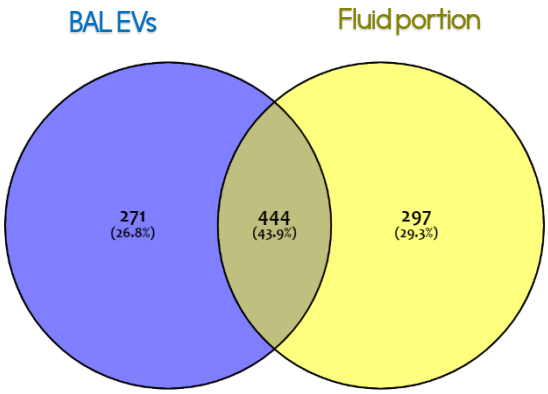

Figure 3. Venn diagram of protein groups identified in EVs and in the fluid portion
Blue area represents protein groups exclusive to EVs; yellow area represents protein groups exclusive to the fluid fraction; grey represents protein groups common to both fractions.

Table 1 summarizes this classification as it reports protein lists of EVs and of the fluid portion, of only their exclusive proteins and of the common ones. Moreover, specific vesicular markers (highlighted in bold in Table 6 proteins lists), such as TSG101, Rab family proteins, ARF6, ADAM10, CD63 and CD151, have been identified, further confirming a good quality isolation of extracellular vesicles from our BALF samples. In order to evaluate how much data sets of EVs and of the fluid part might be correlated, a scatter plot analysis of mass spectrometry data was performed, including whole BALF data set as well. First, Figure 4A shows a scatter plot defined by BALF data

set on x axis and fluid portion data set on y axis, displaying a positive, linear and strong relationship, with an evident correlation. Second, Figure 4B shows a scatter plot defined by fluid fraction data set on x axis and EVs data set on y axis, displaying a positive, linear and weak relationship. At last, Figure 4C shows a scatter graph defined by BALF data set on x axis and EVs data set on y axis, showing a positive, linear and weak relationship, as well

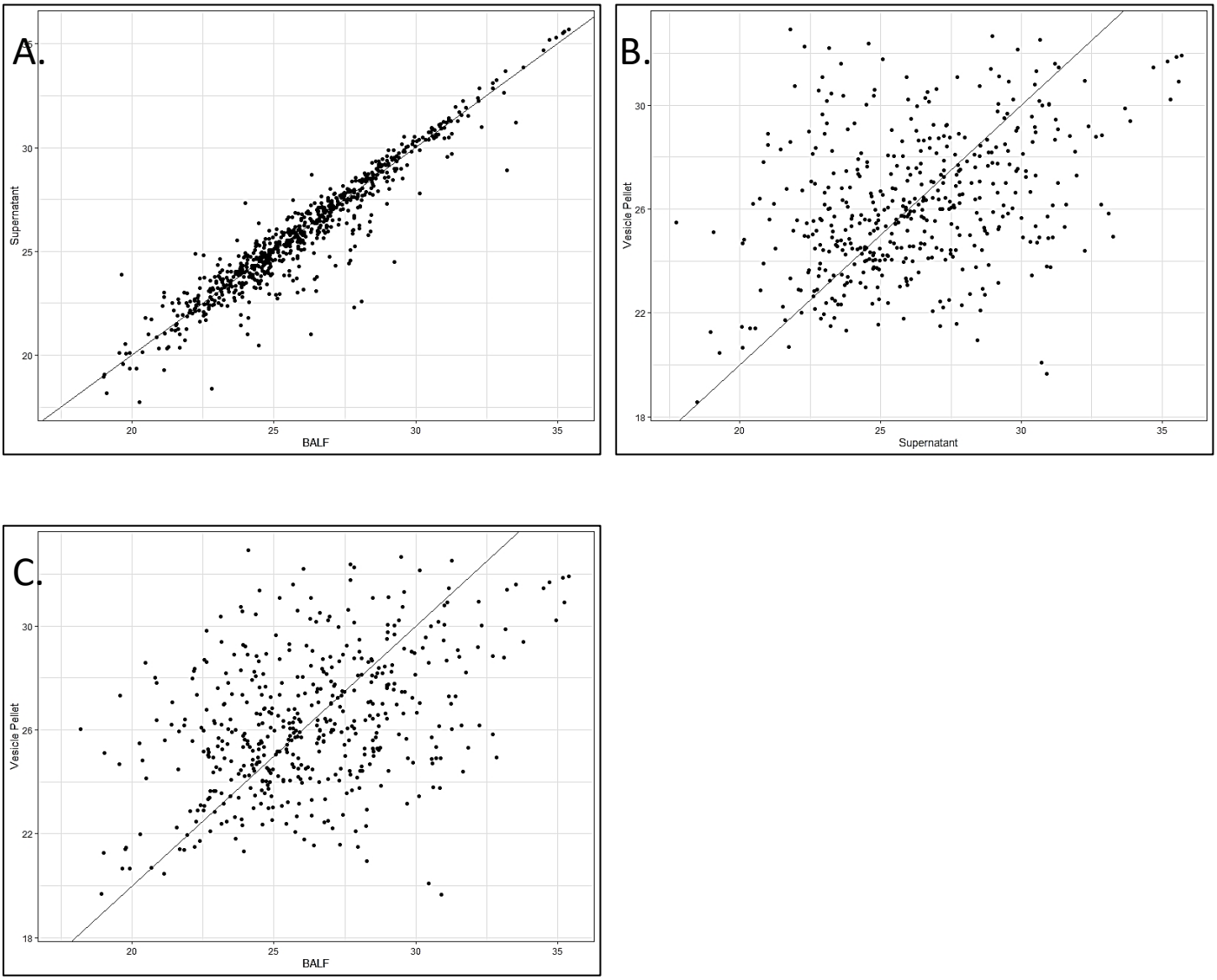

Figure 4. Scatter plots
(A) Whole BALF vs Fluid; **(B)** Fluid vs EVs; **(C)** Whole BALF vs EVs

MetaCore enrichment analysis

Functional analysis of the identified protein groups in the EVs and in the complementary fraction was performed using MetaCore software suite. First, Gene Ontology (GO) enrichment analysis of biological processes (BP) was carried out in order to provide a deeper overview of the two experimental data sets. In detail, Figure 5A displays the ten most significant BPs enriched from the exclusive EVs mass spectrometry data, such as establishment of localization, vesicle-mediated transport, localization, export from cell and Ras protein signal transduction. Likewise, the ten most significant BP enriched from the exclusive protein groups of the fluid portion are shown in Figure 5B, such as leukocyte mediated immunity, secretion, response to organic substance, neutrophil degranulation and neutrophil activation. As a second step, the functional analysis was implemented with a comparison of the most significant enriched pathway maps of the two data sets. In particular, the fifteen most relevant common pathway maps are listed in Figure 6, where the orange-coloured bars refer to the fluid portion data set, while the blue-coloured bars refer to the EVs' one (the complete lists are shown in Figure 7). As Figure 6 shows, EVs exclusive data set is associated with a major involvement in most of the relevant pathways, as it is related to the immune response through antigen presentation, cytoskeleton remodeling, alpha-2 adrenergic receptor regulation of ion channels, adenosine receptors signaling pathways, beta-adrenergic signaling in lung cancer, proinsulin C-peptide signaling and G protein-coupled receptors signaling in lung cancer On the other hand, fluid portion's exclusive data set strongly impacts on other significant pathways, such as the angiotensin system, blood coagulation, cell adhesion and ECM remodeling, release of pro-inflammatory mediators and elastolytic enzymes and the inhibition of WNT signaling in the progression of lung cancer.

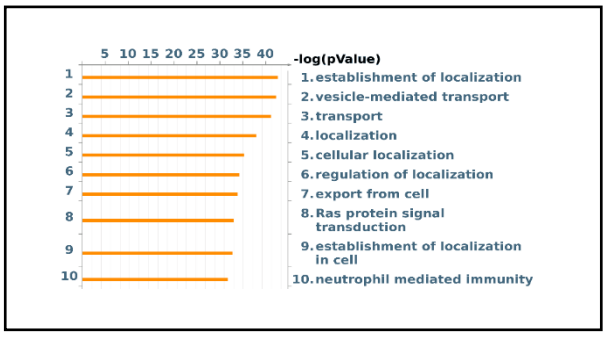

A.

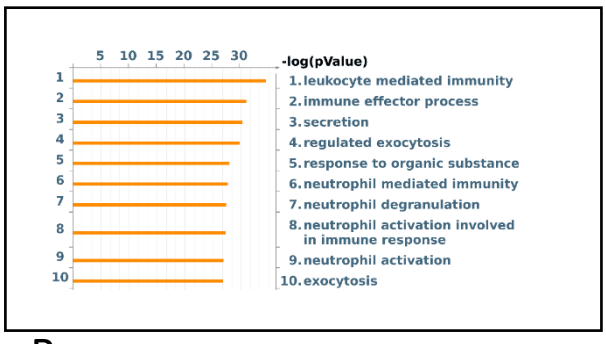

B.

Figure 5. Enrichment analysis of BALF EVs and of the fluid fraction
GO Biological Processes of protein groups exclusive to EVs (**A**) and exclusive to the fluid fraction (**B**)

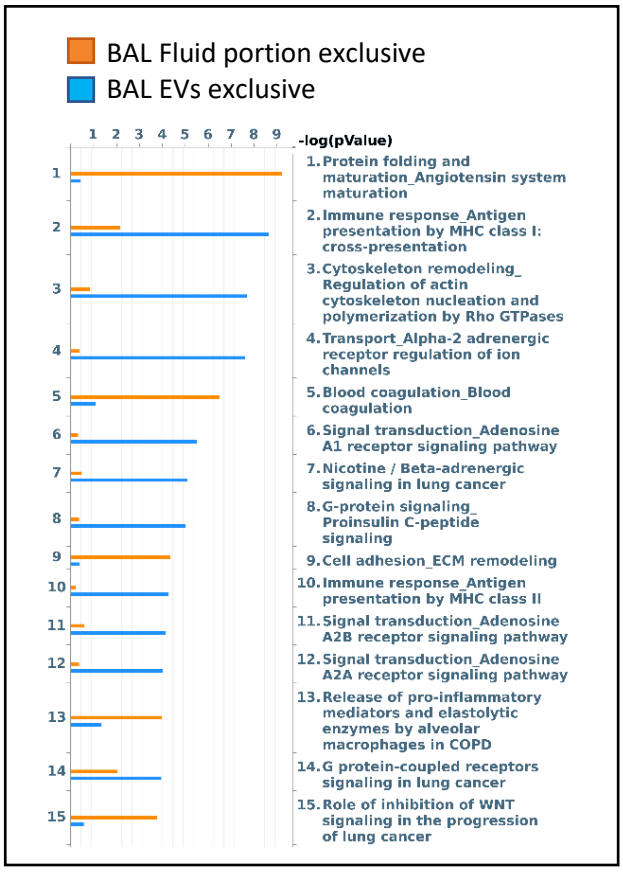

Figure 6. Figure 6. Comparison of major pathway maps of EVs and BALF fluid fraction
Orange bars indicate data set exclusive to BALF fluid fraction; blue bars indicate data set exclusive to BALF EVs.

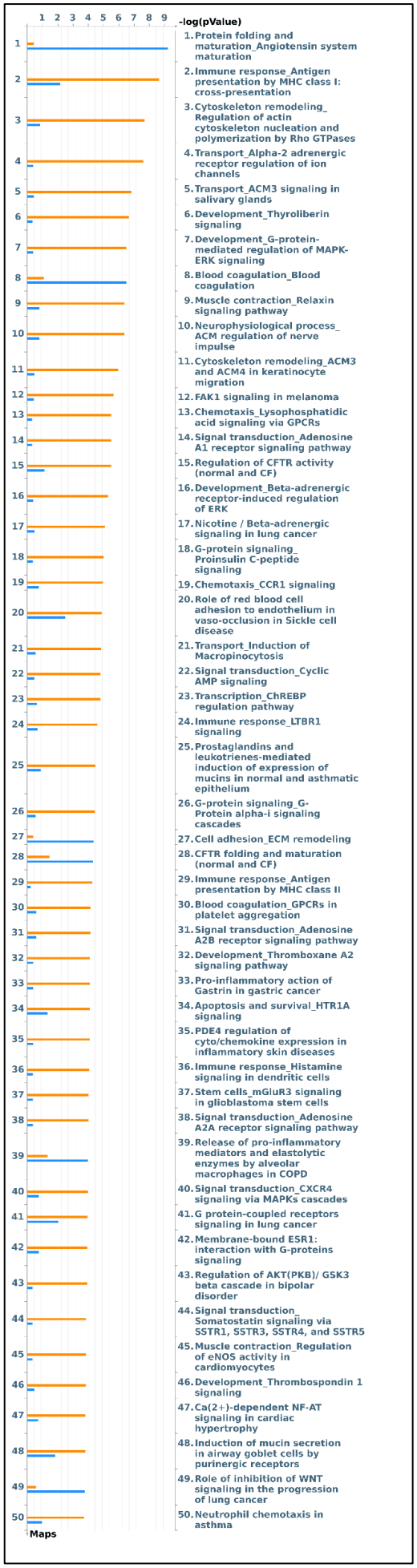

Figure 7. Pathway maps' enrichment: BALF EVs and fluid portion's comparison

Complete list of 50 most statistically significant pathway maps common to both fractions. Orange-coloured bars refer to BALF fluid portion exclusive data set, while blue-coloured bars refer to BALF EVs exclusive data set.

DISCUSSION

Ultracentrifugation as efficient isolation method for various classes of EVs

In the longtime challenge of identifying specific, easily-detectable and reliable biomarkers of pulmonary diseases, alternative biofluids, such as BALF, have been considerably evaluated (117). Numerous studies on BALF proteome have being carried out worldwide, especially directed at widespread diseases such as lung cancer (118,119), cystic fibrosis (120,121), asthma (122,123) and COPD (124,125). Nonetheless, BALF proteomics applied to studies on pulmonary interstitial diseases is progressively strengthening and providing novel and reliable results. In particular, growing effort to investigate the role of extracellular vesicles (EVs) in the physiopathology of ILDs and their potential therapeutic applications is spreading among scientific community (126,127), especially applied to IPF (111,112,115). Although very few, current EVs studies on IPF BALF are focused mainly on acid nucleic content, such as miRNAs (114), however proteomic studies could instead provide valuable insights into the disease (115). To the best of our knowledge, our study is the first shotgun proteomic investigation of EVs isolated from BALF of IPF patients. The main purpose of our analysis was to characterize and explore the individual impact on IPF pathogenesis of not only the vesicular component of BALF, but also its fluid counterpart. To this purpose, ultracentrifugation was chosen as EVs isolation technique (116) and its purification was assessed by TEM (128), 2DE and LC-MS/MS as well. Electron microscopy displays the presence of a broad range of isolated extracellular vesicles, from small particles (70-150 nm in size) to bigger ones (150-2000 nm in size), suggesting that this isolation method is effective in separating various classes of vesicles.

Vesicular and fluid fractions as characteristic and distinct proteomic profiles

2D-Electrophoresis of both vesicular and fluid components of IPF BALF was performed demonstrating a considerable distinction of the two fractions. The fluid fraction resulted similar and comparable to that of a BALF protein pattern, while no evidence of BAL typical protein species can be observed in EVs profile. Our next step included LC-MS/MS by shotgun approach. Scatter plot analysis of mass spectrometry data of both portions confirm previous results in accordance to 2DE-proteomic profiles. Interestingly, these results confirm how distant EVs proteome is with respect to whole BALF and to its fluid counterpart. Furthermore, our findings support the importance of pre-

fractioning procedures in proteomic technologies as they allow to overcome the limit of low abundant species identification in complex samples like BAL. Indeed, most of EVs proteins are not easily detectable in BAL samples both in 2DE/MS and LC-MS/MS proteomic approaches, as usually hidden by major protein species. Consequently, our study confirms the importance of isolating and studying separately the vesicular and fluid fractions as potential sources of biomarkers.

Enrichment analysis highlights distinctive but complementary molecular pathways in IPF pathogenesis

Given this interesting divergence between the two components, we evaluated protein content and protein functions of both vesicular and fluid samples in specific biological processes and molecular pathways. Interestingly, our analysis highlights relevant molecular pathways that result distinctive but complementary in IPF pathogenesis, as two faces of the same coin.

Accordingly, our enrichment results provide a further evidence of EVs predominant involvement in mechanisms of transport, localization and signal mediation, confirming their key roles in intercellular communication in physiological and pathological conditions (129). Conversely, fluid part's analysis highlights the predominance of neutrophil and leukocyte immune-mediated response processes characterized by the secretion of modulating factors.

EVs-associated most significant molecular pathways

Remarkably, the comparison of the most significant molecular pathways of the two parts evidences that EVs proteins are prevalently involved in antigen presentation MHC class I and II, cytoskeleton remodeling, adenosine signaling, adrenergic signaling, G protein signaling and specific G protein C-peptide signaling. C-peptide (proinsulin), prevalently studied in diabetic disease, exerts its biological activities via a specific G-protein coupled receptor also expressed on endothelial cells and fibroblasts (130). Its signaling involves ERK1/2, PI3K-Akt, PKC, eNOS and NF-kB, already well-known factors in TGF-β signaling (131,132), the key regulator of fibrosis, thereby suggesting C-peptide involvement in fibrogenic processes (133). Accordingly, recent studies evidence the association of C-peptide with fibrosis progression in different pathologies (134,135). Furthermore, some studies reported the association of C-peptide with the transcription factor peroxisome proliferator-activated receptor-γ (PPARγ) (136), whose modulation equilibrates adipogenesis or fibrogenesis (137), in line with a metabolic dysregulation as an additional impacting cause of fibrosis, especially in IPF (133,137).

Our identification of several Rho GTPases in EVs suggests their potential action on cytoskeleton remodeling by mediating actin filament rearrangement via ROCK (138). Indeed, interesting studies report ROCK signaling pathways involved in myofibroblasts differentiation and in fibrogenic processes, in particular in pulmonary fibrosis such as IPF (139–141). Curiously, given the growing attention on Wnt signaling in cellular adhesions regulation and involvement in IPF pathogenic mechanisms, *Franco et al* reported that Rho GTPases' regulation modulates cellular migration and polarity via β-catenin-independent Wnt pathway, (142).Another remarkable cytoskeleton-related protein detected in EVs is profilin, which triggers fibrogenic pathways such as PI3K-Akt and ERK 1/2 (143).

Our results indicate the involvement of another interesting pathway which recently is drawing attention as related to fibrogenesis: adenosine signaling pathway. Adenosine exerts its functions by binding to G-protein coupled receptors A2A and A2B, leading to fibroblast activation and collagen synthesis (144). Indeed, several studies already report a correlation between A2B adenosine receptor's (A2BAR) activation and the regulation of inflammation and fibrosis in IPF, specifically indicating macrophages as main mediators (145,146). Moreover, some signal transduction factors of this signaling, such as PKA, are detected in EVs. Curiously, a recent study demonstrates the key role of A2BAR in the modulation of EMT process in IPF by two signaling pathways, cAMP/PKA and MAP/ERK (147). Furthermore, our enrichment analysis suggested a direct link between PKA and CREB1 activation, inducing VEGF-A transcription, one of the major player in IPF onset (148).

Interestingly, our analysis reports another molecular pathway whose relation to IPF pathogenesis is not often taking into account: alpha- and beta-adrenergic systems. Rassler B. demonstrates in rats that a continuous stimulation of beta- and especially alpha-adrenergic signaling lead to pulmonary fibrosis. In detail, the adrenergic-stimulated histologic pulmonary fibrosis is associated to a remarkable increase in TGFβ1, collagen I, MMP-2 and TIMP-2 mRNA expression, suggesting a link between adrenergic stimulation and up-regulation of ECM molecules and promotion of fibrotic processes (149).

Fluid fraction-associated most significant molecular pathways

In line with these findings, ECM remodeling is well reflected by the identification of MMP-9, MMP-13, Matrilysin (MMP-7), Kallikrein 1, TIMP1, MMP-1 and Kallikrein 3 in the fluid fraction. These proteins are reported as strictly related to IPF pathogenesis because their altered homeostasis could induce epithelial-to-mesenchymal transition, through a decrease in level or activity of pro-fibrotic

mediators or a decrease in level of antifibrotic mediators. Moreover, their action leads to abnormal epithelial cell migration and aberrant repair processes, which, together with the phenotype switching of lung macrophage from M1 to M2 type and fibrocyte migration, contribute to IPF pathogenesis (150). At the same time, several MMPs degrading extracellular matrix components are elastase enzymes that release elastin peptide fragments implicated in proinflammatory processes (151). Among these, chitinase-3-like protein 1, identified in the fluid fraction, plays a role in T-helper cell type 2 (Th2) inflammatory response and IL-13-induced inflammation, regulating allergen sensitization, inflammatory cell apoptosis, dendritic cell accumulation and M2 macrophage differentiation (152). Additionally, an altered ECM induces also defects in cell-cell junctions, giving rise to a wide range of dysregulations, such as an alteration of Wnt signaling, suggested by MMP-9, E-cadherin, TIMP1, Vimentin and Keratin 18 identification in the fluid part. Particularly, Wnt signaling represents another pivotal course of action in IPF pathogenesis, as well as lung cancer onset and progression (148,153–155).

Proteins identified in the fluid part of IPF BALF highlighted other two interesting molecular pathways such as angiotensin system maturation and blood coagulation. Dysregulation of RAAS components leads to pro-inflammatory and pro-fibrotic effects in different organs triggering fibrosis development (108,137,156,157) and many metabolic dysfunctions, such as those observed in metabolic syndrome and diabetes mellitus type 2 (158). Interestingly, RAAS by angiotensin-converting enzyme, was also reported as an effector of VEGF (148,159,160), whose chronic exposition quickly relaxes the endothelial cell barrier and regulates its function by modifying components of intercellular junctions (160). Notably, cellular adhesions are modulated by Wnt signaling and interestingly, a recent study of *Du et al* positively correlates the increased level of VEGF with an increased level of Wnt in atherosclerotic rats, further suggesting a metabolic dysregulation as a background scenario in IPF pathogenesis (161). Moreover, numerous proteins identified in the fluid fraction are involved in blood coagulation. Remarkably, a dysregulation of this process was already suggested as a potential additional cause of IPF development by our previous findings, as a two-dimensional electrophoresis analysis provided evidence of a strong up-regulation of annexin A2 (ANXAII) in IPF BAL (108). Annexin A2, expressed on endothelial cells, monocytes and macrophages, acts as cell-surface co-receptor for plasminogen and tissue plasminogen activator (tPA), considerably increasing plasmin generation and fibrinolysis (162). Therefore, it contributes also to the plasmin-mediated activation of matrix metalloproteinases, such as MMP3, MMP9 and MMP13, which, by degrading ECM components, leads to the release of matrix-bound pro-angiogenic growth factors VEGF and FGF, relevant players in IPF (163,164). Accordingly, annexin A2 was identified in this work in both EVs

and fluid fraction, suggesting a potential involvement of procoagulant proteins in the pathogenesis of IPF (108). These results are also supported by *Bargagli et al*, as an up-regulation of pro-coagulant proteins was validated in serum of IPF patients, especially with acute exacerbated (165).

Although these altered molecular pathways were evidenced by proteins directly identified in BAL samples, our results provide evidences of a wider systemic involvement. In other words, fluid proteins-mediated altered processes are regulated by both in situ cellular protein release and by systemic circulating molecules, which could be released in the lung environment by plasma exudation to epithelial lining fluid. Likewise, vesicular proteins could have systemic origin beside being pulmonary. For this reason, altered systemic metabolic pathways could potentially employ extracellular vesicles as communication system to induce specific pro-fibrotic response in lung environment, eventually leading to IPF.

CONCLUSION

In conclusion, EVs isolation and separation from its fluid complementary fractions turned out to be extremely useful for the detection of potential protein biomarkers characterizing IPF patients, which otherwise would be hardly detectable by classic experimental procedure. despite protein content of each BALF component is different and regulates distinct molecular pathways, both display a novel and particular scenario of the disease in which a systemic and metabolic dysregulation contributes as a cause and/or a consequence of the development of IPF. Furthermore, vesicular and fluid proteins potentially cooperate for the pathogenesis and maintenance of the disease through pro-fibrotic and pro-inflammatory signals. These interesting results represent a valuable start point for further analysis by increasing the cohort of patients and comparing IPF samples with controls.

Table 1. Mass spectrometry protein lists

Complete list of MS proteomic data, reported by corresponding gene names, including the total proteins identifications in EVs, total proteins identification of the fluid portion, the list of proteins exclusively identified in EVs, the list of proteins exclusively identified in the fluid portion and the proteins identified in both the EVs and fluid portions.

TOTAL EVs	TOTAL FLUIDIC PORTION	EVs EXCLUSIVE	FLUIDIC PORTION EXCLUSIVE	COMMON PROTEINS
715 proteins	**741 proteins**	**271 proteins**	**297 proteins**	**444 proteins**
MYO1B	LAMC2	MYO1B	LAMC2	SBSN
AHNAK	VIM	AHNAK	VIM	C3
SERPINB2	MMP9	SERPINB2	MMP9	TF
TMC5	APOA4	TMC5	APOA4	FLNA
PPL	STIP1	PPL	STIP1	LAMA3
EPS8L1	PDIA3	EPS8L1	PDIA3	A2M
HSPG2	C2	HSPG2	C2	DSP
EVPL	SERPINC1	EVPL	SERPINC1	MUC5B
FAM129B	AFM	FAM129B	AFM	MYOF
NT5E	IVL	NT5E	IVL	IQGAP1
STXBP2	CFI	STXBP2	CFI	LTF
MVP	DDB1	MVP	DDB1	LAMB3
EHD4	CTSB	EHD4	CTSB	CLTC
SERPINB7	FGB	SERPINB7	FGB	SPTAN1
STEAP4	MRC1	STEAP4	MRC1	CFH
TAGLN	FGG	TAGLN	FGG	TLN1
SLC4A1	F2	SLC4A1	F2	VCL
PRKAR2A	ITIH2	PRKAR2A	ITIH2	FCGBP
CLIC3	HRG	CLIC3	HRG	ANPEP
FER1L6	DPYSL3	FER1L6	DPYSL3	PIGR
CLIC4	HNRNPA2B1	CLIC4	HNRNPA2B1	FLNB
ATP13A4	C6	ATP13A4	C6	CP
PI3	ITIH4	PI3	ITIH4	LAMB1
EHD1	CHI3L1	EHD1	CHI3L1	PDCD6IP
GNAI2	EFEMP1	GNAI2	EFEMP1	SERPINA1
CIB1	HSPD1	CIB1	HSPD1	ACTN4
GNA14	ATP6V1B2	GNA14	ATP6V1B2	MYO1D
TSG101	HNRNPK	**TSG101**	HNRNPK	VCP
ACE	CTSC	ACE	CTSC	LCP1
CACNA2D2	ATP6V1A	CACNA2D2	ATP6V1A	LAMC1
SLC44A2	KLK7	SLC44A2	KLK7	HSPA5
MAP1B	ATP12A	MAP1B	ATP12A	MYH9
FAM129A	KLK10	FAM129A	KLK10	TGFBI
RAB11B; RAB11A	PPIB	**RAB11B;RAB11A**	PPIB	EEF2
NCKAP1	C8A	NCKAP1	C8A	HSPA8
CNP	CHIT1	CNP	CHIT1	TKT
RAB2A; RAB2B	MYO5C	RAB2A;RAB2B	MYO5C	ANXA2;ANXA2P2
FLOT2	AGT	FLOT2	AGT	BPIFB1
SLC15A2	LRG1	SLC15A2	LRG1	EZR
ALOX15	HYOU1	ALOX15	HYOU1	LTA4H
EHD2	MDH2	EHD2	MDH2	MSN
CPNE3	MMP1	CPNE3	MMP1	ENO1
TXNL1	CA1	TXNL1	CA1	MPO
FSCN1	PYGL	FSCN1	PYGL	CFB
CAPN5	C8B	CAPN5	C8B	GC
TMC4	LEG1	TMC4	LEG1	**HSP90AA1**
CAND1	SERPINA4	CAND1	SERPINA4	APOA1
DES	PGLYRP2	DES	PGLYRP2	ANXA1

VAT1L	IGHD	VAT1L	IGHD	C5
GNA11	FASN	GNA11	FASN	P4HB
GNAS	IGFBP7	GNAS	IGFBP7	CLIC6
DSC1	PSAP	DSC1	PSAP	UBA1
PPP3CA; PPP3CB	AKR1B1	PPP3CA;PPP3CB	AKR1B1	SERPINB3;SERPINB4
GGT1;GGT2; GGT3P	PNP	GGT1;GGT2;GGT3P	PNP	ALDH1A1
VILL	GSTO1	VILL	GSTO1	SPTBN1
ATP1A1	AMBP	ATP1A1	AMBP	**HSP90B1**
ATP8B1	HSPA4	ATP8B1	HSPA4	PGK1
PSMB5	NCL	PSMB5	NCL	SFTPB
SYTL1	DDX39B;DDX39A	SYTL1	DDX39B;DDX39A	SLC34A2
SLC9A3R2	PABPC1	SLC9A3R2	PABPC1	BAIAP2
GNAI3	CDH1	GNAI3	CDH1	ECM1
GPRC5C	NRP2	GPRC5C	NRP2	QSOX1
PRKCD	CRYM	PRKCD	CRYM	YWHAE
GIPC1	LZTFL1	GIPC1	LZTFL1	CAT
CTTN	CFD	CTTN	CFD	ALDOA
PTPN13	SERPIND1	PTPN13	SERPIND1	ANXA5
CYFIP1	AZU1	CYFIP1	AZU1	HP;HPR
COPS4	AHSG	COPS4	AHSG	GDI2
STK24	HARS	STK24	HARS	ANXA4
RAB3D	CCT8	RAB3D	CCT8	DMBT1
ABCA3	SEPT7	ABCA3	SEPT7	C7
ATP1B1	PGM2	ATP1B1	PGM2	DPP4
PDCD10	TPM4	PDCD10	TPM4	LMNA
GNG12	CFHR1	GNG12	CFHR1	IDH1
RP2	TFRC	RP2	TFRC	PGD
GBE1	RBP4	GBE1	RBP4	SERPINB1
YES1	CRTAC1	YES1	CRTAC1	SELENBP1
RAB7A	LGALS1	**RAB7A**	LGALS1	HPX
S100A16	TCN1	S100A16	TCN1	ACTN1
PAFAH1B1	F12	PAFAH1B1	F12	PLG
RAB14	ORM1	RAB14	ORM1	NPEPPS
CD36	GANAB	CD36	GANAB	EPS8
SMPDL3B	RPLP0;RPLP0P6	SMPDL3B	RPLP0;RPLP0P6	JUP
VPS28	CA2	VPS28	CA2	TPI1
PLSCR1	GRN	PLSCR1	GRN	ANXA3
RAB27B	APOB	**RAB27B**	APOB	PROM1
GNAI1	ACO1	GNAI1	ACO1	PGM1
CPA4	SERPINI1	CPA4	SERPINI1	ALDH3B1
C6orf132	PPP2R4	C6orf132	PPP2R4	SFN
GGT5	PLEC	GGT5	PLEC	**ANXA11**
RAB10	DPP3	RAB10	DPP3	CNDP2
PPP1CB; PPP1CC; PPP1CA	HNRNPD	PPP1CB;PPP1CC; PPP1CA	HNRNPD	ANXA6
ARRDC1	BLVRA	ARRDC1	BLVRA	SERPINA3
RAB5B	PROS1	**RAB5B**	PROS1	LGALS3BP
CDHR3	PEPD	CDHR3	PEPD	SARG
CPNE2	C1QB	CPNE2	C1QB	AKR1A1
PROM2	LAP3	PROM2	LAP3	ALPL
MYO1G	COTL1	MYO1G	COTL1	MSLN

BAIAP2L1	MMP7	BAIAP2L1	MMP7	SLC9A3R1
MPP5	TIMP1	MPP5	TIMP1	HSPA1A;HSPA1B
GNB2	SERPINF2	GNB2	SERPINF2	GPI
VPS37B	NPC2	VPS37B	NPC2	ICAM1
RAB35	ELANE	**RAB35**	ELANE	CLU
SLC5A1	PRTN3	SLC5A1	PRTN3	IGHM
RAB5C	PDIA6	**RAB5C**	PDIA6	GAPDH
IST1	SARS	IST1	SARS	AMY1A;AMY2B;AMY2A
CYBRD1	HPRT1	CYBRD1	HPRT1	SUSD2
SLC6A14	GOT2	SLC6A14	GOT2	TGM2
TPR	SPINT1	TPR	SPINT1	DPYSL2
EPX	CCT5	EPX	CCT5	ACTR3
GFPT1	CPE	GFPT1	CPE	LDHA
RAB34	PA2G4	RAB34	PA2G4	WDR1
GPR116	PSMD11	GPR116	PSMD11	APOH
TMPRSS2	COPG1	TMPRSS2	COPG1	TPM3
GLIPR2	MUC5AC	GLIPR2	MUC5AC	TGM3
CAMP	SET;SETSIP	CAMP	SET;SETSIP	DSG1
ARF4	PAM	ARF4	PAM	FGA
TACSTD2	VASP	TACSTD2	VASP	YWHAZ
ALPP;ALPI; ALPPL2	FABP4	ALPP;ALPI;ALPPL2	FABP4	CTSD
ARHGAP18	TXNRD1	ARHGAP18	TXNRD1	ANXA7
PACSIN3	IGFBP2	PACSIN3	IGFBP2	GDI1
PDCD6	SERPINA7	PDCD6	SERPINA7	TYMP
ACSL4	PEBP4	ACSL4	PEBP4	A1BG
RAB5A	C1QC	RAB5A	C1QC	AGRN
ASS1	PGLYRP1	ASS1	PGLYRP1	CAPN1
TGM1	BPIFA1	TGM1	BPIFA1	FBP1
RAB1A	ORM2	RAB1A	ORM2	SERPING1
PACSIN2	EML2	PACSIN2	EML2	WARS
TLR5	FOLR3	TLR5	FOLR3	MDH1
S100A14	TSN	S100A14	TSN	**HSP90AB1**
RALB	HNRNPA3	RALB	HNRNPA3	KNG1
RAB8A	GLUL	RAB8A	GLUL	EPS8L2
ENTPD3	RAD23B	ENTPD3	RAD23B	AHCY
GPX4	APOA2	GPX4	APOA2	YWHAH
NCSTN	RBMX	NCSTN	RBMX	PARK7
MVB12A	GPC1	MVB12A	GPC1	LDHB
CHMP2A	ERP29	CHMP2A	ERP29	AZGP1
RHOF	GGH	RHOF	GGH	ALDOC
RRAS	PLD3	RRAS	PLD3	CALR
VAMP8	ADH5	VAMP8	ADH5	SERPINF1
CCT3	CORO1C	CCT3	CORO1C	YWHAQ
HSPA2	KLK11	HSPA2	KLK11	RNH1
RAB22A	PLXDC2	RAB22A	PLXDC2	CD55
DLAT	ADH1C;ADH1A	DLAT	ADH1C;ADH1A	STOM
GNAO1	GLO1	GNAO1	GLO1	PRDX6
AK3	FDPS	AK3	FDPS	ALDH3A1
LIN7C	TPP1	LIN7C	TPP1	CLIC1
FRK	CLEC3B	FRK	CLEC3B	LCN2
PAFAH1B2	SAMHD1	PAFAH1B2	SAMHD1	PLS1

PTPRJ	IGHV3-38	PTPRJ	IGHV3-38	RDX
QDPR	RNASE1	QDPR	RNASE1	MUC4
CCNY	CS	CCNY	CS	C9
CD47	S100A12	CD47	S100A12	EEF1G
SLC44A4	NSFL1C	SLC44A4	NSFL1C	SERPINB12
NEDD4L; NEDD4	FSTL1	NEDD4L;NEDD4	FSTL1	PSMA6
GRB2	EEF1D	GRB2	EEF1D	YWHAG
RAB21	PPA1	RAB21	PPA1	HSPB1
CEP290	FAM49B	CEP290	FAM49B	CALM3;CALM2;CALM1
SCAMP2	EIF5A;EIF5AL1	SCAMP2	EIF5A;EIF5AL1	CAPG
TLR2	PRMT1	TLR2	PRMT1	PPIA
SLC11A2	PLBD1	SLC11A2	PLBD1	TPPP3
MGLL	HNRNPH1; HNRNPH2; HNRNPF	MGLL	HNRNPH1;HNRNPH2;HNRNPF	CAPS
DNAJC5	ST13;ST13P4; ST13P5	DNAJC5	ST13;ST13P4;ST13P5	S100A9
CLDN3	PDIA4	CLDN3	PDIA4	SFTPA2;SFTPA1
RRAS2	DNAH5	RRAS2	DNAH5	PSMA1
ATP11A	PSMD2	ATP11A	PSMD2	NUCB1
RAP1B	CUL4B	RAP1B	CUL4B	PSME1
RAP2B	CTSZ	RAP2B	CTSZ	ITIH1
STOML3	LAMA5	STOML3	LAMA5	CD163
CD82	IL1RN	CD82	IL1RN	CORO1A
TMEM67	PTMA	TMEM67	PTMA	PGAM1
ATP9A	PPP5C	ATP9A	PPP5C	NID1
AP2B1	CCT7	AP2B1	CCT7	PPP2R1A
F11R	GNB2L1	F11R	GNB2L1	STXBP1
WASF2	ESD	WASF2	ESD	LYN
ENPP3	HMGB1	ENPP3	HMGB1	DSTN
SLC2A1	PYCARD	SLC2A1	PYCARD	ALDH9A1
CALB2	SH3BGRL	CALB2	SH3BGRL	BASP1
BDH2	SOD3	BDH2	SOD3	CAPZB
ME1	C4A	ME1	C4A	CKB
MISP	CRISP3	MISP	CRISP3	FTH1
TFG	SCGB1D1	TFG	SCGB1D1	CFL1
RAB6B; RAB6A	C8G	RAB6B;RAB6A	C8G	PRDX5
SH3BP4	IGHV3-15	SH3BP4	IGHV3-15	GSTP1
CHMP4C	RNASE2	CHMP4C	RNASE2	S100A8
BROX	IGHV3-49	BROX	IGHV3-49	IGHA1
RAB27A	KLK13	**RAB27A**	KLK13	PLS3
CRIP2	AK2	CRIP2	AK2	ACTR2
ARF6	PEA15	**ARF6**	PEA15	ATIC
VTA1	TTN	VTA1	TTN	SLK
LAMP3	PTGDS	LAMP3	PTGDS	FABP5
SLC5A8	TXNDC17	SLC5A8	TXNDC17	BLMH
DNAH6	PTGR2	DNAH6	PTGR2	APOE
MUC21	PCBD1	MUC21	PCBD1	YWHAB
CPNE1	GLUD1;GLUD2	CPNE1	GLUD1;GLUD2	GPRC5A

HIST1H1C; HIST1H1E; HIST1H1D; HIST1H1T; HIST1H1A	AARS	HIST1H1C;HIST1H1E; HIST1H1D;HIST1H1T; HIST1H1A	AARS	PRDX1
AQP5	CRK	AQP5	CRK	LGALS3
TMEM231	VSIG8	TMEM231	VSIG8	IGJ
CDSN	SHBG	CDSN	SHBG	IGKC
ARF3;ARF1	ACAT2	ARF3;ARF1	ACAT2	IGHG1
SUGT1	CACYBP	SUGT1	CACYBP	CSTA
RAB25	EIF2S1	RAB25	EIF2S1	VTN
RUVBL1	PPP1R7	RUVBL1	PPP1R7	TTR
RUVBL2	PON1	RUVBL2	PON1	CASP14
SLC22A4	HNRNPC	SLC22A4	HNRNPC	CAPN2
SMIM1	MAPRE1	SMIM1	MAPRE1	MYO6
HLA-DQB1	PRDX4	HLA-DQB1	PRDX4	DDAH1
ACP1	FKBP2	ACP1	FKBP2	PSMB2
TMEM30A	COL6A2	TMEM30A	COL6A2	PSMB1
ARF5	EIF3I	ARF5	EIF3I	KCTD12
SLC1A1	TARS	SLC1A1	TARS	GNB1
SLC3A2	MAT2A	SLC3A2	MAT2A	PSMA7
TMEM30B	DDAH2	TMEM30B	DDAH2	TAGLN2
ADAM10	EEF1B2	**ADAM10**	EEF1B2	AK1
UBL3	BCAM	UBL3	BCAM	PEBP1
MYADM	PRKCSH	MYADM	PRKCSH	CD14
PLLP	NUDC	PLLP	NUDC	FTL
LY6D	HK3	LY6D	HK3	CTSH
PDZK1IP1	BTD	PDZK1IP1	BTD	LCN1
S100A10	TWF2	S100A10	TWF2	HBB
TOLLIP	WFDC2	TOLLIP	WFDC2	NAPSA
AQP1	GPNMB	AQP1	GPNMB	LYZ
GNG5	CHMP2B	GNG5	CHMP2B	IGHG2
CYSTM1	LXN	CYSTM1	LXN	KPNB1
MAL2	FBXO24	MAL2	FBXO24	GNAQ
CLTA	IGKV1-17	CLTA	IGKV1-17	VAT1
PHACTR4	IGLV8-61	PHACTR4	IGLV8-61	ARPC2
MYO1F; MYO1E	PGC	MYO1F;MYO1E	PGC	SERPINB6
NAPRT	IGHV4-28	NAPRT	IGHV4-28	SERPINA6
BBS1	GSN	BBS1	GSN	TALDO1
RAB23	IGHV5-51	RAB23	IGHV5-51	UGP2
NOS2	PRKAR1A	NOS2	PRKAR1A	CAB39
TAOK1	IGHV3-21	TAOK1	IGHV3-21	GSDMA
BBS2	IGHV3-64D	BBS2	IGHV3-64D	PSMA5
DYNC1H1	RPL10A	DYNC1H1	RPL10A	MYL6
ITGA3	FERMT3	ITGA3	FERMT3	CAPZA1
MOB1A; MOB1B	CADM1	MOB1A;MOB1B	CADM1	S100A11
HNMT	GALM	HNMT	GALM	ARHGDIA
MUC16	DAG1	MUC16	DAG1	BPIFB2
ANXA13	IGHV1-18	ANXA13	IGHV1-18	PRDX2
SRC	IGHV1-2	SRC	IGHV1-2	CD44
PRDM5	AGR2	PRDM5	AGR2	PFN1
HLA-DRB4	KRT18	HLA-DRB4	KRT18	SFTPD

CRB3	UBE2V1	CRB3	UBE2V1	IGHG4
PLEKHS1	TBCA	PLEKHS1	TBCA	HBD
MYL12A; MYL12B; MYL9	HEXB	MYL12A;MYL12B; MYL9	HEXB	CMPK1
PMM2	ST6GALNAC1	PMM2	ST6GALNAC1	CCT2
SHANK2	VSIG4	SHANK2	VSIG4	BLVRB
TSTA3	HBG2;HBG1	TSTA3	HBG2;HBG1	ASAH1
CHMP1A	UBE2I	CHMP1A	UBE2I	ZG16B
ABI1	GSTA1;GSTA3	ABI1	GSTA1;GSTA3	BPNT1
KALRN	ITPRIPL1	KALRN	ITPRIPL1	HNRNPA1;HNRNPA1L2
CLIC2	ATP6V1C1	CLIC2	ATP6V1C1	DUOX1
DUOXA1	IGHV2-70; IGHV2-70D	DUOXA1	IGHV2-70;IGHV2-70D	SNAP23
NTM	GPX3	NTM	GPX3	**FLOT1**
RHOG	TP63	RHOG	TP63	STK26
SKP1	DPP7	SKP1	DPP7	MARCKS
PFN2	FKBP1A	PFN2	FKBP1A	SRI
LRRC15	AKR1C3	LRRC15	AKR1C3	PSMA3
SDCBP	PRR4	**SDCBP**	PRR4	PSMA2
SDCBP	RETN	HLA-DRB1	RETN	APOD
SBSN	VIMP	MYO1C	VIMP	CAPNS1
HLA-DRB1	NIT2	UGDH	NIT2	PGLS
MYO1C	CSF1	GNB4	CSF1	RPSA
UGDH	APCS	RAB8B	APCS	CPM
GNB4	STAT4	POF1B	STAT4	TXN
RAB8B	KLKB1;F11	PLCD1	KLKB1;F11	ACTC1;ACTA1;ACTA2;ACTG2
POF1B	KHDRBS1	CYFIP2	KHDRBS1	HIST1H4A
PLCD1	QPCT	RAB13	QPCT	PIP
CYFIP2	LHPP	RHOC	LHPP	SLPI
RAB13	FRAS1	ATP4A	FRAS1	EEF1A1;EEF1A1P5
RHOC	SEC22B		SEC22B	LUM
ATP4A	RANBP1		RANBP1	HBA1
C3	PSMD14		PSMD14	ENO2
TF	SSB		SSB	RNPEP
FLNA	C4B		C4B	C16orf89
LAMA3	CRYZ		CRYZ	GSR
A2M	SERPINH1		SERPINH1	HLA-DRA
DSP	CAP1		IGKV A18;IGKV2D-29;IGKV2D-26	SORD
MUC5B	IGKV A18; IGKV2D-29; IGKV2D-26		IGHV1-3	ARG1
MYOF	GSN		IGLV2-8	CAPZA2
IQGAP1	IGHV1-3		IGHV3-20	LGALS7
LTF	IGLV2-8		IGKV3D-15	APRT
LAMB3	IGHV3-20		IGHV1-46	PSMB3
CLTC	IGKV3D-15		IGKV1-6;IGKV1-12	ATRN
SPTAN1	IGHV1-46		CST4;CST1	PSMA4
CFH	IGKV1-6;IGKV1-12		IGLV3-16	MUC1

TLN1	CST4;CST1		EPPK1	HIST1H2BL;HIST1H2BM; HIST1H2BN;HIST1H2BH; HIST2H2BF;HIST1H2BC; HIST1H2BD;H2BFS; HIST1H2BK;HIST2H2BE; HIST1H2BB;HIST1H2BO; HIST1H2BJ;HIST3H2BB; HIST1H2BA
VCL	IGLV3-16		IGLC7	IGHG3
FCGBP	EPPK1		HIST1H3A;HIST3H3;H3F3C	RAN
ANPEP	IGLC7		ADH1B	GSS
PIGR	HIST1H3A;HIST3H3;H3F3C		IGKV1-8	NAGK
FLNB	ADH1B		IGKV2D-28	EFHD2
CP	IGKV1-8		IGKV2-40	CTSS
LAMB1	IGKV2D-28		PRB4	GLOD4
PDCD6IP	IGKV2-40		IGHV1-69	CTSG
SERPINA1	PRB4		IGHV1-69-2	RAC1;RAC2
ACTN4	IGHV1-69			PSME2
MYO1D	IGHV1-69-2			CBR1
VCP	C3			**CD9**
LCP1	TF			ARHGDIB
LAMC1	FLNA			CST3
HSPA5	LAMA3			PODXL
MYH9	A2M			GOT1
TGFBI	DSP			ARPC1B
EEF2	MUC5B			OTUB1
HSPA8	MYOF			ITGAM
TKT	IQGAP1			CORO1B
ANXA2; ANXA2P2	LTF			GNA13
BPIFB1	LAMB3			CALML5
EZR	CLTC			GMPPB
LTA4H	SPTAN1			CDC42
MSN	CFH			RHOA
ENO1	TLN1			GOLM1
MPO	VCL			PCBP1
CFB	FCGBP			PDXK
GC	ANPEP			UBA52;RPS27A;UBB;UBC
HSP90AA1	PIGR			DBNL
APOA1	FLNB			TPT1
ANXA1	CP			ARPC3
C5	LAMB1			G6PD
P4HB	PDCD6IP			UBE2L3
CLIC6	SERPINA1			ARPC4
UBA1	ACTN4			SOD1
SERPINB3; SERPINB4	MYO1D			ABHD14B
ALDH1A1	VCP			CEACAM5
SPTBN1	LCP1			VPS4B
HSP90B1	LAMC1			CHMP4B
PGK1	HSPA5			PKP1
SFTPB	MYH9			GGCT
SLC34A2	TGFBI			CCT4

BAIAP2	EEF2			ALAD
ECM1	HSPA8			SEPT9
QSOX1	TKT			KLK8
YWHAE	ANXA2;ANXA2P2			UCHL3
CAT	BPIFB1			MYH14
ALDOA	EZR			CPPED1
ANXA5	LTA4H			PSMB8
HP;HPR	MSN			S100P
GDI2	ENO1			DCD
ANXA4	MPO			CSTB
DMBT1	CFB			IGKV4-1
C7	GC			CD59
DPP4	**HSP90AA1**			S100A6
LMNA	APOA1			SCGB1A1
IDH1	ANXA1			HSPH1
PGD	C5			LASP1
SERPINB1	P4HB			S100A7;S100A7A
SELENBP1	CLIC6			KIF5A;KIF5C;KIF5B
HPX	UBA1			FCGR3A;FCGR3B
ACTN1	SERPINB3;SERPINB4			NANS
PLG	ALDH1A1			TUBB4B;TUBB4A
NPEPPS	SPTBN1			IGLV1-51
EPS8	**HSP90B1**			B2M
JUP	PGK1			**TSPAN1**
TPI1	SFTPB			HEBP2
ANXA3	SLC34A2			UBE2N;UBE2NL
PROM1	BAIAP2			USP5
PGM1	ECM1			PEF1
ALDH3B1	QSOX1			NUDT5
SFN	YWHAE			NCCRP1
ANXA11	CAT			MAPK1
CNDP2	ALDOA			PRSS8
ANXA6	ANXA5			**LAMP1**
SERPINA3	HP;HPR			SH3BGRL3
LGALS3BP	GDI2			PKM
SARG	ANXA4			CEACAM6
AKR1A1	DMBT1			SCGB3A1
ALPL	C7			IGLV3-19
MSLN	DPP4			IGHV4-61
SLC9A3R1	LMNA			IGLL5;IGLC1
HSPA1A; HSPA1B	IDH1			RAB1B
GPI	PGD			CSRP1
ICAM1	SERPINB1			HAGH
CLU	SELENBP1			OLA1
IGHM	HPX			PSMB7
GAPDH	ACTN1			NME2;NME2P1
AMY1A; AMY2B; AMY2A	PLG			**CD63**
SUSD2	NPEPPS			IGHV3-72
TGM2	EPS8			IGHV6-1

DPYSL2	JUP			IGLV3-9
ACTR3	TPI1			IGHA2
LDHA	ANXA3			SCGB3A2
WDR1	PROM1			GNG7
APOH	PGM1			BSN
TPM3	ALDH3B1			STX3
TGM3	SFN			IPO5
DSG1	**ANXA11**			LAMP2
FGA	CNDP2			RNASE3
YWHAZ	ANXA6			ITGB2
CTSD	SERPINA3			DNPH1
ANXA7	LGALS3BP			C11orf54
GDI1	SARG			VPS35
TYMP	AKR1A1			HNRNPL
A1BG	ALPL			HLA-C;HLA-H;HLA-A
AGRN	MSLN			SEPT11
CAPN1	SLC9A3R1			PCBP2;PCBP3
FBP1	HSPA1A;HSPA1B			C1S
SERPING1	GPI			CHMP6
SBSN	ICAM1			NAPA
WARS	CLU			PTGES3
MDH1	IGHM			CST6
HSP90AB1	GAPDH			FOLR1
KNG1	AMY1A;AMY2B; AMY2A			DEFA3;DEFA1
EPS8L2	SUSD2			IGKV3D-11
AHCY	TGM2			IGKV3-20
YWHAH	DPYSL2			SNX3
PARK7	ACTR3			CD5L
LDHB	LDHA			PSCA
AZGP1	WDR1			PSMB6
ALDOC	APOH			PRB3
CALR	TPM3			MIF
SERPINF1	TGM3			FN1
YWHAQ	DSG1			IGLV7-46
RNH1	FGA			IGHV3-43D;IGHV3-9
CD55	YWHAZ			IFI30
STOM	CTSD			GSTA2
PRDX6	ANXA7			IGLV1-44;IGLV1-47
ALDH3A1	GDI1			IGKV2-24;IGKV2D-24
CLIC1	TYMP			DMD
LCN2	A1BG			PSMB9
PLS1	AGRN			TMSB4X
RDX	CAPN1			CDK4;CDK14;CDK12;CDK13; CDK16;CDK17;CDK18;CDK9; CDK15;CDK5;CDK6;CDK3; CDK2;CDK1
MUC4	FBP1			KPRP
C9	SERPING1			TBC1D10A
EEF1G	SBSN			CHMP1B
SERPINB12	WARS			**CD151**
PSMA6	MDH1			PHPT1

YWHAG	**HSP90AB1**			FBLN1
HSPB1	KNG1			DNM2;DNM3
CALM3; CALM2; CALM1	EPS8L2			IGLC6
CAPG	AHCY			HSPA6;HSPA7
PPIA	YWHAH			ACTB
TPPP3	PARK7			ACTG1
CAPS	LDHB			IGKV3D-7;IGKV3-7
S100A9	AZGP1			IGHV3-43
SFTPA2; SFTPA1	ALDOC			FBP2
PSMA1	CALR			CAP1
NUCB1	SERPINF1			TUBA1A;TUBA3E
PSME1	YWHAQ			IGKV3D-20
ITIH1	RNH1			ACTBL2
CD163	CD55			SPP1
CORO1A	STOM			NME1
PGAM1	PRDX6			TUBA4A
NID1	ALDH3A1			
PPP2R1A	CLIC1			
STXBP1	LCN2			
LYN	PLS1			
DSTN	RDX			
ALDH9A1	MUC4			
BASP1	C9			
CAPZB	EEF1G			
CKB	SERPINB12			
FTH1	PSMA6			
CFL1	YWHAG			
PRDX5	HSPB1			
GSTP1	CALM3;CALM2; CALM1			
S100A8	CAPG			
IGHA1	PPIA			
PLS3	TPPP3			
ACTR2	CAPS			
ATIC	S100A9			
SLK	SFTPA2;SFTPA1			
FABP5	PSMA1			
BLMH	NUCB1			
APOE	PSME1			
YWHAB	ITIH1			
GPRC5A	CD163			
PRDX1	CORO1A			
LGALS3	PGAM1			
IGJ	NID1			
IGKC	PPP2R1A			
IGHG1	STXBP1			
CSTA	LYN			
VTN	DSTN			
TTR	ALDH9A1			
CASP14	BASP1			
CAPN2	CAPZB			

MYO6	CKB			
DDAH1	FTH1			
PSMB2	CFL1			
PSMB1	PRDX5			
KCTD12	GSTP1			
GNB1	S100A8			
PSMA7	IGHA1			
TAGLN2	PLS3			
AK1	ACTR2			
PEBP1	ATIC			
CD14	SLK			
FTL	FABP5			
CTSH	BLMH			
LCN1	APOE			
HBB	YWHAB			
NAPSA	GPRC5A			
LYZ	PRDX1			
IGHG2	LGALS3			
KPNB1	IGJ			
GNAQ	IGKC			
VAT1	IGHG1			
ARPC2	CSTA			
SERPINB6	VTN			
SERPINA6	TTR			
TALDO1	CASP14			
UGP2	CAPN2			
CAB39	MYO6			
GSDMA	DDAH1			
PSMA5	PSMB2			
MYL6	PSMB1			
CAPZA1	KCTD12			
S100A11	GNB1			
ARHGDIA	PSMA7			
BPIFB2	TAGLN2			
PRDX2	AK1			
CD44	PEBP1			
PFN1	CD14			
SFTPD	FTL			
IGHG4	CTSH			
HBD	LCN1			
CMPK1	HBB			
CCT2	NAPSA			
BLVRB	LYZ			
ASAH1	IGHG2			
ZG16B	KPNB1			
BPNT1	GNAQ			
HNRNPA1; HNRNPA1L2	VAT1			
DUOX1	ARPC2			
SNAP23	SERPINB6			
FLOT1	SERPINA6			

STK26	TALDO1			
MARCKS	UGP2			
SRI	CAB39			
PSMA3	GSDMA			
PSMA2	PSMA5			
APOD	MYL6			
CAPNS1	CAPZA1			
PGLS	S100A11			
RPSA	ARHGDIA			
CPM	BPIFB2			
TXN	PRDX2			
ACTC1; ACTA1; ACTA2; ACTG2	CD44			
HIST1H4A	PFN1			
PIP	SFTPD			
SLPI	IGHG4			
EEF1A1; EEF1A1P5	HBD			
LUM	CMPK1			
HBA1	CCT2			
ENO2	BLVRB			
RNPEP	ASAH1			
C16orf89	ZG16B			
GSR	BPNT1			
HLA-DRA	HNRNPA1; HNRNPA1L2			
SORD	DUOX1			
ARG1	SNAP23			
CAPZA2	**FLOT1**			
LGALS7	STK26			
APRT	MARCKS			
PSMB3	SRI			
ATRN	PSMA3			
PSMA4	PSMA2			
MUC1	APOD			
HIST1H2BL; HIST1H2BM ;HIST1H2BN ;HIST1H2BH ;HIST2H2BF; HIST1H2BC; HIST1H2BD; H2BFS;HIST 1H2BK;HIST 2H2BE;HIST 1H2BB;HIST 1H2BO;HIST 1H2BJ;HIST 3H2BB;HIST 1H2BA	CAPNS1			

IGHG3	PGLS			
RAN	RPSA			
GSS	CPM			
NAGK	TXN			
EFHD2	ACTC1;ACTA1; ACTA2;ACTG2			
CTSS	HIST1H4A			
GLOD4	PIP			
CTSG	SLPI			
RAC1;RAC2	EEF1A1;EEF1A1P5			
PSME2	LUM			
CBR1	HBA1			
CD9	ENO2			
ARHGDIB	RNPEP			
CST3	C16orf89			
PODXL	GSR			
GOT1	HLA-DRA			
ARPC1B	SORD			
OTUB1	ARG1			
ITGAM	CAPZA2			
CORO1B	LGALS7			
GNA13	APRT			
CALML5	PSMB3			
GMPPB	ATRN			
CDC42	PSMA4			
RHOA	MUC1			
GOLM1	HIST1H2BL; HIST1H2BM; HIST1H2BN; HIST1H2BH; HIST2H2BF; HIST1H2BC; HIST1H2BD; H2BFS; HIST1H2BK; HIST2H2BE; HIST1H2BB; HIST1H2BO; HIST1H2BJ; HIST3H2BB; HIST1H2BA			
PCBP1	IGHG3			
PDXK	RAN			
UBA52; RPS27A; UBB; UBC	GSS			
DBNL	NAGK			
TPT1	EFHD2			
ARPC3	CTSS			
G6PD	GLOD4			
UBE2L3	CTSG			
ARPC4	RAC1;RAC2			
SOD1	PSME2			
ABHD14B	CBR1			

CEACAM5	**CD9**			
VPS4B	ARHGDIB			
CHMP4B	CST3			
PKP1	PODXL			
GGCT	GOT1			
CCT4	ARPC1B			
ALAD	OTUB1			
SEPT9	ITGAM			
KLK8	CORO1B			
UCHL3	GNA13			
MYH14	CALML5			
CPPED1	GMPPB			
PSMB8	CDC42			
S100P	RHOA			
DCD	GOLM1			
CSTB	PCBP1			
IGKV4-1	PDXK			
CD59	UBA52;RPS27A; UBB;UBC			
S100A6	DBNL			
SCGB1A1	TPT1			
HSPH1	ARPC3			
LASP1	G6PD			
S100A7; S100A7A	UBE2L3			
KIF5A;KIF5C ;KIF5B	ARPC4			
FCGR3A; FCGR3B	SOD1			
NANS	ABHD14B			
TUBB4B; TUBB4A	CEACAM5			
IGLV1-51	VPS4B			
B2M	CHMP4B			
TSPAN1	PKP1			
HEBP2	GGCT			
UBE2N; UBE2NL	CCT4			
USP5	ALAD			
PEF1	SEPT9			
NUDT5	KLK8			
NCCRP1	UCHL3			
MAPK1	MYH14			
PRSS8	CPPED1			
LAMP1	PSMB8			
SH3BGRL3	S100P			
PKM	DCD			
CEACAM6	CSTB			
SCGB3A1	IGKV4-1			
IGLV3-19	CD59			
IGHV4-61	S100A6			
IGLL5;IGLC1	SCGB1A1			
RAB1B	HSPH1			
CSRP1	LASP1			
HAGH	S100A7;S100A7A			

OLA1	KIF5A;KIF5C;KIF5B			
PSMB7	FCGR3A;FCGR3B			
NME2; NME2P1	NANS			
CD63	TUBB4B;TUBB4A			
IGHV3-72	IGLV1-51			
IGHV6-1	B2M			
IGLV3-9	**TSPAN1**			
IGHA2	HEBP2			
SCGB3A2	UBE2N;UBE2NL			
GNG7	USP5			
BSN	PEF1			
STX3	NUDT5			
IPO5	NCCRP1			
LAMP2	MAPK1			
RNASE3	PRSS8			
ITGB2	**LAMP1**			
DNPH1	SH3BGRL3			
C11orf54	PKM			
VPS35	CEACAM6			
HNRNPL	SCGB3A1			
HLA-C; HLA-H; HLA-A	IGLV3-19			
SEPT11	IGHV4-61			
PCBP2;PCBP3	IGLL5;IGLC1			
C1S	RAB1B			
CHMP6	CSRP1			
NAPA	HAGH			
PTGES3	OLA1			
CST6	PSMB7			
FOLR1	NME2;NME2P1			
DEFA3; DEFA1	**CD63**			
IGKV3D-11	IGHV3-72			
IGKV3-20	IGHV6-1			
SNX3	IGLV3-9			
CD5L	IGHA2			
PSCA	SCGB3A2			
PSMB6	GNG7			
PRB3	BSN			
MIF	STX3			
FN1	IPO5			
IGLV7-46	LAMP2			
IGHV3-43D; IGHV3-9	RNASE3			
IFI30	ITGB2			
GSTA2	DNPH1			
IGLV1-44; IGLV1-47	C11orf54			
IGKV2-24; IGKV2D-24	VPS35			
DMD	HNRNPL			
PSMB9	HLA-C;HLA-H;HLA-A			
TMSB4X	SEPT11			

CDK4;CDK14;CDK12; CDK13; CDK16; CDK17; CDK18; CDK9; CDK15; CDK5; CDK6; CDK3; CDK2; CDK1	PCBP2;PCBP3			
KPRP	C1S			
TBC1D10A	CHMP6			
CHMP1B	NAPA			
CD151	PTGES3			
PHPT1	CST6			
FBLN1	FOLR1			
DNM2; DNM3	DEFA3;DEFA1			
IGLC6	IGKV3D-11			
HSPA6; HSPA7	IGKV3-20			
ACTB	SNX3			
ACTG1	CD5L			
IGKV3D-7; IGKV3-7	PSCA			
IGHV3-43	PSMB6			
FBP2	PRB3			
CAP1	MIF			
TUBA1A; TUBA3E	FN1			
IGKV3D-20	IGLV7-46			
ACTBL2	GHV3-43D;IGHV3-9			
SPP1	IFI30			
NME1	GSTA2			
TUBA4A	IGLV1-44;IGLV1-47			
	IGKV2-24; IGKV2D-24			
	DMD			
	PSMB9			
	TMSB4X			
	CDK4;CDK14; CDK12; CDK13; CDK16; CDK17; CDK18; CDK9; CDK15; CDK5; CDK6; CDK3; CDK2; CDK1			

	KPRP			
	TBC1D10A			
	CHMP1B			
	CD151			
	PHPT1			
	FBLN1			
	DNM2;DNM3			
	IGLC6			
	HSPA6;HSPA7			
	ACTB			
	ACTG1			
	IGKV3D-7;IGKV3-7			
	IGHV3-43			
	FBP2			
	CAP1			
	TUBA1A;TUBA3E			
	IGKV3D-20			
	ACTBL2			
	SPP1			
	NME1			
	TUBA4A			

REFERENCES

1. Lenz C, Dihazi H. Introduction to Proteomics Technologies. Methods Mol Biol Clifton NJ. 2016;1362:3–27.

2. Pertea M, Shumate A, Pertea G, Varabyou A, Chang Y-C, Madugundu AK, et al. Thousands of large-scale RNA sequencing experiments yield a comprehensive new human gene list and reveal extensive transcriptional noise. bioRxiv. 2018 May 29;332825.

3. Aebersold R, Agar JN, Amster IJ, Baker MS, Bertozzi CR, Boja ES, et al. How many human proteoforms are there? Nat Chem Biol. 2018 Feb 14;14(3):206–14.

4. Steffen P, Kwiatkowski M, Robertson WD, Zarrine-Afsar A, Deterra D, Richter V, et al. Protein species as diagnostic markers. J Proteomics. 2016 Feb 16;134:5–18.

5. Smith LM, Kelleher NL, Consortium for Top Down Proteomics. Proteoform: a single term describing protein complexity. Nat Methods. 2013 Mar;10(3):186–7.

6. Aslam B, Basit M, Nisar MA, Khurshid M, Rasool MH. Proteomics: Technologies and Their Applications. J Chromatogr Sci. 2017 Feb;55(2):182–96.

7. Bedia, Carmen. "Experimental approaches in omic sciences." Comprehensive Analytical Chemistry. Vol. 82. Elsevier, 2018. 13-36.

8. Karahalil B. Overview of Systems Biology and Omics Technologies. Curr Med Chem. 2016;23(37):4221–30.

9. Tavassoly I, Goldfarb J, Iyengar R. Systems biology primer: the basic methods and approaches. Essays Biochem. 2018 26;62(4):487–500.

10. Doll S, Dreßen M, Geyer PE, Itzhak DN, Braun C, Doppler SA, et al. Region and cell-type resolved quantitative proteomic map of the human heart. Nat Commun. 2017 13;8(1):1469.

11. Luck K, Sheynkman GM, Zhang I, Vidal M. Proteome-Scale Human Interactomics. Trends Biochem Sci. 2017;42(5):342–54.

12. Kitano H. Systems biology: a brief overview. Science. 2002 Mar 1;295(5560):1662–4.

13. Meleady P. Two-Dimensional Gel Electrophoresis and 2D-DIGE. Methods Mol Biol Clifton NJ. 2018;1664:3–14.

14. Westermeier R. 2D gel-based Proteomics: there's life in the old dog yet. Arch Physiol Biochem. 2016 Dec;122(5):236–7.

15. Lilley KS, Razzaq A, Dupree P. Two-dimensional gel electrophoresis: recent advances in sample preparation, detection and quantitation. Curr Opin Chem Biol. 2002 Feb;6(1):46–50.

16. Han X, Aslanian A, Yates JR. Mass spectrometry for proteomics. Curr Opin Chem Biol. 2008 Oct;12(5):483–90.

17. Claassen M. Inference and validation of protein identifications. Mol Cell Proteomics MCP. 2012 Nov;11(11):1097–104.

18. Kortz L, Helmschrodt C, Ceglarek U. Fast liquid chromatography combined with mass spectrometry for the analysis of metabolites and proteins in human body fluids. Anal Bioanal Chem. 2011 Mar;399(8):2635–44.

19. Oliveira BM, Coorssen JR, Martins-de-Souza D. 2DE: the phoenix of proteomics. J Proteomics. 2014 Jun 2;104:140–50.

20. Khatri P, Sirota M, Butte AJ. Ten years of pathway analysis: current approaches and outstanding challenges. PLoS Comput Biol. 2012;8(2):e1002375.

21. Ashburner M, Ball CA, Blake JA, Botstein D, Butler H, Cherry JM, et al. Gene ontology: tool for the unification of biology. The Gene Ontology Consortium. Nat Genet. 2000 May;25(1):25–9.

22. Binns D, Dimmer E, Huntley R, Barrell D, O'Donovan C, Apweiler R. QuickGO: a web-based tool for Gene Ontology searching. Bioinformatics. 2009 Nov 15;25(22):3045–6.

23. Patel Krishna, Manika Singh, and Harsha Gowda. "Bioinformatics methods to deduce biological interpretation from proteomics data." Proteome Bioinformatics. Humana Press, New York, NY, 2017. 147-161.

24. Wu X, Hasan MA, Chen JY. Pathway and network analysis in proteomics. J Theor Biol. 2014 Dec 7;362:44–52.

25. Wu, Xiaogang, and Jake Y. Chen. "Molecular interaction networks: topological and functional characterizations." Automation in Proteomics and Genomics: An Engineering Case-Based Approach 145 (2009).

26. Harding C, Heuser J, Stahl P. Receptor-mediated endocytosis of transferrin and recycling of the transferrin receptor in rat reticulocytes. J Cell Biol. 1983 Aug;97(2):329–39.

27. Harding CV, Heuser JE, Stahl PD. Exosomes: looking back three decades and into the future. J Cell Biol. 2013 Feb 18;200(4):367–71.

28. Pan BT, Johnstone RM. Fate of the transferrin receptor during maturation of sheep reticulocytes in vitro: selective externalization of the receptor. Cell. 1983 Jul;33(3):967–78.

29. Stahl PD, Raposo G. Exosomes and extracellular vesicles: the path forward. Essays Biochem. 2018 15;62(2):119–24.

30. Doyle LM, Wang MZ. Overview of Extracellular Vesicles, Their Origin, Composition, Purpose, and Methods for Exosome Isolation and Analysis. Cells. 2019 15;8(7).

31. Abels ER, Breakefield XO. Introduction to Extracellular Vesicles: Biogenesis, RNA Cargo Selection, Content, Release, and Uptake. Cell Mol Neurobiol. 2016 Apr;36(3):301–12.

32. Kalra H, Simpson RJ, Ji H, Aikawa E, Altevogt P, Askenase P, et al. Vesiclepedia: a compendium for extracellular vesicles with continuous community annotation. PLoS Biol. 2012;10(12):e1001450.

33. Théry C, Boussac M, Véron P, Ricciardi-Castagnoli P, Raposo G, Garin J, et al. Proteomic analysis of dendritic cell-derived exosomes: a secreted subcellular compartment distinct from apoptotic vesicles. J Immunol Baltim Md 1950. 2001 Jun 15;166(12):7309–18.

34. Yáñez-Mó M, Siljander PR-M, Andreu Z, Zavec AB, Borràs FE, Buzas EI, et al. Biological properties of extracellular vesicles and their physiological functions. J Extracell Vesicles. 2015;4:27066.

35. Yuana Y, Sturk A, Nieuwland R. Extracellular vesicles in physiological and pathological conditions. Blood Rev. 2013 Jan;27(1):31–9.

36. Colao IL, Corteling R, Bracewell D, Wall I. Manufacturing Exosomes: A Promising Therapeutic Platform. Trends Mol Med. 2018;24(3):242–56.

37. Lässer C, Jang SC, Lötvall J. Subpopulations of extracellular vesicles and their therapeutic potential. Mol Aspects Med. 2018;60:1–14.

38. Nourbakhsh B, Mowry EM. Multiple Sclerosis Risk Factors and Pathogenesis. Contin Minneap Minn. 2019 Jun;25(3):596–610.

39. Bishop M, Rumrill PD. Multiple sclerosis: Etiology, symptoms, incidence and prevalence, and implications for community living and employment. Work Read Mass. 2015;52(4):725–34.

40. Dendrou CA, Fugger L, Friese MA. Immunopathology of multiple sclerosis. Nat Rev Immunol. 2015 Sep 15;15(9):545–58.

41. Hellings N, Barée M, Verhoeven C, D'hooghe MB, Medaer R, Bernard CC, et al. T-cell reactivity to multiple myelin antigens in multiple sclerosis patients and healthy controls. J Neurosci Res. 2001 Feb 1;63(3):290–302.

42. Cao Y, Goods BA, Raddassi K, Nepom GT, Kwok WW, Love JC, et al. Functional inflammatory profiles distinguish myelin-reactive T cells from patients with multiple sclerosis. Sci Transl Med. 2015 May 13;7(287):287ra74.

43. Friese MA, Schattling B, Fugger L. Mechanisms of neurodegeneration and axonal dysfunction in multiple sclerosis. Nat Rev Neurol. 2014 Apr;10(4):225–38.

44. Ludwin SK, Rao VT, Moore CS, Antel JP. Astrocytes in multiple sclerosis. Mult Scler Houndmills Basingstoke Engl. 2016;22(9):1114–24.

45. Ponath G, Park C, Pitt D. The Role of Astrocytes in Multiple Sclerosis. Front Immunol. 2018 Feb 19;9:217. doi: 10.3389/fimmu.2018.00217. PMID: 29515568; PMCID: PMC5826071.

46. Correale J, Farez MF. The Role of Astrocytes in Multiple Sclerosis Progression. Front Neurol. 2015;6:180.

47. Liddelow SA, Barres BA. Reactive Astrocytes: Production, Function, and Therapeutic Potential. Immunity. 2017 20;46(6):957–67.

48. Savino MT, Ortensi B, Ferro M, Ulivieri C, Fanigliulo D, Paccagnini E, et al. Rai acts as a negative regulator of autoimmunity by inhibiting antigen receptor signaling and lymphocyte activation. J Immunol Baltim Md 1950. 2009 Jan 1;182(1):301–8.

49. Villanacci V, Bassotti G, Ortensi B, Fisogni S, Cathomas G, Maurer CA, et al. Expression of the Rai (Shc C) adaptor protein in the human enteric nervous system. Neurogastroenterol Motil Off J Eur Gastrointest Motil Soc. 2008 Mar;20(3):206–12.

50. Ferro M, Savino MT, Ortensi B, Finetti F, Genovese L, Masi G, et al. The Shc family protein adaptor, Rai, negatively regulates T cell antigen receptor signaling by inhibiting ZAP-70 recruitment and activation. PloS One. 2011;6(12):e29899.

51. Savino MT, Ulivieri C, Emmi G, Prisco D, De Falco G, Ortensi B, et al. The Shc family protein adaptor, Rai, acts as a negative regulator of Th17 and Th1 cell development. J Leukoc Biol. 2013 Apr;93(4):549–59.

52. Ulivieri C, Savino MT, Luccarini I, Fanigliulo E, Aldinucci A, Bonechi E, et al. The Adaptor Protein Rai/ShcC Promotes Astrocyte-Dependent Inflammation during Experimental Autoimmune Encephalomyelitis. J Immunol Baltim Md 1950. 2016 15;197(2):480–90.

53. Ulivieri C, De Tommaso D, Finetti F, Ortensi B, Pelicci G, D'Elios MM, et al. A T Cell Suppressive Circuitry Mediated by CD39 and Regulated by ShcC/Rai Is Induced in Astrocytes by Encephalitogenic T Cells. Front Immunol. 2019;10:1041.

54. Harlow E, Lane D. Bradford assay. CSH Protoc. 2006 Nov 1;2006(6).

55. Bjellqvist B, Pasquali C, Ravier F, Sanchez JC, Hochstrasser D. A nonlinear wide-range immobilized pH gradient for two-dimensional electrophoresis and its definition in a relevant pH scale. Electrophoresis. 1993 Dec;14(12):1357–65.

56. Hochstrasser DF, Patchornik A, Merril CR. Development of polyacrylamide gels that improve the separation of proteins and their detection by silver staining. Anal Biochem. 1988 Sep;173(2):412–23.

57. Nagano F, Sasaki T, Fukui K, Asakura T, Imazumi K, Takai Y. Molecular cloning and characterization of the noncatalytic subunit of the Rab3 subfamily-specific GTPase-activating protein. J Biol Chem. 1998 Sep 18;273(38):24781–5.

58. Werner P, Pitt D, Raine CS. Multiple sclerosis: altered glutamate homeostasis in lesions correlates with oligodendrocyte and axonal damage. Ann Neurol. 2001 Aug;50(2):169–80.

59. Jayakumar AR, Norenberg MD. Glutamine Synthetase: Role in Neurological Disorders. Adv Neurobiol. 2016;13:327–50.

60. Iovino L, Tremblay ME, Civiero L. Glutamate-induced excitotoxicity in Parkinson's disease: The role of glial cells. J Pharmacol Sci. 2020 Nov;144(3):151–64.

61. Lewerenz J, Maher P. Chronic Glutamate Toxicity in Neurodegenerative Diseases-What is the Evidence? Front Neurosci. 2015;9:469.

62. Macrez R, Stys PK, Vivien D, Lipton SA, Docagne F. Mechanisms of glutamate toxicity in multiple sclerosis: biomarker and therapeutic opportunities. Lancet Neurol. 2016;15(10):1089–102.

63. Baas D, Bourbeau D, Sarliéve LL, Ittel M-E, Dussault JH, Puymirat J. Oligodendrocyte maturation and progenitor cell proliferation are independently regulated by thyroid hormone. Glia. 1997;19(4):324–32.

64. You D, Yin B-C, Li Z-H, Zhou Y, Yu W-B, Zuo P, et al. Sirtuin-dependent reversible lysine acetylation of glutamine synthetases reveals an autofeedback loop in nitrogen metabolism. Proc Natl Acad Sci U S A. 2016 14;113(24):6653–8.

65. Arito M, Nagai K, Ooka S, Sato T, Takakuwa Y, Kurokawa MS, et al. Altered acetylation of proteins in patients with rheumatoid arthritis revealed by acetyl-proteomics. Clin Exp Rheumatol. 2015 Dec;33(6):877–86.

66. Haque A, Ray SK, Cox A, Banik NL. Neuron specific enolase: a promising therapeutic target in acute spinal cord injury. Metab Brain Dis. 2016;31(3):487–95.

67. Zeis T, Graumann U, Reynolds R, Schaeren-Wiemers N. Normal-appearing white matter in multiple sclerosis is in a subtle balance between inflammation and neuroprotection. Brain J Neurol. 2008 Jan;131(Pt 1):288–303.

68. Mutze K, Vierkotten S, Milosevic J, Eickelberg O, Königshoff M. Enolase 1 (ENO1) and protein disulfide-isomerase associated 3 (PDIA3) regulate Wnt/β-catenin-driven trans-differentiation of murine alveolar epithelial cells. Dis Model Mech. 2015 Aug 1;8(8):877–90.

69. Wang W-T, Sun L, Sun C-H. PDIA3-regulted inflammation and oxidative stress contribute to the traumatic brain injury (TBI) in mice. Biochem Biophys Res Commun. 2019 Oct 22;518(4):657–63.

70. Chen JY-F, Hung C-C, Huang K-L, Chen Y-T, Liu S-Y, Chiang W-F, et al. Src family kinases mediate betel quid-induced oral cancer cell motility and could be a biomarker for early invasion in oral squamous cell carcinoma. Neoplasia N Y N. 2008 Dec;10(12):1393–401.

71. Chen X, Liu X, Lang H, Zhang S, Luo Y, Zhang J. S100 calcium-binding protein A6 promotes epithelial-mesenchymal transition through β-catenin in pancreatic cancer cell line. PloS One. 2015;10(3):e0121319.

72. Yamada J, Jinno S. Upregulation of calcium binding protein, S100A6, in activated astrocytes is linked to glutamate toxicity. Neuroscience. 2012 Dec 13;226:119–29.

73. Fisher AB. The phospholipase A2 activity of peroxiredoxin 6. J Lipid Res. 2018;59(7):1132–47.

74. Luoma AM, Kuo F, Cakici O, Crowther MN, Denninger AR, Avila RL, et al. Plasmalogen phospholipids protect internodal myelin from oxidative damage. Free Radic Biol Med. 2015 Jul;84:296–310.

75. Liu Y, Zhang X, Yang B, Zhuang H, Guo H, Wei W, et al. Demethylation-Induced Overexpression of Shc3 Drives c-Raf-Independent Activation of MEK/ERK in HCC. Cancer Res. 2018 01;78(9):2219–32.

76. Yun H-M, Park K-R, Kim E-C, Hong JT. PRDX6 controls multiple sclerosis by suppressing inflammation and blood brain barrier disruption. Oncotarget. 2015 Aug 28;6(25):20875–84.

77. Giurdanella G, Motta C, Muriana S, Arena V, Anfuso CD, Lupo G, et al. Cytosolic and calcium-independent phospholipase A(2) mediate glioma-enhanced proangiogenic activity of brain endothelial cells. Microvasc Res. 2011 Jan;81(1):1–17.

78. Anfuso CD, Lupo G, Romeo L, Giurdanella G, Motta C, Pascale A, et al. Endothelial cell-pericyte cocultures induce PLA2 protein expression through activation of PKCalpha and the MAPK/ERK cascade. J Lipid Res. 2007 Apr;48(4):782–93.

79. Jiang Y-Y, Shang L, Shi Z-Z, Zhang T-T, Ma S, Lu C-C, et al. Microtubule-associated protein 4 is an important regulator of cell invasion/migration and a potential therapeutic target in esophageal squamous cell carcinoma. Oncogene. 2016 15;35(37):4846–56.

80. Vouyiouklis DA, Brophy PJ. Microtubule-associated proteins in developing oligodendrocytes: transient expression of a MAP2c isoform in oligodendrocyte precursors. J Neurosci Res. 1995 Dec 15;42(6):803–17.

81. Hu X, Liu ZZ, Chen X, Schulz VP, Kumar A, Hartman AA, et al. MKL1-actin pathway restricts chromatin accessibility and prevents mature pluripotency activation. Nat Commun. 2019 12;10(1):1695.

82. Hampe L, Radjainia M, Xu C, Harris PWR, Bashiri G, Goldstone DC, et al. Regulation and Quality Control of Adiponectin Assembly by Endoplasmic Reticulum Chaperone ERp44. J Biol Chem. 2015 Jul 17;290(29):18111–23.

83. Zhang K, Guo Y, Ge Z, Zhang Z, Da Y, Li W, et al. Adiponectin Suppresses T Helper 17 Cell Differentiation and Limits Autoimmune CNS Inflammation via the SIRT1/PPARγ/RORγt Pathway. Mol Neurobiol. 2017;54(7):4908–20.

84. Liu X, Xu L, Liu Y, Tong X, Zhu G, Zhang XC, et al. Crystal structure of the hexamer of human heat shock factor binding protein 1. Proteins. 2009 Apr;75(1):1–11.

85. Puglia M, Landi C, Gagliardi A, Breslin L, Armini A, Brunetti J, et al. The proteome speciation of an immortalized cystic fibrosis cell line: New perspectives on the pathophysiology of the disease. J Proteomics. 2018 06;170:28–42.

86. Eroglu B, Min J-N, Zhang Y, Szurek E, Moskophidis D, Eroglu A, et al. An essential role for heat shock transcription factor binding protein 1 (HSBP1) during early embryonic development. Dev Biol. 2014 Feb 15;386(2):448–60.

87. Heilman PL, Song S, Miranda CJ, Meyer K, Srivastava AK, Knapp A, et al. HSPB1 mutations causing hereditary neuropathy in humans disrupt non-cell autonomous protection of motor neurons. Exp Neurol. 2017 Nov;297:101–9.

88. van Horssen J, Schreibelt G, Drexhage J, Hazes T, Dijkstra CD, van der Valk P, et al. Severe oxidative damage in multiple sclerosis lesions coincides with enhanced antioxidant enzyme expression. Free Radic Biol Med. 2008 Dec 15;45(12):1729–37.

89. Anderson MA, Burda JE, Ren Y, Ao Y, O'Shea TM, Kawaguchi R, et al. Astrocyte scar formation aids central nervous system axon regeneration. Nature. 2016 Apr 14;532(7598):195–200.

90. Haindl MT, Köck U, Zeitelhofer-Adzemovic M, Fazekas F, Hochmeister S. The formation of a glial scar does not prohibit remyelination in an animal model of multiple sclerosis. Glia. 2019 Mar;67(3):467–81.

91. Mohan H, Krumbholz M, Sharma R, Eisele S, Junker A, Sixt M, et al. Extracellular matrix in multiple sclerosis lesions: Fibrillar collagens, biglycan and decorin are upregulated and associated with infiltrating immune cells. Brain Pathol Zurich Switz. 2010 Sep;20(5):966–75.

92. Yamagami T, Pleasure DE, Lam KS, Zhou CJ. Transient activation of Wnt/β-catenin signaling reporter in fibrotic scar formation after compression spinal cord injury in adult mice. Biochem Biophys Res Commun. 2018 Feb 19;496(4):1302–7.

93. Howe MD, Furr JW, Munshi Y, Roy-O'Reilly MA, Maniskas ME, Koellhoffer EC, et al. Transforming growth factor-β promotes basement membrane fibrosis, alters perivascular cerebrospinal fluid distribution, and worsens neurological recovery in the aged brain after stroke. GeroScience. 2019 Oct;41(5):543–59.

94. Camby I, Belot N, Rorive S, Lefranc F, Maurage CA, Lahm H, et al. Galectins are differentially expressed in supratentorial pilocytic astrocytomas, astrocytomas, anaplastic astrocytomas and glioblastomas, and significantly modulate tumor astrocyte migration. Brain Pathol Zurich Switz. 2001 Jan;11(1):12–26.

95. Rinaldi M, Thomas L, Pasquini LA. Galectin-1 in myelin repair. Oncotarget. 2016 Dec 13;7(50):81979–80.

96. Kim J-E, Kang T-C. PKC, AKT and ERK1/2-Mediated Modulations of PARP1, NF-κB and PEA15 Activities Distinctly Regulate Regional Specific Astroglial Responses Following Status Epilepticus. Front Mol Neurosci. 2019;12:180.

97. Kumar D, Ambasta RK, Kumar P. Ubiquitin biology in neurodegenerative disorders: From impairment to therapeutic strategies. Ageing Res Rev. 2020 Aug;61:101078.

98. Hodge CD, Spyracopoulos L, Glover JNM. Ubc13: the Lys63 ubiquitin chain building machine. Oncotarget. 2016 Sep 27;7(39):64471–504.

99. Capello M, Ferri-Borgogno S, Cappello P, Novelli F. α-Enolase: a promising therapeutic and diagnostic tumor target. FEBS J. 2011 Apr;278(7):1064–74.

100. Cappello P, Principe M, Bulfamante S, Novelli F. Alpha-Enolase (ENO1), a potential target in novel immunotherapies. Front Biosci Landmark Ed. 2017 Jan 1;22:944–59.

101. Tannahill GM, Iraci N, Gaude E, Frezza C, Pluchino S. Metabolic reprograming of mononuclear phagocytes in progressive multiple sclerosis. Front Immunol. 2015;6:106.

102. Reynolds HY. Use of bronchoalveolar lavage in humans--past necessity and future imperative. Lung. 2000;178(5):271–93.

103. Govender P, Dunn MJ, Donnelly SC. Proteomics and the lung: Analysis of bronchoalveolar lavage fluid. Proteomics Clin Appl. 2009 Sep;3(9):1044–51.

104. Carvalho AS, Matthiesen R. Bronchoalveolar Lavage: Quantitative Mass Spectrometry-Based Proteomics Analysis in Lung Diseases. Methods Mol Biol Clifton NJ. 2017;1619:487–94.

105. Nguyen EV, Gharib SA, Schnapp LM, Goodlett DR. Shotgun MS proteomic analysis of bronchoalveolar lavage fluid in normal subjects. Proteomics Clin Appl. 2014 Oct;8(9–10):737–47.

106. Travis WD, Costabel U, Hansell DM, King TE, Lynch DA, Nicholson AG, et al. An official American Thoracic Society/European Respiratory Society statement: Update of the international multidisciplinary classification of the idiopathic interstitial pneumonias. Am J Respir Crit Care Med. 2013 Sep 15;188(6):733–48.

107. Efared B, Ebang-Atsame G, Rabiou S, Diarra AS, Tahiri L, Hammas N, et al. The diagnostic value of the bronchoalveolar lavage in interstitial lung diseases. J Negat Results Biomed. 2017 Mar 1;16(1):4.

108. Landi C, Bargagli E, Carleo A, Bianchi L, Gagliardi A, Prasse A, et al. A system biology study of BALF from patients affected by idiopathic pulmonary fibrosis (IPF) and healthy controls. Proteomics Clin Appl. 2014 Dec;8(11–12):932–50.

109. Carleo A, Landi C, Prasse A, Bergantini L, D'Alessandro M, Cameli P, et al. Proteomic characterization of idiopathic pulmonary fibrosis patients: stable versus acute exacerbation. Monaldi Arch Chest Dis Arch Monaldi Mal Torace. 2020 Apr 30;90(2).

110. Rollet-Cohen V, Bourderioux M, Lipecka J, Chhuon C, Jung VA, Mesbahi M, et al. Comparative proteomics of respiratory exosomes in cystic fibrosis, primary ciliary dyskinesia and asthma. J Proteomics. 2018 15;185:1–7.

111. Njock M-S, Guiot J, Henket MA, Nivelles O, Thiry M, Dequiedt F, et al. Sputum exosomes: promising biomarkers for idiopathic pulmonary fibrosis. Thorax. 2019;74(3):309–12.

112. Yamada M. The Roles of MicroRNAs and Extracellular Vesicles in the Pathogeneses of Idiopathic Pulmonary Fibrosis and Acute Respiratory Distress Syndrome. Tohoku J Exp Med. 2020;251(4):313–26.

113. Lee H, Groot M, Pinilla-Vera M, Fredenburgh LE, Jin Y. Identification of miRNA-rich vesicles in bronchoalveolar lavage fluid: Insights into the function and heterogeneity of extracellular vesicles. J Control Release Off J Control Release Soc. 2019 28;294:43–52.

114. Liu B, Jiang T, Hu X, Liu Z, Zhao L, Liu H, et al. Downregulation of microRNA-30a in bronchoalveolar lavage fluid from idiopathic pulmonary fibrosis patients. Mol Med Rep. 2018 Dec;18(6):5799–806.

115. Martin-Medina A, Lehmann M, Burgy O, Hermann S, Baarsma HA, Wagner DE, et al. Increased Extracellular Vesicles Mediate WNT5A Signaling in Idiopathic Pulmonary Fibrosis. Am J Respir Crit Care Med. 2018 15;198(12):1527–38.

116. Théry C, Amigorena S, Raposo G, Clayton A. Isolation and characterization of exosomes from cell culture supernatants and biological fluids. Curr Protoc Cell Biol. 2006 Apr;Chapter 3:Unit 3.22.

117. Wheelock CE, Goss VM, Balgoma D, Nicholas B, Brandsma J, Skipp PJ, et al. Application of 'omics technologies to biomarker discovery in inflammatory lung diseases. Eur Respir J. 2013 Sep;42(3):802–25.

118. Sim SY, Choi YR, Lee JH, Lim JM, Lee S-E, Kim KP, et al. In-Depth Proteomic Analysis of Human Bronchoalveolar Lavage Fluid toward the Biomarker Discovery for Lung Cancers. Proteomics Clin Appl. 2019;13(5):e1900028.

119. Matthiesen R. MS-Based Biomarker Discovery in Bronchoalveolar Lavage Fluid for Lung Cancer. Proteomics Clin Appl. 2020;14(1):e1900077.

120. Liessi N, Pedemonte N, Armirotti A, Braccia C. Proteomics and Metabolomics for Cystic Fibrosis Research. Int J Mol Sci. 2020 Jul 30;21(15).

121. Braccia C, Tomati V, Caci E, Pedemonte N, Armirotti A. SWATH label-free proteomics for cystic fibrosis research. J Cyst Fibros Off J Eur Cyst Fibros Soc. 2019;18(4):501–6.

122. Landi C, Cameli P, Vantaggiato L, Bergantini L, d'Alessandro M, Peruzza M, et al. Ceruloplasmin and oxidative stress in severe eosinophilic asthma patients treated with Mepolizumab and Benralizumab. Biochim Biophys Acta Proteins Proteomics. 2020 Nov 8;1869(2):140563.

123. Xu P, Wang L, Chen D, Feng M, Lu Y, Chen R, et al. The application of proteomics in the diagnosis and treatment of bronchial asthma. Ann Transl Med. 2020 Feb;8(4):132.

124. Moon J-Y, Leitao Filho FS, Shahangian K, Takiguchi H, Sin DD. Blood and sputum protein biomarkers for chronic obstructive pulmonary disease (COPD). Expert Rev Proteomics. 2018;15(11):923–35.

125. Liu Y, Liu H, Li C, Ma C, Ge W. Proteome Profiling of Lung Tissues in Chronic Obstructive Pulmonary Disease (COPD): Platelet and Macrophage Dysfunction Contribute to the Pathogenesis of COPD. Int J Chron Obstruct Pulmon Dis. 2020;15:973–80.

126. Neri T, Tavanti L, De Magistris S, Lombardi S, Romei C, Falaschi F, et al. Endothelial Cell-Derived Extracellular Vesicles as Potential Biomarkers in Chronic Interstitial Lung Diseases. Ann Clin Lab Sci. 2019 Sep;49(5):608–10.

127. McVey MJ, Maishan M, Blokland KEC, Bartlett N, Kuebler WM. Extracellular vesicles in lung health, disease, and therapy. Am J Physiol Lung Cell Mol Physiol. 2019 01;316(6):L977–89.

128. Cizmar P, Yuana Y. Detection and Characterization of Extracellular Vesicles by Transmission and Cryo-Transmission Electron Microscopy. Methods Mol Biol Clifton NJ. 2017;1660:221–32.

129. G Kugeratski F, Kalluri R. Exosomes as mediators of immune regulation and immunotherapy in cancer. FEBS J. 2020 Sep 10;

130. Yaribeygi H, Maleki M, Sathyapalan T, Sahebkar A. The effect of C-peptide on diabetic nephropathy: A review of molecular mechanisms. Life Sci. 2019 Nov 15;237:116950.

131. Venugopal SK, Mowery ML, Jialal I. C Peptide. 2020 Jul 2. In: StatPearls [Internet]. Treasure Island (FL): StatPearls Publishing; 2021 Jan–. PMID: 30252282.

132. Kitamura T, Kimura K, Jung BD, Makondo K, Okamoto S, Cañas X, et al. Proinsulin C-peptide rapidly stimulates mitogen-activated protein kinases in Swiss 3T3 fibroblasts: requirement of protein kinase C, phosphoinositide 3-kinase and pertussis toxin-sensitive G-protein. Biochem J. 2001 Apr 1;355(Pt 1):123–9.

133. Zhao X, Kwan JYY, Yip K, Liu PP, Liu F-F. Targeting metabolic dysregulation for fibrosis therapy. Nat Rev Drug Discov. 2020;19(1):57–75.

134. Wang N, Wang Y, Zhang W, Chen Y, Chen X, Wang C, et al. C-peptide is associated with NAFLD inflammatory and fibrotic progression in type 2 diabetes. Diabetes Metab Res Rev. 2020;36(2):e3210.

135. Li Y, Zhong Y, Gong W, Gao X, Qi H, Liu K, et al. C-peptide prevents SMAD3 binding to alpha promoters to inhibit collagen type IV synthesis. J Mol Endocrinol. 2018;61(1):47–56.

136. Chima RS, LaMontagne T, Piraino G, Hake PW, Denenberg A, Zingarelli B. C-peptide, a novel inhibitor of lung inflammation following hemorrhagic shock. Am J Physiol Lung Cell Mol Physiol. 2011 May;300(5):L730-739.

137. Bargagli E, Refini RM, d'Alessandro M, Bergantini L, Cameli P, Vantaggiato L, et al. Metabolic Dysregulation in Idiopathic Pulmonary Fibrosis. Int J Mol Sci. 2020 Aug 7;21(16).

138. Stempien-Otero A, Kim D-H, Davis J. Molecular networks underlying myofibroblast fate and fibrosis. J Mol Cell Cardiol. 2016 Aug;97:153–61.

139. Guillotin D, Taylor AR, Platé M, Mercer PF, Edwards LM, Haggart R, et al. Transcriptome analysis of IPF fibroblastic foci identifies key pathways involved in fibrogenesis. Thorax. 2020 Nov 19;

140. Knipe RS, Tager AM, Liao JK. The Rho kinases: critical mediators of multiple profibrotic processes and rational targets for new therapies for pulmonary fibrosis. Pharmacol Rev. 2015;67(1):103–17.

141. Carleo A, Bargagli E, Landi C, Bennett D, Bianchi L, Gagliardi A, et al. Comparative proteomic analysis of bronchoalveolar lavage of familial and sporadic cases of idiopathic pulmonary fibrosis. J Breath Res. 2016 Apr 15;10(2):026007.

142. Franco CA, Liebner S, Gerhardt H. Vascular morphogenesis: a Wnt for every vessel? Curr Opin Genet Dev. 2009 Oct;19(5):476–83.

143. Yang D, Liu W, Ma L, Wang Y, Ma J, Jiang M, et al. Profilin-1 contributes to cardiac injury induced by advanced glycation end-products in rats. Mol Med Rep. 2017 Nov;16(5):6634–41.

144. Shaikh G, Cronstein B. Signaling pathways involving adenosine A2A and A2B receptors in wound healing and fibrosis. Purinergic Signal. 2016 Jun;12(2):191–7.

145. Philip K, Mills TW, Davies J, Chen N-Y, Karmouty-Quintana H, Luo F, et al. HIF1A up-regulates the ADORA2B receptor on alternatively activated macrophages and contributes to pulmonary fibrosis. FASEB J Off Publ Fed Am Soc Exp Biol. 2017 Nov;31(11):4745–58.

146. Collum SD, Molina JG, Hanmandlu A, Bi W, Pedroza M, Mertens TCJ, et al. Adenosine and hyaluronan promote lung fibrosis and pulmonary hypertension in combined pulmonary fibrosis and emphysema. Dis Model Mech. 2019 May 15;12(5).

147. Giacomelli C, Daniele S, Romei C, Tavanti L, Neri T, Piano I, et al. The A2B Adenosine Receptor Modulates the Epithelial- Mesenchymal Transition through the Balance of cAMP/PKA and MAPK/ERK Pathway Activation in Human Epithelial Lung Cells. Front Pharmacol. 2018;9:54.

148. Landi C, Carleo A, Vantaggiato L, Bergantini L, d'Alessandro M, Cameli P, et al. Common molecular pathways targeted by nintedanib in cancer and IPF: A bioinformatic study. Pulm Pharmacol Ther. 2020 Sep 5;64:101941.

149. Rassler B. Role of α- and β-adrenergic mechanisms in the pathogenesis of pulmonary injuries characterized by edema, inflammation and fibrosis. Cardiovasc Hematol Disord Drug Targets. 2013 Dec;13(3):197–207.

150. Craig VJ, Zhang L, Hagood JS, Owen CA. Matrix metalloproteinases as therapeutic targets for idiopathic pulmonary fibrosis. Am J Respir Cell Mol Biol. 2015 Nov;53(5):585–600.

151. Wells JM, Gaggar A, Blalock JE. MMP generated matrikines. Matrix Biol J Int Soc Matrix Biol. 2015 Jul;44–46:122–9.

152. Lee CG, Hartl D, Lee GR, Koller B, Matsuura H, Da Silva CA, et al. Role of breast regression protein 39 (BRP-39)/chitinase 3-like-1 in Th2 and IL-13-induced tissue responses and apoptosis. J Exp Med. 2009 May 11;206(5):1149–66.

153. Nusse R, Clevers H. Wnt/β-Catenin Signaling, Disease, and Emerging Therapeutic Modalities. Cell. 2017 Jun 1;169(6):985–99.

154. Baarsma HA, Königshoff M. 'WNT-er is coming': WNT signalling in chronic lung diseases. Thorax. 2017;72(8):746–59.

155. Stewart DJ. Wnt signaling pathway in non-small cell lung cancer. J Natl Cancer Inst. 2014 Jan;106(1):djt356.

156. Landi C, Bargagli E, Bianchi L, Gagliardi A, Carleo A, Bennett D, et al. Towards a functional proteomics approach to the comprehension of idiopathic pulmonary fibrosis, sarcoidosis, systemic sclerosis and pulmonary Langerhans cell histiocytosis. J Proteomics. 2013 May 27;83:60–75.

157. Abdul-Hafez A, Mohamed T, Omar H, Shemis M, Uhal BD. The renin angiotensin system in liver and lung: impact and therapeutic potential in organ fibrosis. J Lung Pulm Respir Res. 2018;5(1).

158. Figueiredo VP, Barbosa MA, de Castro UGM, Zacarias AC, Bezerra FS, de Sá RG, et al. Antioxidant Effects of Oral Ang-(1-7) Restore Insulin Pathway and RAS Components Ameliorating Cardiometabolic Disturbances in Rats. Oxid Med Cell Longev. 2019;2019:5868935.

159. Landi C, Bergantini L, Cameli P, d'Alessandro M, Carleo A, Shaba E, et al. Idiopathic Pulmonary Fibrosis Serum proteomic analysis before and after nintedanib therapy. Sci Rep. 2020 Jun 10;10(1):9378.

160. Li Y, Yan Z, Chaudhry K, Kazlauskas A. The Renin-Angiotensin-Aldosterone System (RAAS) Is One of the Effectors by Which Vascular Endothelial Growth Factor (VEGF)/Anti-VEGF Controls the Endothelial Cell Barrier. Am J Pathol. 2020 Jun 23;

161. Du J, Li J. The role of Wnt signaling pathway in atherosclerosis and its relationship with angiogenesis. Exp Ther Med. 2018 Sep;16(3):1975–81.

162. Kim J, Hajjar KA. Annexin II: a plasminogen-plasminogen activator co-receptor. Front Biosci J Virtual Libr. 2002 Feb 1;7:d341-348.

163. Liu W, Hajjar KA. The annexin A2 system and angiogenesis. Biol Chem. 2016 Oct 1;397(10):1005–16.

164. Schuliga M, Jaffar J, Berhan A, Langenbach S, Harris T, Waters D, et al. Annexin A2 contributes to lung injury and fibrosis by augmenting factor Xa fibrogenic activity. Am J Physiol Lung Cell Mol Physiol. 2017 May 1;312(5):L772–82.

165. Bargagli E, Madioni C, Bianchi N, Refini RM, Cappelli R, Rottoli P. Serum analysis of coagulation factors in IPF and NSIP. Inflammation. 2014 Feb;37(1):10–6.